Discrete element simulation for the loading of a steep incline side wall conveyor

RF Fourie

orcid.org/0000-0001-9782-2112

Dissertation submitted in partial fulfilment of the requirements for the degree *Master of Engineering in Mechanical Engineering* at the North-West University

Supervisor: Dr PVZ Venter

Co-supervisor: Prof M van Eldik

Graduation ceremony: May 2019

Student number: 21735387

ABSTRACT

The blast furnace progress team evaluated the equipment operational life of the two different charging systems used at the blast furnace plant. It was determined that the steep incline sidewall conveyor charging system had a lower operational life due to damages caused by the constant spill of material during operation. A need was identified for a discrete element model that can simulate the loading point of the steep incline sidewall conveyor, and then used to evaluate possible design changes to reduce the spilled material percentage.

The development of the discrete element model simulation was initiated by determining the applicable material model parameters, and the methods used to calibrate them. A combination of the direct and bulk calibration approaches along with the V-model methodology was used. A test rig was built which allowed for a screened material sample to be drained through a containment hopper, interact with a deflection plate and settle to the material angle of repose. These events were captured with a high speed camera and the footage was used for the validation of the material parameters within the discrete element model simulation.

Following the model material parameter calibration, the steep incline sidewall conveyor model was developed. This was done by firstly evaluating the plant equipment layout and operational strategy. The conveyor movement was incorporated into the simulation with the use of the overset mesh tool. The validation of the simulation model was done with the use of high speed camera footage of the loading point. Three categories of validation were established, namely particle speed assessment, particle trajectory assessment and particle-belt interaction assessment.

The model was then used to determine if plant design changes can be made in order to reduce the material spillage percentage. This was done by evaluating two different modification options. Firstly the effect of a variable speed drive installation was investigated by simulating a belt velocity increase and decrease of 50%. Secondly the effect of material particle velocity variation was simulated by increasing and decreasing the discharge chute angle with 10 degrees respectively. It was determined that the chute angle modification had the greatest effect on the material spillage reduction.

It was concluded that the combination of the direct and bulk calibration approaches were applicable in calibrating the required material model parameters. The discrete element model accurately simulated the loading point of a steep incline sidewall conveyor. The

simulated results indicated that the spillage percentage can be reduced significantly if the material's relative velocity is matched to the belt velocity by increasing the discharge chute angle.

KEY WORDS

Numerical modelling

Discrete element model

Hertz Mindlin contact model

Calibration

Direct measuring approach

Bulk calibration approach

Test bench

High speed camera

Steep incline sidewall conveyor

Coke particles

ACKNOWLEDGEMENTS

I thank God the Father, his son Jesus Christ and the Holy Spirit for all the blessings and opportunities bestowed on me.

I thank my wife Anja Fourie for her undying love, support and unfaltering patience. Your kind words and loving prayers are the energy source that keeps me going.

I thank my parents and brother Marie, John and Charl Fourie for all the support and guidance. An example worth aspiring towards.

I thank grandfather Wim Skinner for setting me on the path of post graduate studies. You are sorely missed and I cheerfully await the day of our reconciliation.

I thank my study leaders Prof. Martin van Eldik and Dr. Philip Venter for their continuous guidance.

I thank Christian de Wet, Cronier van Niekerk and Ruan Nagel for the assistance throughout the study.

TABLE OF CONTENT

LIST OF FIGURES

LIST OF TABLES

1. INTRODUCTION

1.1. BACKGROUND

At the heart of a typical iron making industry lays the blast furnace plant. The blast furnace plant is responsible for converting iron baring raw materials into molten iron through a counter current process of heat and mass transfer. For the blast furnace to operate at peak performance an uninterrupted raw material supply is required, in specific batches, and with a specific quality. While these raw materials are loaded into the top of the furnace, hot air, pulverised coal and pure oxygen are blown into the furnace, through tuyeres, just above the hearth section. The introduction of the hot air into the furnace results in the combustion of pulverised coal and coke at the outlet of the tuyeres. This combustion process causes an increase in gas temperature which results in the carbon dioxide rich gas to rise to the top of the furnace. The hot gas rising process is an important element in the blast furnace operation, because it is required for the formation of carbon monoxide (due to the Boudouard reaction when in contact with coke) which is required for the oxygen reduction process (Ricketts, 2012).

The oxygen reduction process occurs when the carbon monoxide is in contact with iron ore (Hematite) and results in an increase in particle temperature and carbon dioxide gas. At lower regions of the furnace the reduction process reaches a stage where the iron particles start to melt and drip down to the bottom of the furnace. Due to the melting of iron particles (reduction process) and consumption of coke (Boudouard reaction and combustion) voids are formed which results in the material burden moving downward (Ricketts, 2012). This downward movement of the material is known as the driving of a furnace and is monitored closely, because the rate at which the furnace is driving determines the rate at which raw materials are loaded into the furnace. Therefore the raw material feed and hot air supply are constantly monitored and adjusted in order to ensure that the blast furnace operates at the required production volumes while producing quality liquid iron.

The quality of the raw material supply to the furnace is controlled by the RMH (Raw Material Handling) plant. The RMH plant is responsible for quality verification, screening, sorting and conveying of all the material required by the blast furnace. In the blast furnace plant a network of conveyors converge toward the stock house section. At the stock house all of the processed materials such as iron ore, manganese, dolomite, silica ore, sinter and coke are loaded into dedicated bunkers. Each of these materials are extracted in specific batches and loaded into the blast furnace via two methods; 1) a skip loading system (illustrated by Figure

1) and 2) a conveyor loading system (illustrated by Figure 2), of which both are used at Arcelor Mittal (Ricketts, 2012).

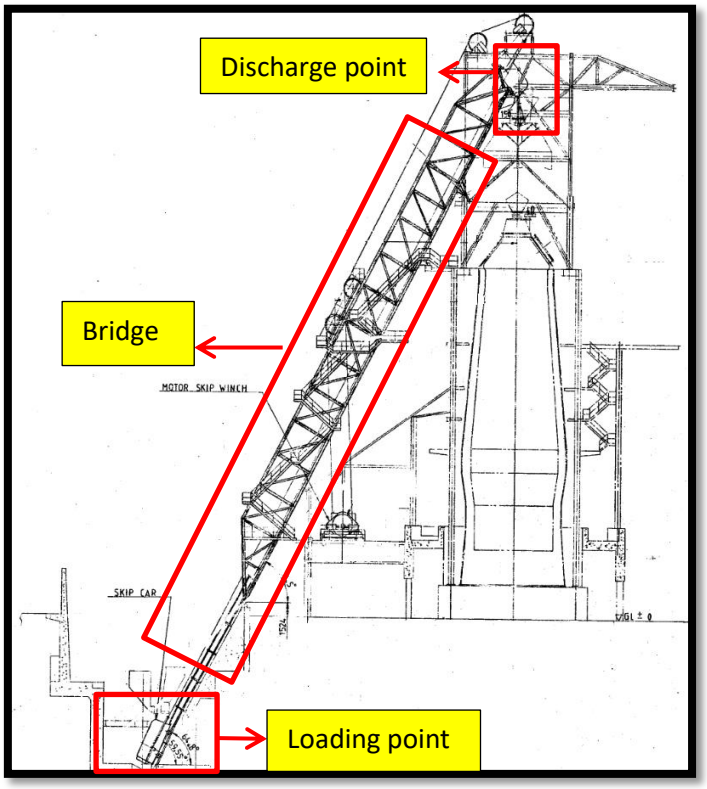

Figure 1 Typical skip furnace loading system (Ricketts, 2012)

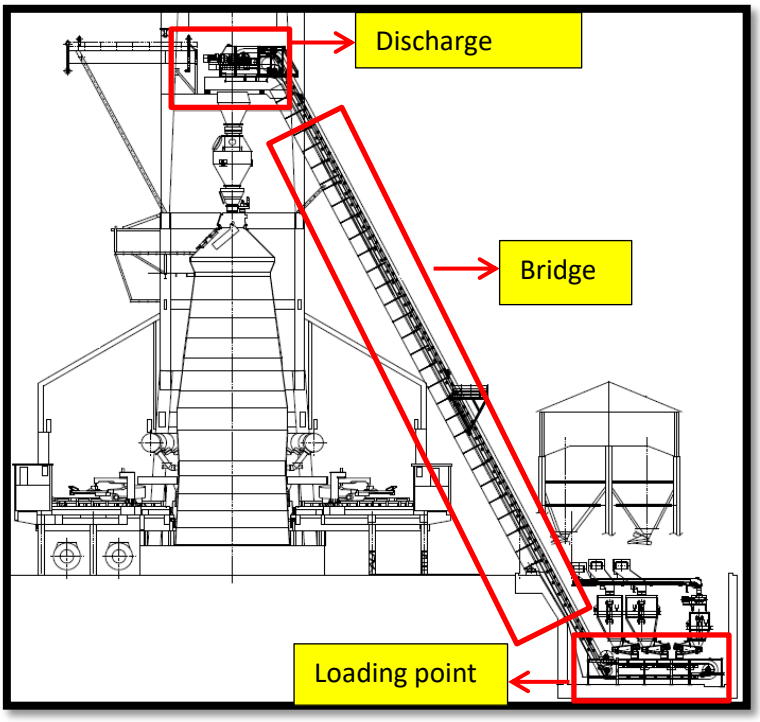

Figure 2 Steep incline sidewall conveyor arrangement (Ricketts, 2012)

The skip loading system is the older of the two charging methods. With this system two large bucket trolleys, also known as skips, running on rail tracks are pulled up to the furnace top via a winch system. This design allows for one skip to be pulled up to the furnace top, loaded with a specific batch of material, while the second empty skip is lowered down to the stock house for loading. The system is synchronised so that as the full skip reaches the furnace top for discharge, the empty skip stops in the stock house ready for loading (illustrated by Figure 1). The loading mechanism is therefore based on a hopper (fed by stock house conveyors) discharging into the stationary skip bucket. As a result, the feed rate capacity is limited to the skip size and the skip travel time.

The second design has a network of conveyors situated underneath each of the material bunkers in the stock house. These conveyors transport the material in the required batches to three separate transfer point hoppers, also known as surcharge hoppers. The transfer points are divided into 1) ore and additives, 2) sinter and 3) coke. These transfer point hoppers weigh and load each of the material batches onto a continuously moving steep incline sidewall conveyor, which transports the material to the furnace top for discharge. With this design the loading mechanism is based on the surcharge hoppers discharging the material onto a moving conveyor. The feed rate capacity of this design is limited by the size and velocity of the conveyor.

As part of the blast furnace maintenance improvement project it was determined that the skip system has a longer operational life than the steep incline sidewall conveyor system. A further investigation revealed that the steep incline sidewall conveyor system has a constant spillage emanating from the loading section of the belt, and the skip system doesn't. It was highlighted that the constant material spillage causes the material to build up on the sides of the belt. This material build-up causes the belt to move through material, which increases the abrasion wear on the belt edges, resulting in a shortened operational life.

In an attempt to increase the operational life of the steep incline sidewall conveyor system, two possible solutions were proposed to address the material spillages. The first was to install a variable speed drive which would alter the belt velocity relative to the material discharge velocity. The second was to re-design the discharge chutes above the steep incline sidewall conveyor loading point in order to better match the material trajectory to the belt movement direction.

1.2. NEED

Any changes suggested to reduce material spillages will require plant modifications and therefore capital investment. To support the decision making process a need was identified for a mathematical model capable of simulating the current loading conditions. Such a model would be used to determine if the spillages are affected more by the material trajectory coming from the surcharge hoppers, or due to the belt velocity. The benefit of the model would be to simulate design changes without physically interfering with plant production, reducing the costs associated with trial and error installations.

1.3. SCOPE

This study will determine if a discrete element model (DEM) is capable of simulating coke material bulk behaviour when discharged from a hopper onto a steep inclined sidewall conveyor. Thereafter it will be determined which of the suggested design changes would have the greatest effect on reducing the material spillages. The software package used for this study is Simcenter STAR-CCM+ (Siemens PLM, 2018).

Included in the study will be the measuring of specific coke material parameters required for the DEM formulation. Each of the material parameters will be validated with the use of a material flow test bench rig which will be designed and built for the purpose of this study. A DEM simulation will be developed for the current coke material loading point of the steep inclined sidewall conveyor setup. The simulation model will be validated by taking high speed camera footage of the coke loading section of the steep inclined sidewall conveyor. Upon validating the current loading operation, the suggested design changes will be evaluated by comparing material spillage percentage between the different options.

Items that will be excluded from this study include the skip loading system, as the focus is on the steep incline sidewall conveyor. The conveying of the material after the loading point, i.e. the bridge section as illustrated by Figure 2 will also be excluded along with the discharge mechanism. The sinter as well as the ore and additive loading interfaces will not be included due to the sinter having a large percentage of small particles requiring a detailed particle size analysis. The ore and additives have a complex particle-particle interaction characteristic because the quantity of material charged is dependent on the furnace condition and therefore makes this loading interface complex.

1.4. METHODOLOGY

The methodology for this study is as follows:

1.4.1. LITERATURE STUDY

A literature study will be conducted in order to evaluate what research has been published with regards to the use of Discrete Element Modelling (DEM).The first section will focus on the different types of software packages that are available. This will provide a better understanding with regards to cost, user friendliness and possible post processing capabilities. The second section will investigate what research has been done in the field of material micro and bulk properties. The aim of this section will be to identify key material properties for the DEM calibration process.

The third section will focus on the calibration techniques used to validate the DEM simulation model. Here it will be investigated if test benches or procedures have been developed that are capable of validating the material behaviour, and at what point is the simulation model deemed calibrated. The fourth section will focus on the industrial use of the DEM simulation model as a design tool. Here it is important to determine what the DEM model has been used for and how close did the DEM simulation results match the actual plant installation. It should also be determined if there are possible limitations to the DEM model in the industry and if it is even possible of developing an accurate steep incline sidewall conveyor DEM model.

1.4.2. THEORY

The theoretical background chapter will focus on the Discrete Element Model and the relevant mathematical formulations incorporated within the model. This includes the boundary conditions, conservation equations and material characteristics required to define the model. In understanding the input requirements and how they are used within the software, significant time can be saved in the calibration and validation process of the simulation model.

1.4.3. MODEL CALIBRATION

A material assessment will be done to determine specific material properties that will form part of the direct material calibration approach. These include particle size distribution, density, material modulus of elasticity and particle shape evaluation. The next step will be to design and build a material testing rig that will assist with the bulk calibration approach. The material properties investigated by the bulk calibration approach will be the material's static friction coefficient, rolling coefficient, modulus of elasticity and the coefficient of restitution. A high speed camera will be used to capture the material as it passes through the testing rig in order to verify if the material's behaviour within the DEM simulation matches the material's

behaviour within the test rig. Specific material properties will be adjusted until the DEM model replicates the actual high speed camera footage. Upon the point that the material's behaviour within the DEM simulation replicates the high speed camera footage of the test rig, the material will be deemed calibrated and ready for the steep incline sidewall conveyor simulation.

1.4.4. STEEP INCLINE SIDEWALL CONVEYOR SIMULATION

For the steep incline sidewall conveyor simulation only the bottom third of the coke discharge hopper and the conveyor will be incorporated into the simulation. The total length of the conveyor will not be included into the simulation model due to the fact that the majority of the spillage originates from the loading point of the belt. As a result, only the loading point will be simulated, where the bridge and discharge sections (as illustrated by Figure 2) will be excluded. High speed camera footage will be taken at the coke loading point which will be used to validate the accuracy of the simulation model.

1.4.5. DESIGN MODIFICATIONS AND RECOMMENDATIONS

This section will focus on the possible plant modification options to reduce material spillage. The simulation will be modified by decreasing and increasing the belt velocity and evaluating what happens to the interaction between the material and the belt. The chute design modification will also be investigated by increasing and decreasing the angle of inclination of the discharge chute. The material interaction with the belt will, thereafter, be evaluated.

1.4.6. CONCLUSION

In the final chapter of this study a conclusion will be reached firstly on whether or not the bulk calibration approach (test rig built) is an acceptable means of calibrating a DEM simulation model. Secondly it will be established if a DEM simulation model is an appropriate model to use for design decisions on a steep incline sidewall conveyor. Thirdly it will be concluded if the current design is adequate, or if a change in belt velocity or chute angle is capable of improving the loading interface and therefore reducing the material spillages.

2. LITERATURE STUDY

Over the past few decades the development in computer processing power resulted in the advancement of numerical simulation methods such as the Discrete Element Modelling (DEM) method. With the use of these numerical simulation methods complex raw material characteristics can be simulated with regards to component design as well as for total system optimisation. Due to these advancements in the computing capabilities it has become more financially viable to simulate raw material processes numerically than to build physical prototypes (Nordell, 1997).

Throughout literature a wide range of DEM simulation software packages have been used to simulate different types of material handling processes. These processes are encapsulated in industries such as mining, agricultural, pharmaceutical, civil, steel, and transport (to name a few). It is therefore required to understand what software packages are currently available on the market, and what are some of the key aspects that distinguish one from the other.

2.1. DISCRETE ELEMENT MODELLING SOFTWARE PACKAGES

One of the main distinguishing factors between software packages are open source packages vs. commercial packages.

2.1.1. OPEN SOURCE DEM SOFTWARE PACKAGES

There are a number of open source DEM software packages available that have been developed for a wide range of material handling applications. Some of the greatest advantages of open source software packages are that it is free of charge, and it allows the user to modify the solver equation formulation in order to be application specific. With all of the freedom that an open source software package provides the user carries a greater risk that the model is not defined correctly and that the result (if even reached) is accurate. None the less a few open source packages that have been used with success are discussed below.

LIGGGHTS® is an open source software package that utilizes DEM for particulate matter simulation for industrial and research purposes (DCS Computing and CFDEMresearch, 2018). LIGGGHTS® incorporates the capability of importing complex geometries, allows for mesh movement with conveyor features, provides a variety of particle-particle contact implementation and allows specific defined particle stream injection.

ESyS-Particle is a Linux and Windows based open source DEM simulation package that has been used with success in the simulation of silo flow, earthquake nucleation, communication in shear cells and rock fragmentation (Canonical Ltd., 2018). ESyS-Particle also provides a variety of particle-particle contacts, a scriptable geometry feature and rotational spherical particles.

MECHSYS is an open source DEM package that also incorporates Computational Fluid Dynamic (CFD) capabilities (University of Queensland, 2015). The development of MECHSYS has been sponsored by the University of Queensland Australia and this platform has mainly been used for the research of the interaction of particles within an active fluid domain.

2.1.2. COMMERCIAL DEM SOFTWARE PACKAGES

The main advantage of a commercial software package is the user friendliness and support that is provided when using the software. With commercial packages the user is guided with specific selection criteria which the solver needs in order to numerically solve a specific scenario. Like any other software package the result is still dependent on the user, and it is therefore important that the user understand all of the input criteria required for an accurate solution. There are a number of software packages that specialize in only DEM whereby other packages are more multi-discipline and combine DEM with FEA and CFD.

EDEM is one of the leading commercially available software packages that specialises in the simulation of bulk material handling (DEM Solutions Ltd, 2018). EDEM is also used for both the industry as well as for academic research. Like most of the commercial packages EDEM incorporates CFD and FEA analyses, however, with DEM as the main foundation.

Rocky is a DEM software package that is developed by a Brazilian based company ESSS (Engineering Simulation and Scientific Software, 2018). Rocky specialise in DEM simulations within the mining and material handling industry and is renowned for the realistic material shape library that is available within the software.

Other software packages that specialise in DEM simulation are Newton (Advanced Conveyor Technologies, 2018) and PFC-3D (ITASCA Consulting group, Inc., 2018).

Simcenter STAR-CCM+ is a CFD software package that has been developed by CD-adapco and is owned by Siemens PLM. What makes this package different is that it is a CFD specializing company that has incorporated DEM in a CFD environment (Siemens PLM,

2018). Thus the capability of coupling DEM particles in a multi-phase environment is readily available.

2.2. MATERIAL PROPERTY ANALYSES AND DEM PARTICLE PARAMETERS

Throughout literature there are a number of papers that have investigated the different material properties and which of these properties have the greatest influence on the DEM model's accuracy. Most of these papers evaluated the input parameter requirements by the specific DEM contact model. This was followed by an evaluation to determine which of those parameters produced a model capable of replicating specific material bulk behaviour.

Coetzee has written an extensive paper that reviews the different DEM parameters that have been investigated, and what tests were used to validate the actual material behaviour with regards to the model results. The aim of that paper was to critically evaluate different validation (model calibration) techniques and if there was a definite model parameter or calibration technique that can be used to produce the most accurate result. The model parameters that were evaluated were: particle shape, size, density, stiffness, rolling resistance, inter particle and boundary friction coefficients, coefficient of restitution, cohesive properties and adhesive properties (Coetzee, 2017).

Thompson investigated the calibration of different DEM model parameters for dry and wet granular materials, in order to determine if the model is capable of replicating material bulk behaviour. The parameters that Thompson identified for both the particles and boundaries were as follow:

- Size distribution.
- Shape distribution.
- Density.
- Stiffness.
- Rolling resistance.
- Static and dynamic friction coefficients.
- Adhesive distance.
- Stiffness friction.
- Coefficient of restitution.

Within this study Thompson also evaluated if a specific sample size of material could be used for model calibration purposes (Thompson, 2008).

Marigo and Stitt used a rotating drum as validation mechanism for the DEM model developed for the evaluation of the influence that particle shape detail has on material bulk behaviour. Additional critical calibration parameters that were identified were: particle size, density, shear modulus, Poisson's ratio, inter particle and boundary static and rolling friction coefficients and the inter particle and boundary coefficient of restitution (Marigo & Stitt, 2015).

Grima and Wypych investigated the sensitivity of the variation of various DEM parameters on the impact reaction force of polyethylene pallets on a plate. Within this paper it was attempted to determine if certain scaling rules could be applied in order to minimise computational time by reducing the number of particles included into the DEM simulation (Grima & Wypych, 2011).

Horn conducted a study on the calibration of relatively large ore aggregate particles by using a large scale shear box. The main parameters that were identified within this report were: particle shape, size, density, bulk density, material porosity, Young's modulus and the internal friction angle. Small scale test were used for the validation of the calibrated DEM model, and it was concluded that the model replicated the material bulk behaviour within an acceptable margin (Horn, 2012).

2.2.1. PARTICLE SHAPE

The most common particle shape that is used when setting up a DEM analyses is a spherical particle shape. The reason for this is that a spherical particle shape provides efficient contact detection criteria which allow the solving time of the simulation to be reduced (Coetzee, 2016).

Coetzee investigated the difference in DEM parameters when spherical clumps comprising of 2, 4 and 8 spheres were used. The study used different validation tests in order to determine if each of the clumps (with their unique set of parameters) we able to replicate the material bulk behaviour. It was concluded that a manually generated spherical clump particle replicated the material behaviour more accurately than a single sphere particle. It was furthermore found that the detail in the portrayal of the particle increased when using more clumps. It was noted that the increase in detail did not provide a significant difference in model accuracy between 4 and 8 clumps (Coetzee, 2016).

Pasha et al investigated the difference in modelled bulk material behaviour of corn grains in a rotary batch seed coater if spherical particles with an additional friction factor are used vs.

optimised particle clumps without a friction factor. Pasha et al obtained the detailed particles with X-ray tomography and software that was capable of clumping spheres together in order to replicate the scanned image. This software allowed for a different number of spheres to be selected from which Pasha et al decided to develop DEM models for 5, 10, 15 and 20 spheres. The results pointed out that a larger number of spherical clumps did not perform significantly better than lower number spherical clumps. It was stated that particles comprising of 5 spheres in a clump will be able to produce adequate results for material bulk behaviour (Pasha, et al., 2016).

Höhner et al conducted an experiment to evaluate the material bulk behaviour as it flows out of a hopper when this material is modelled with the use of different particle shapes. For this experiment acrylic glass shapes were made and allowed to drain from the hopper. DEM models were developed for each of the shapes used and it was determined that the models could replicate the hopper draining behaviour for each of the shapes (Höhner, et al., 2015).

Markauskas and Kačianauskas developed a rice grain particle simulation with the use of a hopper draining test and simulated particles shaped like axisymmetric clumps. The aim of this paper was to determine if the material bulk behaviour could be replicated by only focussing on the shape of the particle. It was found that even though the shape closely resembled actual rice grains the model still required some calibration with regards to other parameters in order to accurately replicate the material bulk behaviour (Markauskas & Kačianauskas, 2011).

2.2.2. PARTICLE SIZE

Throughout literature the size of the particles in the DEM simulation is considered as an important parameter that has to be included in the calibration of the model. For most of the cases the size of the particle has to be scaled up in order to reduce the number of particles in the simulation so that the computational time can be reduced. Roessler and Katterfeld stated that the total degrees of freedom are affected when the particles are scaled and that the scaled particles should be calibrated with regards to the material bulk behaviour (Roessler & Katterfeld, 2016). When conducting laboratory tests with a small number of particles it is possible to size the particles closer to the actual value, but when industrial size simulations (typically hopper or silo discharge) is simulated the user is forced to reduce the number of particles in the simulation.

Shigeto et al investigated the influence of scaling up fine power particles for a screw conveyor application. In this report spherical particles were used and it was found that

particles could be scaled up to 4 times while still producing accurate material bulk behaviour (Shigeto, et al., 2011).

Grima and Wypych determined that care should be taken when scaling rules are applied to particles when impact force is evaluated. They concluded that the size of the particles had an effect on the resolution of the result and therefore if the particle scaling was too great a variation in the impact area would be obtained (Grima & Wypych, 2011).

Xie et al used a similar conveyor design set up as Grima and Wypych in order to investigate the wear process of a conveyor transfer chute. Within this study spherical particles were used and scaled to a size from 4mm, 8mm and 12mm up to 16mm. It was determined that the 4mm particles represented the actual material trajectory accurately, but when the particle size increased beyond 8mm the material stream started to separate. The main difference came with the impact force that was measured between the particle sizes. It was found that when the particle size was increased to 8mm the impact force doubled which resulted in increased wear predictions. A similar conclusion was reached by Xie et al and Grima and Wich which stated that care should be taken when particles are scaled for computational time purposes. It was further concluded that the particle size should not be scaled by more than a factor of 2 when conveyor transfer chutes are modelled (Xie, et al., 2016).

Ucgul et al investigated the draft force of a tillage tool when it is passed through a washed and air dried cohesionless sand. The actual particle size was approximately 600μm which was then scaled up to a model particle size of 9,5mm and 10.5mm. These particles were then individually calibrated by using a penetration test along with the angle of repose analyses. It was determined that the scaling of the particles could replicate the force required by the penetration test but an increase in the rolling resistance and the coefficient of friction would be required. This increase was determined to follow a quadratic trend (Ucgul, et al., 2014).

2.2.3. PARTICLE STIFFNESS

The particle stiffness parameter or Young's modulus is a parameter which is dependent on the type of contact model used within the DEM model. This is also one of the model parameters that can be used to decrease the computational time. Coetzee stated that the size of the stable time step required for the time integration is inversely proportional to the square root of the contact stiffness (Coetzee, 2017). Therefore if the particle stiffness is reduced it means that the time step between iterations can be reduced which results in a reduction in computational time.

Lommen et al investigated what effect the reduction in particle stiffness had on the simulated material bulk behaviour. Three different test scenarios were simulated and within each scenario the particle stiffness was varied. Lommen et al determined that a variation in particle stiffness had an effect on simulated particle properties such as bulk stiffness and bulk restitution. It was also determined that it is possible to reduce the particle stiffness but it has to be limited so that the particle radius does not exceed 0.3% of the particle contact normal overlap or the calculated shear modulus has to be kept above 10^7Pa. Due to the possibility of undesirable results obtained when the particle stiffness is lowered it was advised to rather conduct a particle scaling analyses than just lowering particle stiffness (Lommen, et al., 2014).

Research done by Härtl & Ooi determined that when the shear modulus of glass beads are reduced with a factor of a 100 and then later to a 1000 there were no significant effect on the results between the shear force measured in the simulation model and the actual test (Härtl & Ooi, 2011).

Paulick et al determined that a linear relation can be found between the contact stiffness and the bulk stiffness. It was also stated that care should be taken when selecting particle stiffness when the system is denser. It was concluded that the particle stiffness should be selected such that the particle contact overlap is not greater that 1% of the particle radius (Paulick, et al., 2015).

2.2.4. PARTICLE DENSITY

In the industry the density of the material is generally defined as the bulk density or the heap density. The bulk density is defined as the mass of a sample of material per unit volume which the sample of material occupies. Horn determined the specific particle density of a medium size ore aggregate (40mm) by measuring the volume of water being displaced when a known mass of material is submerged in the container. The bulk density was then determined by filling the large scale shear box tester volume with the material, measuring the mass of the container and dividing it by the known volume of the shear box tester container. Additional properties like the void ratio and porosity were then calculated with the use of the particle density and the bulk density. These values were then used for the calibration of the DEM particle density (Horn, 2012).

2.2.5. ROLLING RESISTANCE

Coetzee stated the property of rolling resistance can be defined differently in different DEM software packages and it has to be ensured by the user to know how the code uses this property in order to calibrate it correctly (Coetzee, 2017).

Ai et al stated that the rolling resistance model is an attempt used to incorporate a rolling torque and the rolling friction generated by a particle. The paper reviewed commonly used rolling resistance models and recommended a general model (Ai, et al., 2011).

LI et al stated that both the particle-particle static friction coefficient as well as the rolling resistance had an effect on the angle of repose of the material. Both of these properties caused and increase in the angle of repose when increased (LI, et al., 2013).

2.2.6. PARTICLE-PARTICLE FRICTION COEFFICIENT

The particle-particle friction coefficient is a parameter that is used within the DEM analyses which dictates the particle's resistance against sliding when in contact with another. This is a parameter which is not easily measurable and is also reliant on other parameters. For instance if a sample of raw material is illustrated via spheres in a DEM analyses these particles will not experience the same interlocking characteristics due to the difference in shape. This means that if the spherical particles are dropped onto a flat surface the particles will just roll off each other and no heap will be formed. The particle-particle friction coefficient is therefore used to assist the simulation with a restriction in the movement so that the spherical particles replicate the actual material bulk behaviour.

Asaf et al. used the particle-particle friction coefficient and the particle stiffness as the two most important parameters for the calibration process of the simulation of a tillage tool penetration in soil. An onsite penetration test was done with a flat plate, a 30º wedge and a 90º wedge and the load displacement curves were plotted for all three of the scenarios. A DEM model was then set up to replicate the three tool scenarios and the particle-particle friction was then adjusted until the load displacement curves could be replicated. Asaf et al determined that this method provided accurate results (Asaf, et al., 2007).

As mentioned previously from Ucgul et al, scaling effects also had an influence on the particle friction coefficient. It was reported that the simulation model was capable of replicating the material bulk behaviour for the different sized particles, but the particle-

particle friction coefficient had to be individually calibrated for the different particle sizes (Ucgul, et al., 2014).

Coetzee and Els used the direct shear test for the calibration of the particle-particle friction coefficient and the particle stiffness. In the study it was found that the particle-particle friction coefficient as well as the particle stiffness had an effect on the model results when compared to the direct shear test results (Coetzee & Els, 2009).

2.2.7. PARTICLE-BOUNDARY FRICTION COEFFICIENT

The particle-boundary friction coefficient is a parameter that is used to describe a particle's resistance against motion when it is in contact with a boundary surface (normally the container it is placed in or a surface the particle interacts with like a chute or a conveyor).

Research performed by Horn determined the particle-boundary friction coefficient by placing a particle on the surface of the boundary to be assessed. The boundary surface was then lifted until the particle started to slide. The angle at which the particle slid was then recorded and a friction coefficient was calculated with the use of this angle. This test was repeated and an average value was used as the parameter for the DEM simulation (Horn, 2012).

Thompson used a similar method to determine the particle boundary friction coefficient. A tilt table was used along with the confined compression test, where a normal load was added while conducting the confined compression test. The table was tilted until the load cell started to slide, from where the angle after sliding was recorded (Thompson, 2008).

2.2.8. COEFFICIENT OF RESTITUTION

The coefficient of restitution is a parameter used in DEM to illustrate the damping mechanism which occurs when a particle makes contact with a boundary surface or another particle. Thus if a particle is dropped from a specific height the height at which it will bounce back to will be influenced by the coefficient of restitution.

Thompson stated that there is no viable test available to test the coefficient of restitution between particles and it is recommended that a default value of 0.3 should be used when simulating hard rock ores (Thompson, 2008).

Just et al investigated the DEM parameters required to model a tablet coating process. Here the coefficient of restitution was tested with a drop test which was recorded with high speed

cameras. It was however found that the coefficient of restitution did not have an effect on the dynamic angle of repose within the test (Just, et al., 2013).

Coetzee stated that some researches followed the drop test to determine the coefficient of restitution but when particles with varying shapes are used a reverse calibration technique was followed. Thus a simulation model was set up and the coefficient of restitution was changed until it matched the actual drop test result (Coetzee, 2017).

2.2.9. COHESIVE AND ADHESIVE PROPERTIES

Thompson stated that different DEM codes use different formulations in order to simulate the effects of adhesive and cohesive forces (Thompson, 2008). Thompson used ROCKY DEM for the simulations and described that in ROCKY there are two models defining cohesive and adhesive forces. The first is the constant force model which applies a constant force during the impact of particles and the force is proportional to the mass of the particles. The second is the linear force model which applies a force that is proportional to the overlap distance generated when the particles make contact with other particles or boundaries. Thompson concluded that if either of these models are activated the consolidation pressure would be greater and would result in greater angle of repose results. Therefore these models are generally implemented when moisture content is taken into consideration during the simulation.

2.3. METHODS USED FOR CALIBRATION OF DEM PARAMETERS

According to Coetzee there are mainly two calibration approaches followed in literature when it comes to obtaining DEM parameters (Coetzee, 2017). Coetzee describes the first as the bulk calibration approach which is defined as the method of conducting in situ or laboratory experiments. With this method the experiment is used to measure specific material bulk properties. A simulation model is then developed to replicate the experiment after which DEM parameters are iteratively changed until the simulation results replicate the experimental results. Coetzee states that one of the risks associated with this approach is that more than one parameter can influence the simulation outcome, which means that different combinations of DEM parameters may provide similar material bulk behaviour. It is also advised that the calibration experiment should be different from the final analyses scenario, because if the calibration experiment is the same as the application which is designed for the DEM parameters will be unique only for that application. This means that there will be a possibility that if design changes are required for the specific scenario, the simulation will not be able to provide accurate material bulk behaviour.

The second approach is known as the direct measuring approach. With this approach the input parameters are determined by directly measuring properties on a particle or contact level. This approach sounds more promising but Coetzee states further that if all of the parameters are measured accurately it still does not guarantee that the simulation model will replicate the material bulk behaviour accurately. This is due to the fact that the simulation still has to include for the exact particle shape, size and correct contact model. For most industrial cases it is not possible to model the exact size of the particles because this will result in too many particles and therefore extensive computational time. It is also not always possible to model the exact shape and therefore the particle behaviour will not always replicate the exact material bulk behaviour. There is an advantage to this approach though, which is that the DEM parameters are not design specific and could therefore be used to simulate different applications.

2.3.1. BULK CALIBRATION APPROACH EXPERIMENTS

Coetzee stated than in most cases researchers use a combination of the bulk calibration approach and the direct measuring approach (Coetzee, 2017). This means that certain parameters like particle shape, size, density and particle-boundary friction coefficient are measured directly and that other properties like particle stiffness and particle-particle friction coefficient are determined via experimental tests. Coetzee (Coetzee, 2017) also summarised typical bulk calibration approaches that have been used throughout literature as the following:

- Penetration test

Test that has been used for the calibration of particle contact stiffness and particle-particle sliding and rolling friction coefficients.

- Direct/ring shear test for bulk friction angle

Researchers have used this test to determine particle contact stiffness, particle-particle sliding and rolling friction coefficient and damping/restitution coefficient

- Direct/ring shear test for angle of dilatancy

This test has been used to determine the particle-particle sliding friction coefficient.

- Uniaxial compression test

Researchers have used this test to determine the bulk stiffness parameter.

- Static angle of repose with a slump tester and pile formation analyses

This is one of the most used tests and it is used for the calibration of particle density, contact stiffness, particle-particle and particle-boundary friction coefficient and particle-particle and particle-boundary rolling coefficient.

- Dynamic angle of repose with a rotating drum or vibrating surface

Researchers have used this test to calibrate parameters like particle-particle sliding friction coefficient, particle-particle and particle-boundary rolling friction coefficient and damping/restitution coefficient

- Hopper or silo discharge rate and time evaluation

This test has been used for the calibration of particle contact stiffness, particle-particle and particle-boundary sliding friction coefficient and particle-particle and particle-boundary rolling friction coefficient.

- Hopper or silo flow profile analyses

Researchers use this test to calibrate the particle contact stiffness and particle-particle and particle-boundary sliding friction coefficient.

- Box fill test

This is a test that has been used for the calibration of the particle density and the bulk density.

- Triaxial/Biaxial test for load displacement and volumetric strain

Researchers have used this test for the calibration of a variety of parameters such as particle contact stiffness, contact ratio, particle-particle sliding friction coefficient, particle-particle rolling friction coefficient, particle damping/restitution coefficient and contact cohesion.

- Soil-tool interaction for draught force

Researchers have used this test for particle contact stiffness, particle-particle sliding friction coefficient, particle damping/restitution coefficient, bond stiffness and bond strength.

- In-situ ring shear and vane tester

This test has been used to calibrate the particle contact stiffness, particle-particle sliding friction coefficient and the bond strength.

- Artificial neural networks with angle of repose and shear test

This was one calibration method developed to calibrate particle density, particle-particle sliding friction coefficient, particle-particle rolling friction coefficient and particle damping/restitution coefficient.

2.3.2. DIRECT MEASURING APPROACH EXPERIMENTS

The direct measuring approach attempts to measure material properties via an experimental procedure and then these properties are used as the DEM simulation parameters. Typical calibration tests that are used in the direct measuring approached are listed by Coetzee (Coetzee, 2017) as:

- Inclined plane test

Researchers have used this test to calibrate the particle-boundary sliding friction coefficient, particle-particle and particle-boundary rolling friction coefficient.

- Direct shear test

This test has been used to calibrate the particle-boundary friction coefficient.

- Particle impact test

This test has been used to calibrate the particle contact stiffness.

- Tribometer

Researches have used this test to calibrate particle-particle and particle-boundary sliding friction coefficients.

- Rheometer and drop test

This test has mainly be used to calibrate the damping/restitution coefficient between particle-particle and particle-boundary

- Pycnometer

Researchers have used this test to determine particle densities.

- Compression test

This test has been used to determine particle contact stiffness and the stiffness ratio.

- Double pendulum test

The double pendulum test has been used in an attempt to determine the particle-particle damping/restitution coefficient.

2.4. INDUSTRIAL APPLICATIONS OF DEM

Within this section the aim was to focus on the applications of DEM in the material handling industry. Literature was gathered to determine how researchers have set up DEM simulation parameters with regards to conveyor systems, transfer chutes, bucket conveyors and hopper and belt interaction points.

Minkin et al investigated the application of a steep inclined pipe conveyor for an open cast mine. This research was done in order to determine the deformation areas on a pipe conveyor with the use of a FEM analyses. A DEM analyses was then used in order to determine what the maximum angle of inclination could be at which the conveyor can operate without material sliding down on the conveyor. The DEM simulation parameters were calibrated with the use of a Jenike shear cell and also evaluating the angle of repose. These tests were a combination of the bulk and direct measuring approach and resulted in a simulation that could replicate the material bulk behaviour. From this paper it was stated that a pipe conveyor test rig is being designed that would enable further validation of the theoretical DEM values (Minkin, et al., 2016).

Sinnot et al simulated the discharge of a vertical bucket conveyor with a coupled particle-gas numerical model. Finite differences were used to solve the gas flow, an immersed boundary method to encapsulate the bucket movement and a discrete element model to solve the particle movement. The aim of this research was to investigate what effect the gas flow had on the discharge of the particles in a bucket conveyor. It was found that the gas flow did have an effect on the trajectory of the particles and reduced the trajectory efficiency (Sinnot, et al., 2017).

Katterfeld et al used a DEM simulation to investigate the wear and flow behaviour of a high feed rate conveyor transfer station. The aim of the research was to determine if it was possible to predict the wear of transfer chute liners and the flow characteristics (possible blockage or spillage) in the transfer between the conveyors. Qualitative measurements were done with regards to the material trajectory and quantitative measurements were done with regards to the force that the material exerts when it comes in contact with the transfer chute liners. It was determined that the DEM simulation provided a good correspondence to the conveyor measured results. It was concluded that the DEM simulation was capable to predict wear and to improve transfer chute flow (Katterfeld, et al., n.d.).

Xie et al investigated the wear on conveyors and transfer chutes due to particle size, feed rate, belt speed, chute structure design and impact force generated by the particles. From this research it was determined that the wear rate on the transfer chute as well as the receiving belt was more severe when the feed rate increased and the particle size decreased. It was also determined that when the receiving belt velocity was decreased a thicker material layer started forming on the receiving belt which resulted in less wear (Xie, et al., 2016)

2.5. CONCLUSION

This chapter highlighted some key points that researchers focussed on in the development of the DEM simulation method. It followed from the study that two main categories of software are used, which is open source and commercial packages. Some advantages as well as disadvantages between the options were discussed and some key features of each were highlighted.

The different parameters within the contact models selected were listed and a perspective was obtained on how many parameters are required for the generation of a DEM simulation. Each of these parameters was discussed in more details focussing on the impact that these parameters had on different material bulk behaviour tests. Clarity was obtained on which of these parameters would be applicable to the study at hand.

From literature it followed that two different calibration techniques are used for the development of a DEM simulation. These techniques were discussed along with the tests that accompany them. Research showed that a combination of these techniques is typically used for the calibration and the validation of the DEM simulations.

Further research was performed on the use of the DEM simulation technique in industry. It was found that the majority of research was based on flat conveyors, chute design, agricultural equipment, hopper filling and material mixing. No research articles were found for the DEM simulation of a steep incline sidewall conveyor loading process.

Now that the different aspects of DEM based literature has been discussed, the theory of the DEM formulation will be assessed.

3. THEORY BEHIND THE DISCRETE ELEMENT MODEL

The previous chapter provided the necessary insight into relevant research in the field of DEM simulations. Key parameters required by the various contact models were identified and the impact that these parameters have on the models were discussed. This chapter will now focus on the formulation of the discrete element model and how this model is included into the conservation equations. A discussion on the computational time requirement will also be included into this chapter.

The discrete element model is a granular particle simulation tool designed to simulate flows that contain a high density of particles where the inter-particle interaction is of importance within the computational boundary. The DEM formulation was established by Cundall and Strack (Cundall & Strack, 1979), and is an extension of the Lagrangian framework that includes the inter-particle interaction within the particle conservation of momentum equation. Therefore to better understand the DEM formulation it is first required to understand the Lagrangian particle equation of motion formulation.

3.1. LAGRANGIAN PARTICLE CONSERVATION OF MOMENTUM

Within Simcenter STAR-CCM+ the particle conservation of momentum is formulated in terms of the Lagrangian framework. It states that the change in momentum is equal to the sum of the surface and body forces that act on the particle (Siemens Product Lifecycle Management Software Inc., 2018). Therefore the conservation of linear momentum of the particle of mass (m_p) is given by Equation (1).

$$m_p \frac{dv_p}{dt} = F_s + F_b \quad (1)$$

Where

v_p : Instantaneous particle velocity

F_s : Resultant of the surface forces acting on the particle

F_b : Resultant of the body forces acting on the particle

The surface and body forces can be calculated with:

$$F_s = F_d + F_p + F_{vm} \quad (2)$$

$$F_b = F_g + F_{MRF} + F_u + F_c + F_{Co} \quad (3)$$

Where

F_d : Drag force

F_p : Pressure gradient force

F_{vm} : Virtual mass force

F_g : Gravity force

F_{MRF} : Force due to moving reference frame

F_u : User defined body force

F_c : Particle contact force

F_{Co} : Coulomb force

The conservation of angular momentum is also accounted for within the DEM model and it is described by Equation (4).

$$I_p \frac{d\omega_p}{dt} = M_b + M_c \quad (4)$$

Where

I_p : Particle moment of inertia

ω_p : Particle angular velocity

M_b : Drag torque

M_c : Total moment from contact forces

When DEM is used within Simcenter STAR-CCM+ the contact forces generated are of importance in both the conservation of linear and angular momentum. These forces are defined by Equations (5) and (6).

$$F_c = \sum_{contacts} F_{cm} \quad (5)$$

$$M_c = \sum_{contacts} (r_c \times F_{cm} + M_{cm}) \quad (6)$$

Where

F_{cm} : Contact force model chosen within Simcenter STAR-CCM+

r_c : Position vector from particle centre of gravity to the contact point

M_{cm} : Moment acting on particle form rolling resistance

Following the conservation of momentum equations within the Lagrangian framework, the DEM formulation can now be defined.

3.2. DISCRETE ELEMENT MODEL FORMULATION

A plane can be drawn at the point of contact between any two spherical particles, as illustrated in Figure 3.

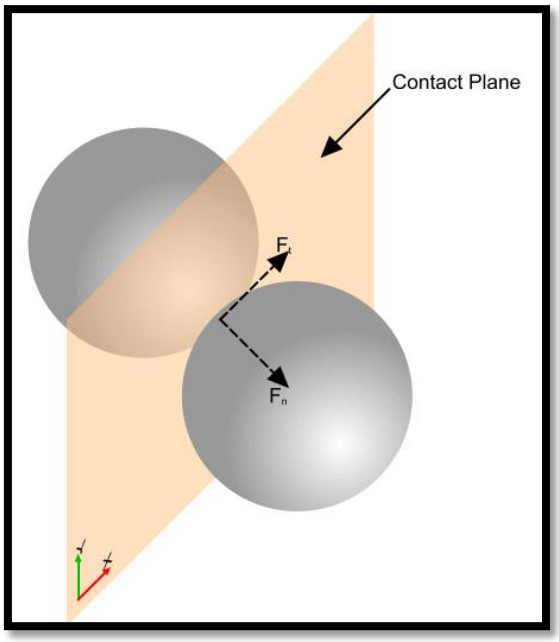

Figure 3 Illustration of the contact plane between two spherical particles (Siemens Product Lifecycle Management Software Inc., 2018)

Within Simcenter STAR-CCM+ the contact force is formulated with a spring-dashpot model illustrated by Figure 4. The spring represents a repulsive force pushing the particles apart and the dashpot allows for damping, which represents a collision that is not perfectly elastic.

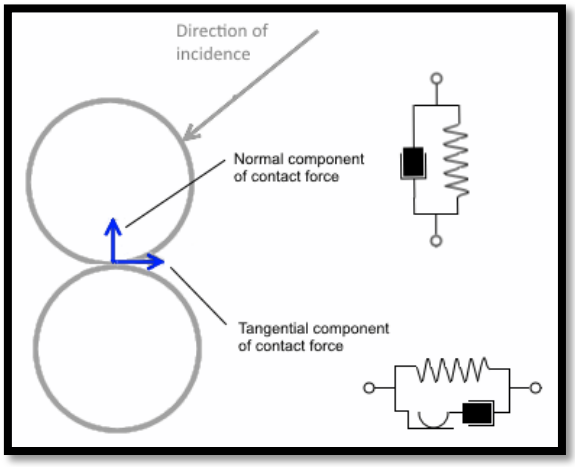

Figure 4 Spring-dashpot contact formulation within DEM (Siemens Product Lifecycle Management Software Inc., 2018)

Figures 3 and 4 illustrate that a force is present in both the normal and tangential direction relative to the contact plane. The normal force is modelled by a parallel connection between a linear spring and a dashpot, and the tangential force is modelled by a parallel connection between a linear spring and a series connection between a dashpot with a slider. For both the normal and the tangential force the spring accounts for the elastic portion of the collision and the dashpot accounts for the energy loss during the collision.

Within Simcenter STAR-CCM+ there are three variations of contact model that can be selected; Hertz Mindlin Contact Model (with option of including particle slip), Linear Spring Contact Model and the Walter Braun Contact model. For the purpose of this paper only the Hertz Mindlin No-slip Contact model will be discussed.

The contact force required by the Lagrangian conservation of momentum equation (F_c) is formulated by the Hertz Mindlin No-Slip Contact Model as follow:

$$F_c = F_n + F_t \tag{7}$$

Where

F_n : Force in the normal direction of the contact plane

F_t : Force in the transverse direction of the contact plane

The normal force (F_n) is divided into the elastic and damping components by Equations (8), (9), (10) and (11).

$$F_n = -K_n d_n - N_n v_n \tag{8}$$

$$K_n = \frac{4}{3} E_{eq} \sqrt{d_n R_{eq}} \tag{9}$$

$$N_n = \sqrt{(5 K_n M_{eq})}\, N_{n\,damp} \tag{10}$$

$$N_{n\,damp} = \frac{-\ln(C_{n\,rest})}{\sqrt{\pi^2 + \ln(C_{n\,rest})^2}} \tag{11}$$

The tangential force (F_t) is divided into the elastic and damping components by Equations (12), (13), (14), (15) and (16)

$$F_t = -K_t d_t - N_t v_t \quad if \quad |K_t d_t| < |K_n d_n| C_{fs} \tag{12}$$

$$F_t = \frac{|K_n d_n| C_{fs} d_t}{|d_t|} \quad if \quad |K_t d_t| > |K_n d_n| C_{fs} \tag{13}$$

$$K_t = 8 G_{eq} \sqrt{d_t R_{eq}} \tag{14}$$

$$N_t = \sqrt{(5 K_t M_{eq})}\, N_{t\ damp} \tag{15}$$

$$N_{t\ damp} = \frac{-\ln(C_{t\ rest})}{\sqrt{\pi^2 + \ln(C_{t\ rest})^2}} \tag{16}$$

And the following equivalent Equations are used for both the normal and tangential forces.

$$R_{eq} = \frac{1}{\frac{1}{R_A} + \frac{1}{R_B}} \tag{17}$$

$$M_{eq} = \frac{1}{\frac{1}{M_A} + \frac{1}{M_B}} \tag{18}$$

$$E_{eq} = \frac{1}{\frac{1 - v_A{}^2}{E_A} + \frac{1 - v_B{}^2}{E_B}} \tag{19}$$

$$G_{eq} = \frac{1}{\frac{2(2 - v_A)(1 + v_B)}{E_A} + \frac{2(2 - v_B)(1 + v_B)}{E_B}} \tag{20}$$

Where

K_n and K_t : Normal and tangential spring stiffness

d_n and d_t : Normal and tangential overlap at the contact point

N_n and N_t : Normal and tangential damping

v_n and v_t : Normal and tangential velocity components of relative sphere surface at contact

$N_{n\ damp}$ and $N_{t\ damp}$: Normal and tangential damping coefficient

C_{fs} : Static friction coefficient

$C_{n\ rest}$ and $C_{t\ rest}$: Normal and tangential coefficient of restitution

R_{eq} : Equivalent radius

M_{eq} : Equivalent particle mass

E_{eq} : Equivalent Young's modulus

G_{eq} : Equivalent shear modulus
R_A and R_B : Radii of spheres A and B assessed in contact
M_A and M_B : Mass of spheres A and B assessed in contact
E_A and E_B : Young's modulus of spheres A and B assessed in contact
v_A and v_B : Poisson's ratio of spheres A and B assessed in contact

It should be noted that these equations are formulated for the collisions between particles and the boundary. When a particle comes in contact with a boundary the values of R_B and M_B are taken as infinite which results in $R_{eq} = R_A$ and $M_{eq} = M_A$, from Equations (17) and (18).

3.3. DISCRETE ELEMENT MODEL TIME SCALE

Within the DEM a time-step is used for which all of the above mentioned conservation equations are calculated in order to determine the position, orientation and velocity of each of the particles. Simcenter STAR-CCM+ uses 3 rules that limit the maximum time-step that can be used within the simulation model.

Firstly, the time-step is limited by the time it takes the Rayleigh wave to propagate across the surface of the sphere to the opposite pole. The material properties applied in the simulation dictates the velocity of the Rayleigh wave. Therefore the first limit can be expressed as:

$$\tau_1 = \pi \frac{R_{min}}{V_{Rayleigh}} \tag{21}$$

The second limiting criterion is with regards to the contact duration of two perfectly elastic spheres and is expressed by Timoshenko's equation (Timoshenko, 1951).

$$\tau_2 = 2.94 \left(\frac{5\sqrt{2}\pi\rho}{4} \frac{1-v^2}{E}\right)^{\frac{2}{5}} \frac{R}{\sqrt[5]{v_{impact}}} \tag{22}$$

The final time-step limiting criterion is based on the theory that a time-step must be small enough in order not to miss possible contacts with particles or boundaries. This criterion is formulated by:

$$\tau_3 = \left(\frac{R}{v_{particle}}\right) \tag{23}$$

Thus in conclusion the maximum time-step allowed for an iteration is governed by the minimum value between τ_1, τ_2 and τ_3.

3.4. CONCLUSION

In this chapter it was discussed how the discrete element model fits into the conservation equations. The formulation of the Hertz Mindlin contact model was discussed for both particle-particle contact as well as particle-boundary contact. The time step limitation factors were also discussed and key properties were highlighted that may affect the model's computational time. With the fundamental theory behind the Hertz Mindlin contact model discussed, the next chapter will address the calibration of each of the model parameters.

4. CALIBRATION OF DEM PARAMETERS

With the DEM formulation and theory analyses completed in the previous chapter, the impact of each material parameter on the contact model is evident. With this formulation completed the current chapter focusses on the parameter calibration process.

For the simulation of the steep incline sidewall conveyor it was decided to follow a combination of the direct measuring and bulk calibration approaches. This decision was made in order to improve the accuracy of the calibration process (as stated in section 2.3). The software package that was used was Simcenter STAR-CCM+ and the DEM contact model selected was the Hertz Mindlin No-slip contact model. The reason for using the Hertz Mindlin No-slip contact model is due to the fact that there is no evidence that the other models are better at predicting bulk behaviour after calibration has been completed. Coetzee stated that research done on particles impacting a plate from a conveyor yielded no significant difference on macro/bulk properties when using the linear spring or the Hertz Mindlin contact models (Coetzee, 2017).

When using the Hertz Mindlin contact model Simcenter STAR-CCM+ requires the following particle and boundary input parameters:

1. Shape.
2. Size.
3. Density.
4. Poisson's ratio.
5. Young's modulus.
6. Static friction coefficient between particle and boundary.
7. Normal and tangential coefficient of restitution between particle and boundary.
8. Coefficient of rolling resistance between particle and boundary.
9. Static friction coefficient between particles.
10. Normal and tangential coefficient of restitution between particles.
11. Coefficient of rolling resistance between particles.

Based on the work done by Coetzee (Coetzee, 2017) it was decided to use the direct measuring calibration approach for parameters 1, 2, 3, 6 and 7. Parameters 3, 4, 5, 8, 10 and 11 would be obtained from literature and Simcenter STAR-CCM+ default values. This decision was made due to the testing facilities available. Parameters 7 and 9 would be calibrated using the bulk calibration approach which would be conducted on a test bench setup.

4.1. BULK CALIBRATION METHODOLOGY AND TEST BENCH DESIGN

The design of the test setup as well as the method used for the bulk calibration was based on the work done by Quist and Evertsson. The aim of the work done by Quist and Evertsson was to develop a calibration framework that could assist in the validation of DEM simulations and govern the quality and the accuracy of the simulation results (Quist & Evertsson, 2015). Quist and Evertsson proposed the V-model for DEM calibration and validation. The V-model comprised of 3 levels, each with a link between the simulation domain and the experimental domain.

Quist and Evertsson stated that the calibration process starts at the first level, which is the laboratory single property test. This level correlates with the direct measuring approach stated by Coetzee (Coetzee, 2017). These properties are typically associated with the particle shape, size, density, Young's modulus, particle-boundary friction coefficient and coefficient of restitution. These parameters are then included into the simulation domain and a first level validation is done.

The second level is defined by multiple flow regime experiments. This level aims to determine if the bulk behaviour produced by the individually calibrated parameters correspond within a degree of accuracy to the experimental tests. Once again this level corresponds with the bulk calibration procedure defined by Coetzee (Coetzee, 2017). Within this level it is typically found that not all of the parameters defined by the individual tests produce the required bulk behaviour. Therefore additional parameter adjustments can be made until the simulation model correlates with the experimental results. Quist and Evertsson proposed that when the point is reached that all of the model parameters produce the required bulk behaviour, the experimental setup should be altered in order to test if these parameters still replicate the experimental results.

The third level is defined by the industrial scale experiment. For this level the model parameters are validated further with actual material handling processes such as conveyor systems, transfer chutes or hopper filling or discharging. At this point, according to (Coetzee, 2017), it can be determined if the model parameters are within an acceptable region of accuracy, after which the parameters can be deemed calibrated.

4.1.1. TEST BENCH DESIGN

Based on level 2 of the V-model Quist and Evertsson developed a test bench that was capable of calibrating multiple parameters of material bulk flow behaviour. This test bench also allowed for the capability of adjusting specific parameters such as hopper gate opening

and deflector plate angle which would affect the result of the material bulk flow behaviour. This was done in order to validate if the calibrated model parameters were capable of replicating multiple design scenarios. Therefore if the simulation results replicated the experimental results the model parameters would be deemed calibrated.

The test bench built for the calibration of model parameters for the simulation of a steep incline sidewall conveyor was based on the design developed by Quist and Evertsson and is illustrated by Figure 5.

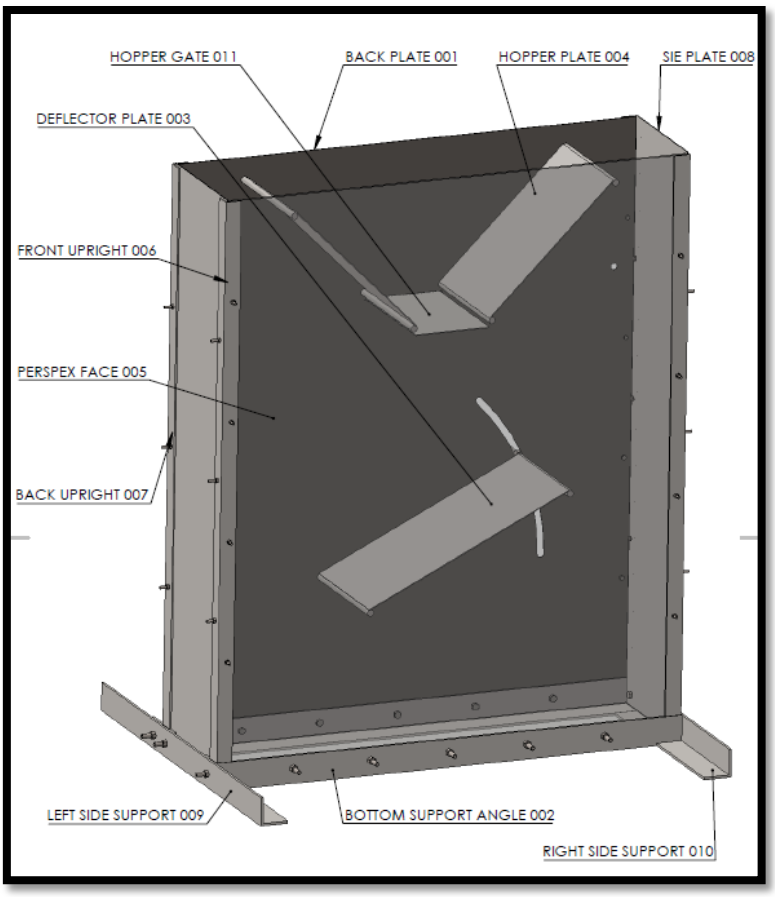

Figure 5 Model parameter calibration test bench

The main features of the test bench were the top containment hopper (with a trapdoor mechanism), the adjustable deflector plate and the bottom and side containment walls. The containment hopper was built so that the left and right hopper plate angles could be adjusted. This adjustment could allow for variable hopper draining rates which would allow for the validation of the simulation model parameters. The adjustable deflector plate was built so that it could rotate around the left side fastening point. This would allow for multiple angles of inclination that would generate different material bulk behaviour, which could be used for the validation of model parameters. The containment hopper side plates, the deflector plate, together with the bottom and side containment walls were designed so that

different types of material could be secured to it. This would allow for the calibration of multiple boundary friction parameters within the simulation model.

4.1.2. CALIBRATION METHODOLOGY

The guidelines for a calibration methodology were provided by the work done by Quist and Evertsson's V-model approach. This methodology was assessed and made applicable to the steep incline sidewall conveyor simulation and is illustrated by Figure 6.

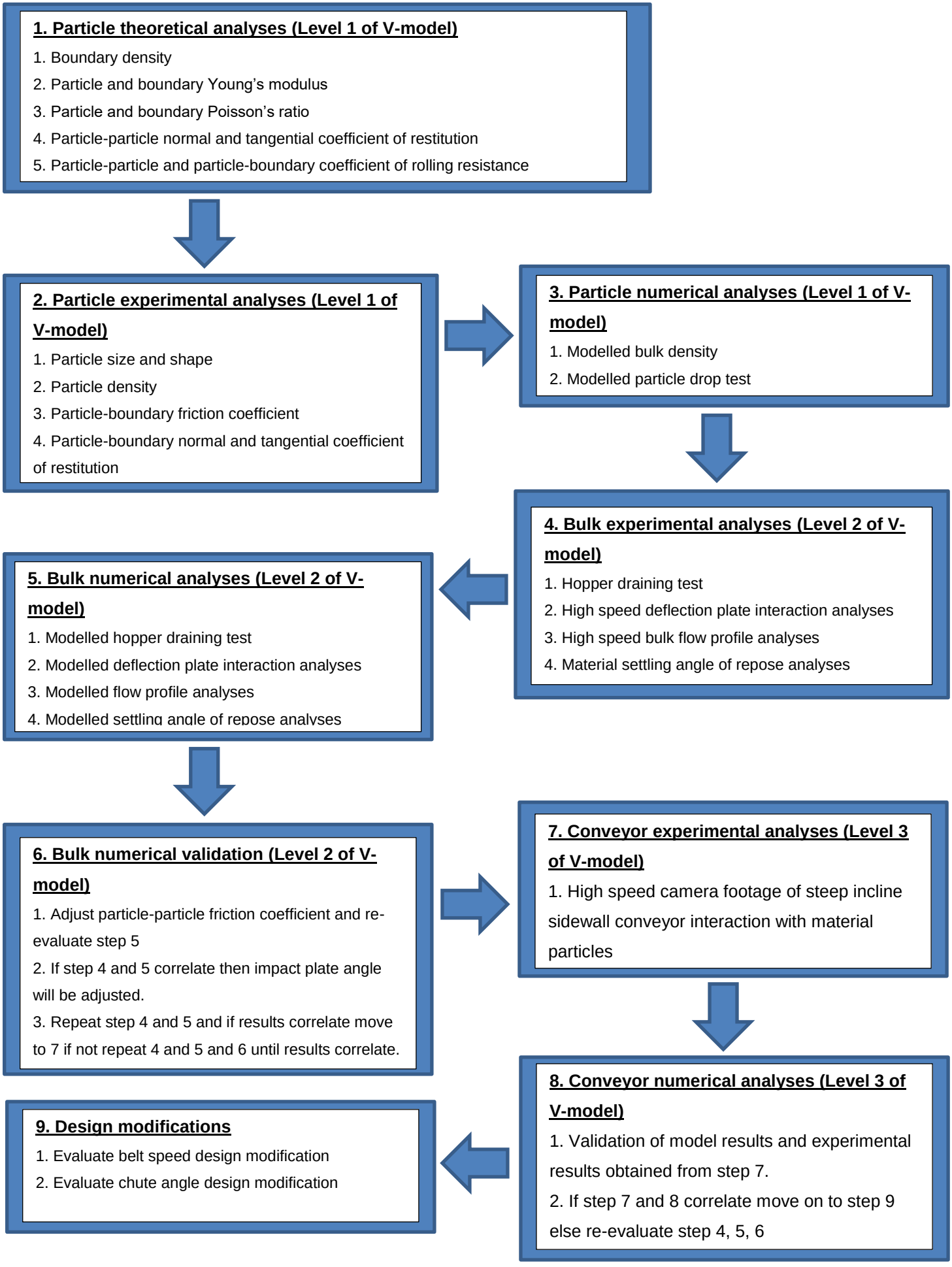

Figure 6 Calibration methodology

4.2. PARTICLE SIZE AND SHAPE CALIBRATION

For the particle size and shape analyses a sample of coke material was gathered from the conveyor that was feeding the coke surcharge hopper, which feeds onto the steep incline sidewall conveyor. This provided a good representation of the coke material that interacts with the steep incline sidewall conveyor.

4.2.1. PARTICLE SIZE CALIBRATION

A coke particle size distribution analyses was obtained from the RMH plant and is summarized by Table 1. It has to be noted that Table 1 represents the particle size distribution of material before it reaches the blast furnace plant and further screening was required.

Table 1 Plant coke size distribution analyses

Size distribution [mm]	>100 Average	80 - 100 Average	60 - 80 Average	40 - 60 Average	35 - 40 Average	30 – 35 Average	20-30 Average	10 - 20 Average	<10 Average
% Coke per size	0,32	8,02	21,45	55,52	7,45	3,73	1,31	0,59	1,61

When comparing the RMH sample analyses from Table 1 with the sample gathered from the conveyor it was found that some of the <30mm and >100mm particles were screened out. It was thus decided to use the RMH analyses for the steep incline sidewall conveyor simulation, but the percentage >100mm particles was combined with the 80mm-100mm and 60mm-80mm particles. This percentage of particles was then simulated as 80mm particles. The 40mm-60mm and 35mm-40mm particle percentage was kept the same as the RMH sample and was simulated as 60mm and 40mm particles respectively. Like with the >100mm particles it was decided to combine the <30mm particle percentage with the 30mm-35mm percentage. These particles were then simulated as 35mm particles. Table 2 summarizes the particle size distribution used for the steep incline sidewall conveyor simulation.

Table 2 Steep incline sidewall conveyor particle size distribution

Steep incline sidewall conveyor particle size distribution						
	>100 Average	80-100 Average	60-80 Average	40-60 Average	35-40 Average	30-35 Average
% Coke per size	30%			56%	7%	7%
Modelled size	80mm			60mm	40mm	35mm

Additional screening was required for the particles used in the test rig experiment. This was due to size constraints presented by the trap door mechanism. It was therefore decided to

screen out the >60mm particles. The particles simulated for the test rig was only 60mm, 40mm and 35mm particles. A summary of the particle size distribution used in the test rig simulation is presented by Table 3.

Table 3 Test rig particle size distribution

Test rig particle size distribution						
	>100 Average	80-100 Average	60-80 Average	40-60 Average	35-40 Average	30-35 Average
% Coke per size	0%			83%	11%	6%
Modelled size	80mm			60mm	40mm	35mm

4.2.2. PARTICLE SHAPE CALIBRATION

For the particle shape calibration 14 random particles were selected from the 60mm screened sample (sample that was used for the test rig analyses). The particle shape calibration was done via a visual analysis, which was conducted as follow. Each particle was placed on a grid representing a 60mm x 60mm block. A photo of the material was taken which could be imported into a CAD program so that representative shapes could be drawn on scale. The result obtained is illustrated in Figure 7.

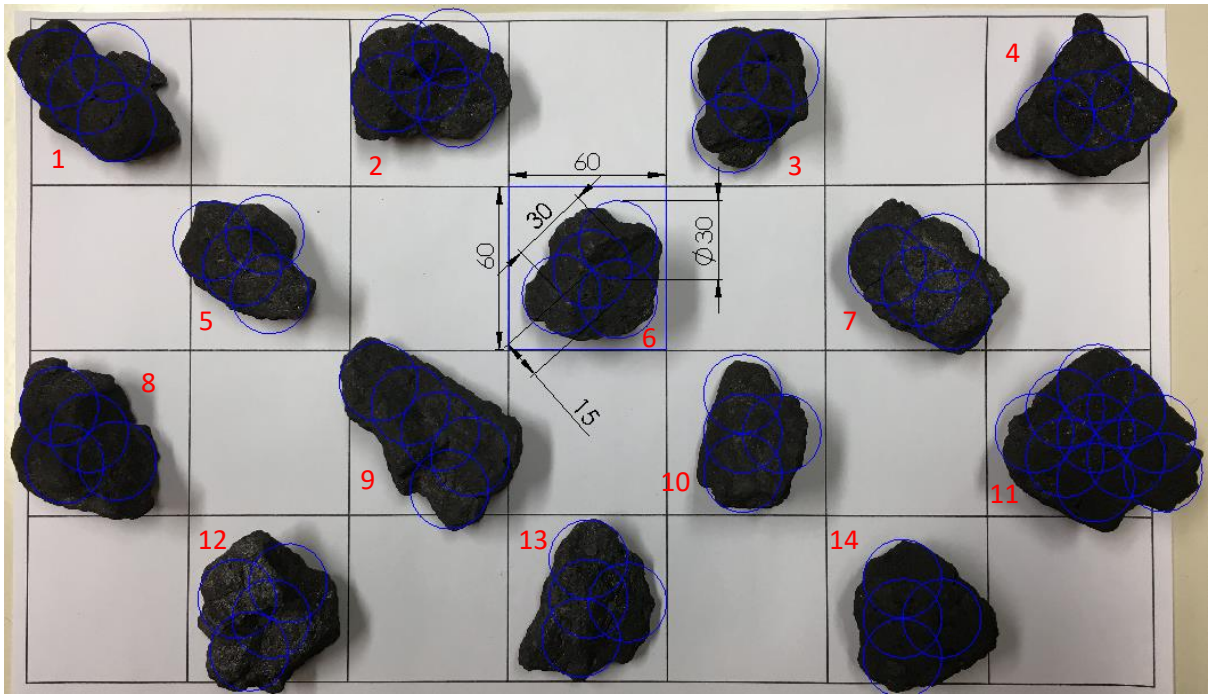

Figure 7 Visual particle shape analyses

From Figure 7 it can be seen that 11 out of 14 particles could be represented by a triangular cluster of spheres, 2 out of 14 could be represented by a square cluster of spheres (#2 and

#11) and 1 out of 14 could be represented by a string cluster of spheres (#9). It was decided to represent all of the particles with a triangular cluster of spheres. The size distribution of the particles was obtained by changing the spheres within the cluster according to the total particle diameter required. The diameter of sphere used per particle size was as follow:

- 80mm particle = 40mm spheres in triangular cluster
- 60mm particle = 30mm spheres in triangular cluster
- 40mm particle = 20mm spheres in triangular cluster
- 35mm particle = 17,5mm spheres in triangular cluster

4.2.3. MODEL SIMULATED SIZE AND SHAPE CALIBRATION

Within Simcenter STAR-CCM+ spherical clusters can be built in a number of arrangements on a unit scale. This means that the particle built does have a specific arrangement but it still has to be given a specific size. The size of the particle is defined when the particle injection into the simulation is defined. Here the size is just defined by one diameter. Simcenter STAR-CCM+ represents the size of the spherical cluster built with regards to a single sphere with the diameter specified in the input parameters. This means that the individual sphere sizes (as required by the size analyses) are not defined. This was overcome by modelling each of the 4 spherical cluster sizes required in a CAD program. Here the cluster volume could be calculated from which a diameter could be calculated which would result in a single sphere of having the same volume as the spherical cluster. Thus the diameter of a single sphere required by Simcenter STAR-CCM+ could be such that the spherical clusters would be the exact size as required. The particle input diameters required by Simcenter STAR-CCM+ are listed below for each particle size required.

- 80mm particle = 62,822mm single sphere diameter
- 60mm particle = 47,116mm single sphere diameter
- 40mm particle = 31,411mm single sphere diameter
- 35mm particle = 27,484 mm single sphere diameter

The final spherical cluster used in the simulation models is illustrated by Figure 8.

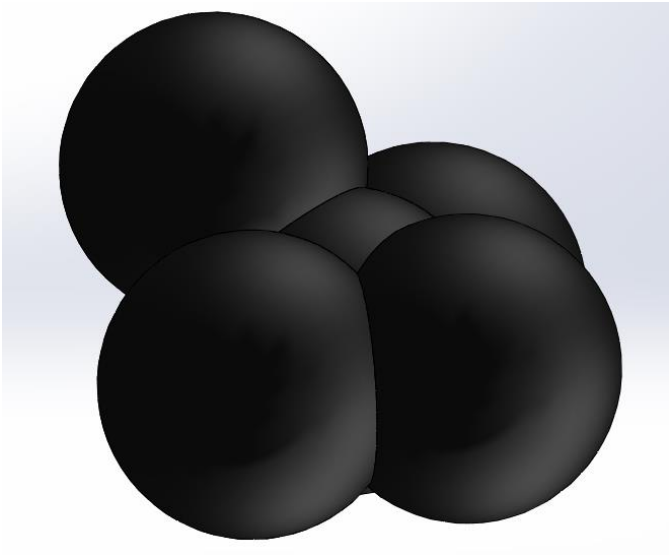

Figure 8 Coke particle representative spherical cluster

4.3. PARTICLE DENSITY AND BULK DENSITY CALIBRATION

The particle density and bulk density was calculated with the use of the direct measurement approach. A sample from the screened <60mm particles was taken for the calculation of the particle density as well as for the bulk density.

4.3.1. PARTICLE DENSITY CALCULATION

The formula used for the calculation of the particle density (ρ_p) is illustrated by Equation (24).

$$\rho_p = \frac{m_p}{V_p} \qquad (24)$$

Where

m_p : mass of the particle

V_p : Volume of the particle

Even though the mass of the particle could readily be measured a single particle volume could not be measured. It was therefore decided to take the <60mm particle sample and submerge it in a volume of water so that the displacement of water could be measured. It was noted that due to the porous structure of coke a small portion of the sample was not fully submerged in the water. It was decided to use a small section of plate to ensure that the entire sample is submerged under the water. With the assumption that the particles didn't absorb the water, the water volume displaced (minus the water displaced by the section of plate) was used as the particle volume of the sample. The mass of the <60mm sample was measured on an electric scale before it was submerged in the water. The average particle

density could be calculated by taking the sample mass and dividing it by the sample volume (volume of water displaced).

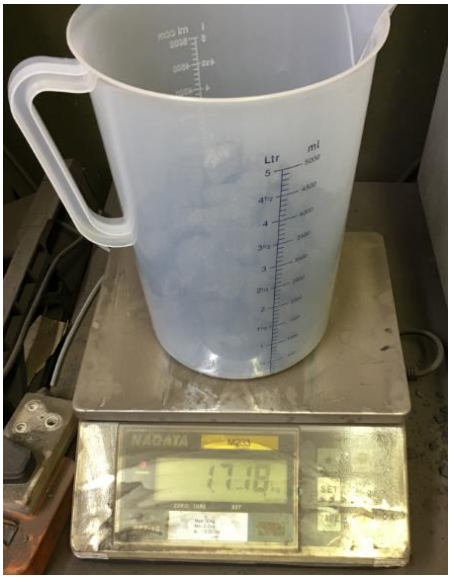

Figure 9 -60mm coke particle sample measured weight

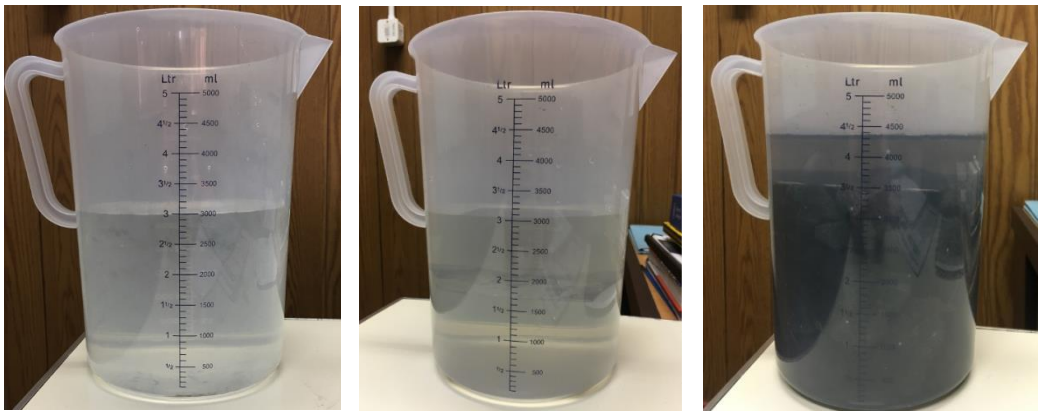

Figure 10 Water volume displacement of <60mm coke particle sample

By using Equation (24) the results in Table 4 were obtained.

Table 4 Particle density calculation results

Particle density calculation		
Weight of container	0,390	kg
Weight of material without container [m_p]	1,328	kg
Volume of water without material sample	0,003	m^3
Calculated volume of material [V_p]	0,001	m^3
Particle density [ρ_p]	1021,538	kg/m^3

The calculated particle density of 1021,538 kg/m^3 was also verified to be within the typical boundary of 800 - 1200 kg/m^3 (obtained from blast furnace plant information), and therefore this value was used directly in Simcenter STAR-CCM+ material input parameters.

4.3.2. PARTICLE BULK DENSITY CALCULATION

Horn defined the bulk density as the mass of a material sample divided by the volume which that material sample occupies (Horn, 2012). With the formulation provided it is evident that the bulk density includes the voids that are formed between the particles as illustrated by Figure 11.

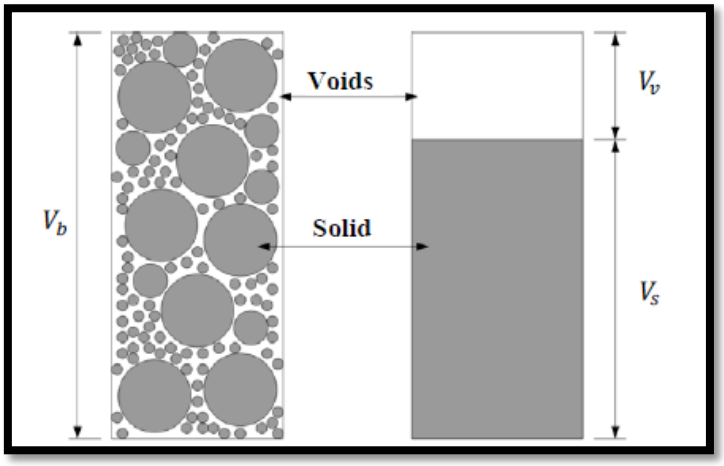

Figure 11 Bulk volume, voids volume and total solid volume (Horn, 2012)

From the definition of the bulk density, Equation (25) can be used to calculate the sample bulk density (ρ_b).

$$\rho_b = \frac{m_b}{V_b} \qquad (25)$$

Where

m_p : mass of the bulk sample

V_p : Volume of the bulk sample

An important parameter that is derived from the bulk density and the particle density is the voids ratio (e). The voids ratio is a term used to describe the ratio between the volume occupied by the voids (V_v in Figure 11) and the volume occupied by the solid material (V_s in Figure 11). The voids ratio is therefore calculated with the use of Equation (26).

$$e = \frac{\rho_p}{\rho_b} - 1 \qquad (26)$$

Where

ρ_p : particle density

ρ_b : bulk density

The voids ratio value is then used to calculate the material porosity (n) and is given by Equation (27).

$$n = 100\left(\frac{e}{e+1}\right) \qquad (27)$$

Where

e : voids ratio

The material porosity is defined as the ratio between the voids volume and the bulk volume and is expressed as a percentage value (Horn, 2012). The porosity value is an important parameter of defining how densely packed a specific volume is with a specific material.

Therefore in order to calculate the coke material bulk density the <60mm particle sample was placed within a known volume, weighed and the bulk density calculated using Equation (25). The voids ratio was calculated using the particle density calculated in Table 4 and the sample porosity was calculated with the calculated voids ratio value. The results obtained from these calculations are summarised in Table 5.

Table 5 Bulk density calculation results

Bulk density calculation		
Bulk density [ρ_b]	428,387	kg/m^3
Void fraction [e]	1,385	-
Porosity [n]	58,065	%

The bulk density result of 428,387 kg/m^3 and porosity result of 58,065% were verified to be within typical plant and conveyor design limits of 400 – 600 kg/m^3 and 50% respectively. Therefore it was decided to move on to the next phase of the calibration.

4.3.3. MODEL SIMULATED PARTICLE DENSITY AND BULK DENSITY CALIBRATION

For the validation of the simulated particle density and bulk density the test rig simulation was used. Within Simcenter STAR-CCM+ a random injector was defined which would only inject particles in the containment hopper volume. Due to the fact that the volume of the containment hopper was known, the random injector could be defined to inject the three different particle sizes (60mm, 40mm and 35mm) to within the calculated porosity limit. It should be noted here that Simcenter STAR-CCM+ defines the porosity limit within the random injector as follow:

$$Porosity = \frac{Total\ volume\ of\ injected\ particles}{Volume\ of\ region\ assigned\ to\ the\ injector} \qquad (28)$$

By taking Equation 28 into consideration it is evident that if the random injector porosity limit were to be used the porosity input value would be 1 minus the calculated material porosity. Thus the porosity value used for the random injector was 0.4194.

When using the random injector porosity limit for all three of the particle sizes (injected simultaneously), it was found that the particle size distribution was random and not correlating with the experimentally determined size distribution. To ensure that the simulated particle size distribution correlates with the experimental size distribution, the random injector porosity limit was used to calculate the number of particles associated with each of the simulated particle sizes. The random injector could then be defined in such a way that a specific number of each of the particle sizes could be injected into the containment hopper. This would then ensure that the simulated particle size distribution matched that of the experimental particle size distribution while ensuring that the correct porosity limit was maintained. The results of the random injector input parameters are summarized by Table 6 and the result of the particle settling is illustrated by Figure 12.

Table 6 Random injector parameter definition

Random injector parameter definition						
	>100 Average	80 - 100 Average	60 - 80 Average	40 - 60 Average	35 - 40 Average	30 - 35 Average
Particle size distribution	0%	0%	0%	83%	11%	6%
Test hopper particles -60mm porosity division	0	0	0	0,3491	0,0468	0,0234
Simulated particle size distribution	80mm			60mm	40mm	35mm
Number of particles	0			274	124	93

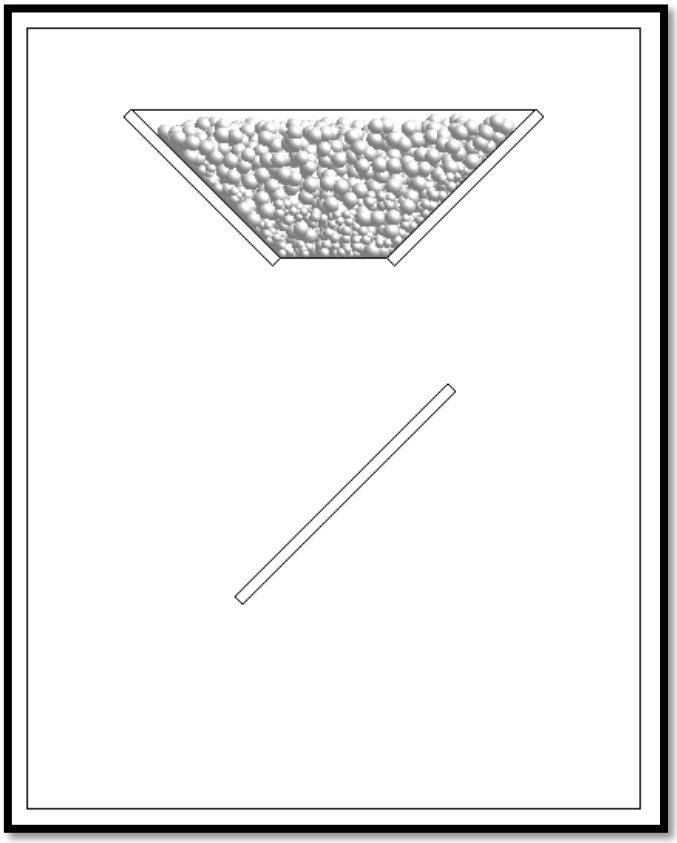

Figure 12 Simulated particle settling within the containment hopper of the test rig

The validation of the bulk density was done with the use of a built in function (within Simcenter STAR-CCM+) that was capable of calculating the total mass of the particles injected into a specific region. This mass was then divided by the containment hopper volume in order to determine the simulated bulk density. The results that were obtained are tabulated in Table 7.

Table 7 Simulated bulk density results

Hopper filled with 35, 40, 60mm particles with Simcenter STAR-CCM+ particle count that matches the total porosity limit of 0,4194		
Total material weight	18,417	kg
Particle count	491	-
Hopper volume	0,043	m^3
Bulk density	428,223	kg/m^3

From Table 7 it follows that the simulated bulk density is 428.223 kg/m^3 and the experimental tests yielded a bulk density of 428.387 kg/m^3 which illustrates a good correlation between the simulated and experimental bulk density.

This result was validated further by taking the screened <60mm sample and filling the experimental test rig to the same height as the simulated result of the filled containment hopper. The material sample was then drained into a bag which was weighed in order to calculate the bulk density of the material. The calculated experimental bulk density result is listed in Table 8.

Table 8 Experimental test rig containment hopper filled with <60mm particles and calculated bulk density result

Experimental test rig containment hopper filling result		
Hopper volume	0,043	m^3
Material weight	18,168	kg
Bulk density	422,433	kg/m^3
Void fraction	1,418	-
Porosity	58,647	%

It was found that the simulated bulk density was within 2% of both of the experimental bulk density results. It can therefore be concluded that the particle size, shape and density is correctly calibrated for the specific material application.

4.4. PARTICLE-BOUNDARY FRICTION COEFFICIENT CALIBRATION

The particle-boundary friction coefficient is required because this value describes the interaction between the material and a typical boundary like a conveyor or a hopper liner. If this value is not calibrated correctly it will influence the velocity at which material exits the discharge chute and therefore influence the interaction of the steep incline sidewall conveyor and the material.

This value was readily calculated by using the direct approach for each of the different boundary materials included into the simulation. The methodology which was followed was to place a particle on a piece of material (which would be simulated as a boundary) and then to rotate the boundary material until the particle started to slide. The angle at which the particle slid was recorder and the friction coefficient was calculated by using Equation (29).

$$\mu_b = \tan(\theta) \qquad (29)$$

Where

μ_b : Boundary friction coefficient

θ : Inclination angle at which particle slides on the boundary material

The deflection plate of the test rig was used for this calculation. Thus only two materials would be included in the simulation boundaries and these were rubber (steep incline sidewall conveyor material) and liner plate (coke surcharge hopper chute liner). Each of these materials was individually fastened to the test rig deflection plate, a particle was placed on the deflection plate and the deflection plate was rotated until the particle started to slide. The angle at which the particle started to slide was recorded with a protractor. This test was repeated 20 times and an average particle-boundary friction coefficient was calculated for the interaction between coke-conveyor and coke-ceramic liner plate.

The test rig setup for the particle-boundary friction coefficient calculation is illustrated by Figure 13 and the results obtained for rubber and ceramic liner plate are listed in Table 9. The full list of results of all 20 tests can be found in Appendix 1.

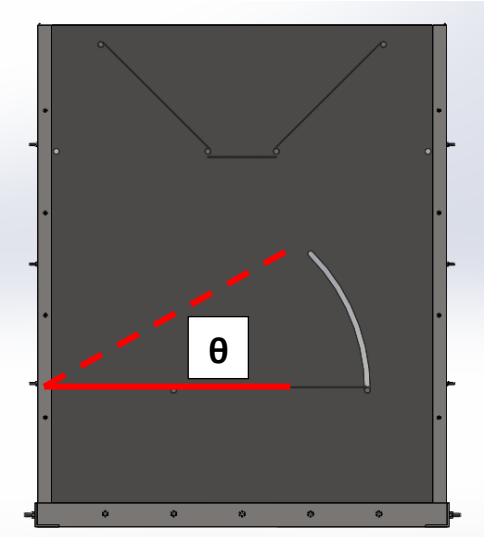

Figure 13 Test rig setup for particle-boundary friction coefficient calculation

Table 9 Particle-boundary friction coefficient results

Particle-boundary friction coefficient results		
Material	**Average angle [deg]**	**Average friction coefficient**
Rubber	40.23	0.852
Ceramic liner plate	13.5	0.240

The values listed in Table 9 were directly inserted into Simcenter STAR-CCM+ boundary coefficient of friction parameters.

4.5. YOUNG'S MODULUS, POISSON'S RATIO AND PARTICLE ROLLING RESISTANCE CALIBRATION

Simcenter STAR-CCM+ requires an input value for the particle and boundary Young's modulus, Poisson's ratio and rolling resistance (when using the Hertz Mindlin contact model). In the literature study it was stated that the shear modulus is also an input parameter in some of the software packages, but Simcenter STAR-CCM+ uses the particle or boundary (depending on the contact material in question) and calculates an equivalent shear modulus with the Young's modulus and Poisson's ratio. Therefore it was only necessary to obtain a Young's modulus, Poisson's ratio and rolling resistance for the coke particles, conveyor rubber and the ceramic liner plate material.

4.5.1. YOUNG'S MODULUS CALIBRATION

Firstly taking a look at the boundary material Young's modulus, it was decided to use the built in Simcenter STAR-CCM+ values. This was done due to the lack of testing equipment available and to prevent an additional parameter that had to be calibrated via an iterative method within the simulation model. The boundary material for the conveyor was selected as rubber and the ceramic liner plate was set as carbon steel. These selections provided a Young's modulus as stipulated in Table 10.

Table 10 Boundary material Young's modulus selection

Boundary material Young's modulus		
Boundary	**Material**	**Young's modulus**
Steep incline sidewall conveyor	Rubber	1 MPa
Hopper and chute liner plate	Carbon steel	200 GPa

The coke particles' Young's modulus was obtained from literature. A paper written by Haapakangas on coke properties in a simulated blast furnace used a cold Young's modulus

of E = 1337.1 MPa (Haapakangas, 2016). Lommen et al stated that the particle's Young's modulus can be reduced (in order to reduce computational time) and stated that the average normal contact overlap should be kept below 0.3% of the particle radius or the shear modulus should be kept above 10^7 Pa (Lommen, et al., 2014). Therefore taking this into consideration the test rig was simulated with the particles (according to the calibrated size, shape and porosity) already injected into the containment hopper. A monitor report was generated in Simcenter STAR-CCM+ that would track the contact overlap generated between the coke particles when the trap door would be opened, and the material allowed to bounce off the deflection plate and settle at the bottom of the test rig. The Young's modulus value would then be changed from 1MPa, 10MPa, 100MPa and a 1000MPa respectively. Figures 14 and 15 illustrate the difference in the different number of contacts that has to be tracked when the particle Young's modulus is changed from 1MPa to 1000 MPa. This also provides a perspective into why the Young's modulus has an influence on the time step required and therefore the computational time.

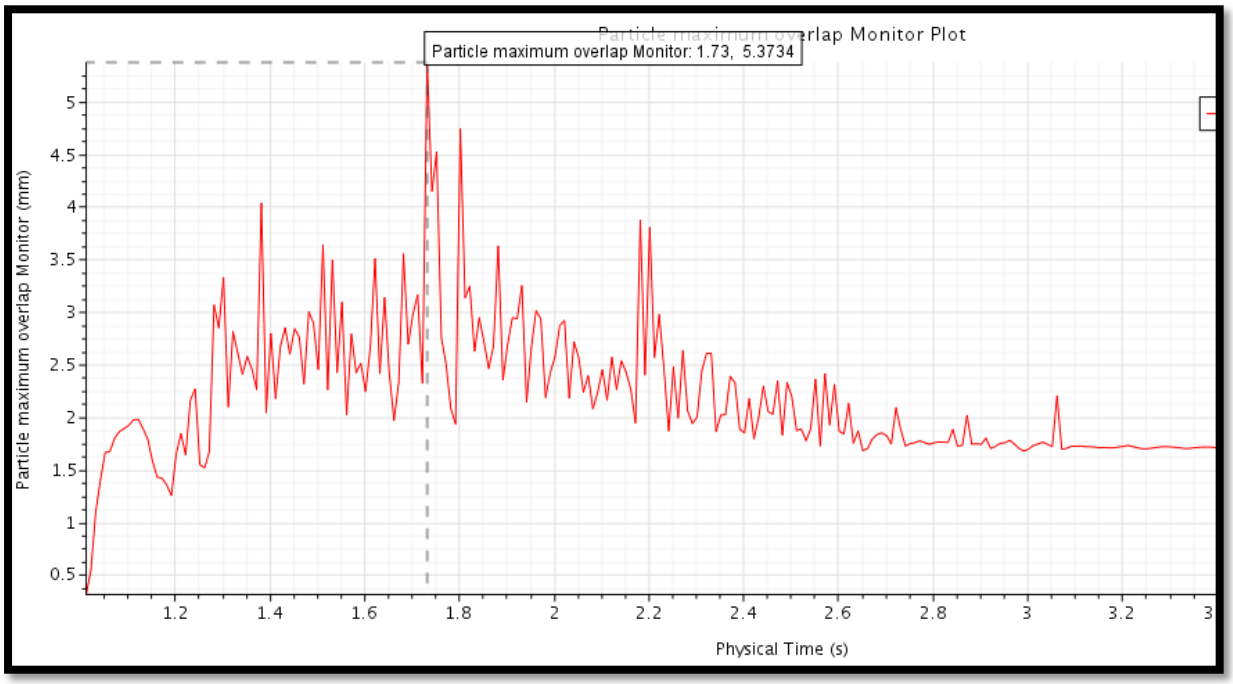

Figure 14 Maximum contact overlap tracked for E=1MPa

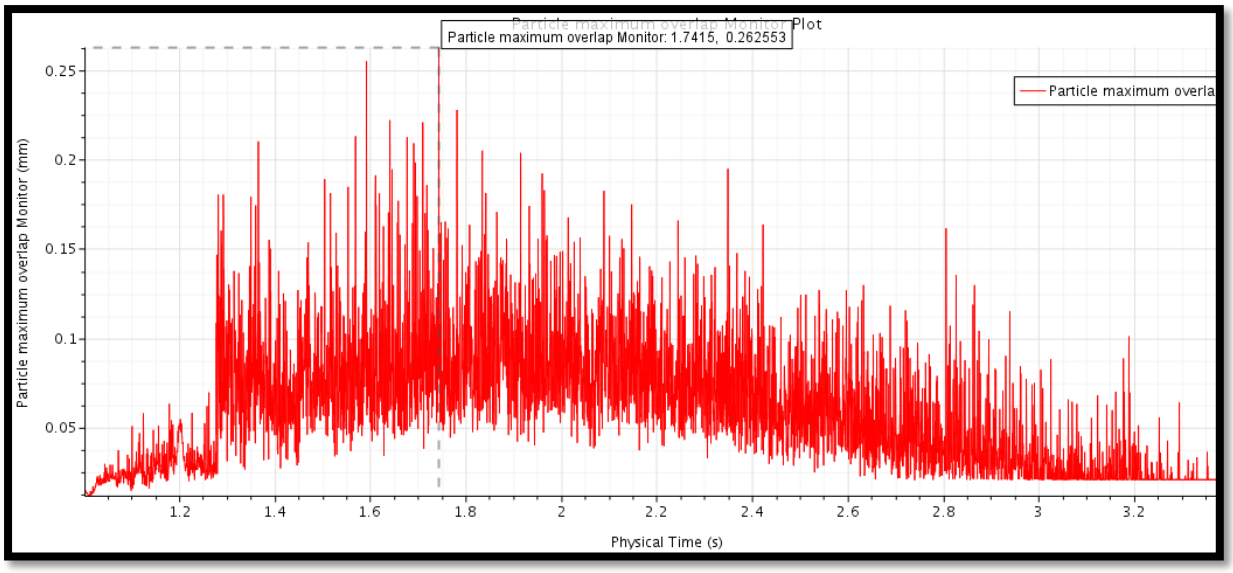

Figure 15 Maximum contact overlap tracked for E=1000MPa

The values generated for the contact overlap analyses revealed that a Young's modulus between 100MPa and 1000MPa would generate an average contact overlap of lower than 0.3% of the particle radius. When calculating the shear modulus with the use of the variable Young's modulus it was determined that a Young's modulus of 100MPa would provide a shear modulus above 10^7Pa. Therefore it was decided to use a Young's modulus of 100Mpa and not the theoretical 1337.1 MPa in order to save computational time.

4.5.2. POISSON'S RATIO CALIBRATION

The Poisson's ratio for the boundary materials was used from the Simcenter STAR-CCM+ build in properties. The Poisson's ratio for the coke particle material was used as an estimate value and kept constant throughout the simulation process, due to the lack of a testing facility. The values used are listed in Table 11.

Table 11 Poisson's ratio for boundary and coke particle material

Poisson's ratio for boundary and coke particle material		
Boundary or particle	**Material**	**Poisson's ratio**
Steep incline sidewall conveyor	Rubber	0.45
Hopper and chute liner plate	Carbon steel	0.285
Particles	Coke	0.05

4.5.3. ROLLING RESISTANCE COEFFICIENT CALIBRATION

The particle rolling resistance coefficient was set to a force proportional model for both the particle-boundary and particle-particle interactions. Here it was once again decided to use

the built in default value for the particle-boundary and particle-particle interaction. This decision was made as this is one parameter that has been calibrated with the use of the bulk calibration approach (Coetzee, 2017). Taking this into consideration revealed that if the test rig were to be used for the calibration of the rolling resistance, multiple values for particle sliding friction factor and rolling resistance would yield the same angle of repose and hopper draining rates. Therefore the particle and boundary rolling resistance was kept constant throughout the study. Table 12 lists the values used.

Table 12 Rolling resistance coefficient for different interactions

Rolling resistance coefficient for different interactions		
Interaction	**Material**	**Rolling resistance coefficient**
Particle with steep incline sidewall conveyor	Coke and Rubber	0.001
Particle with hopper and chute liner plate	Coke and Carbon steel	0.001
Particle with other particles	Coke and Coke	0.001

4.6. COEFFICIENT OF RESTITUTION CALIBRATION

Simcenter STAR-CCM+ requires an input parameter for the normal and tangential coefficient of restitution. These coefficients are used in order to allow for the damping portion of the contact force calculation in both the normal and tangential directions. This means that a coefficient of restitution has to be provided for each of the phases which will come into contact, or in other words a restitution coefficient has to be given for the Coke-Coke interaction, Coke-Rubber interaction and the Coke-Liner plate interaction.

It was stated by both Coetzee (Coetzee, 2017) and Thompson (Thompson, 2008) that a typical test that is used for the evaluation of the coefficient of restitution is the material drop test. Here a single particle is secured at a known height above the boundary material which will be investigated. The particle is dropped and allowed to bounce on the boundary material while the movement of the particle is captured with a high speed camera. The displacement height which the particle obtains after contact is measured and the velocity directly after the contact is calculated. It is also assumed that the resistance caused by the air does not have a significant effect on the particle velocity and that it experiences constant acceleration due to gravity. Equation 30 can then be used to calculate the velocity directly after impact.

$$v_f^2 = v_i^2 + 2g(x_f - x_i) \quad (30)$$

Where

v_f : Final velocity

v_i : Initial velocity

g = Gravitational acceleration

x_f : Final position

x_i : Initial position

One point of difficulty with an actual material particle is that it does not have an exact spherical shape which would allow for an exact bounce displacement analyses. To overcome this issue, particles from the <60mm sample were assessed in order to find the most spherical shaped particles. With the necessary theory and particles obtained the following method was used for the coefficient of restitution assessment.

The material test rig was adjusted so that the bottom deflection plate was in the fully horizontal position. A grid was fastened to the back plate which had 20mm x 20mm blocks printed over the entire area. This grid would allow for the measurement of the total displacement height achieved after the point of impact. It was also decided to only conduct this test for the rubber material due to the fact that the particle bounce mechanism would not be required for the chute liner plate material. The particle would be released from the trap door position by hand in order to ensure that the trap door does not influence the motion of the particle. Figure 16 illustrates the experimental test setup.

Figure 16 Coke-Rubber coefficient of restitution experimental test setup

This test was repeated 10 times and the average values obtained are tabulated in Table 13.

Table 13 Coke-Rubber velocity calculation result

Coke-Rubber velocity calculation result		
Particle displacement after impact	0,14	m
Gravity	-9,81	m/s^2
End velocity	0	m/s
Initial velocity	1,657	m/s

After obtaining the experimental test results a test rig setup similar to the experiment was modelled in Simcenter STAR-CCM+. A single particle was injected into the containment hopper with a specific orientation in order to attempt a similar bounce result. The particle was allowed to settle after which the trap door mechanism was removed and the particle fell to the horizontally positioned deflection plate. Figure 17 illustrates the simulation setup for the coefficient of restitution analyses.

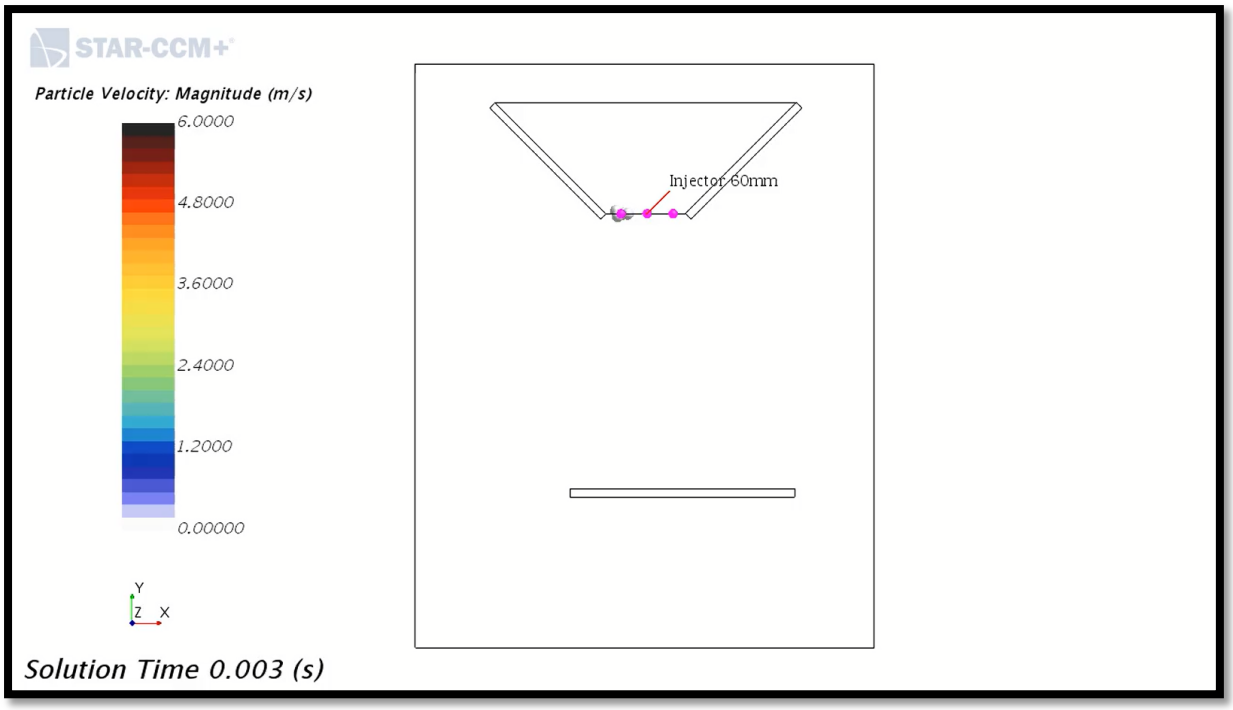

Figure 17 Coefficient of restitution simulation model setup

A monitor plot was set up within Simcenter STAR-CCM+ which tracked the maximum velocity of the particle as it interacted with the deflection plate. This simulation was repeated with a restitution coefficient ranging from 0.2, 0.4, 0.6, 0.8 and 1. It should also be noted that the normal and tangential coefficient of restitution were made the same as to allow for a spherical interaction.

From the simulation results it was found that with an increase in the coefficient of restitution a decrease in damping was obtained. This means that the velocity of the particle after impact increased as the coefficient of restitution increased. Figures 18 and 19 illustrate the difference in the velocity after impact when a restitution coefficient of 0.2 and 0.8 were used. All of the results obtained are illustrated in Appendix 2.

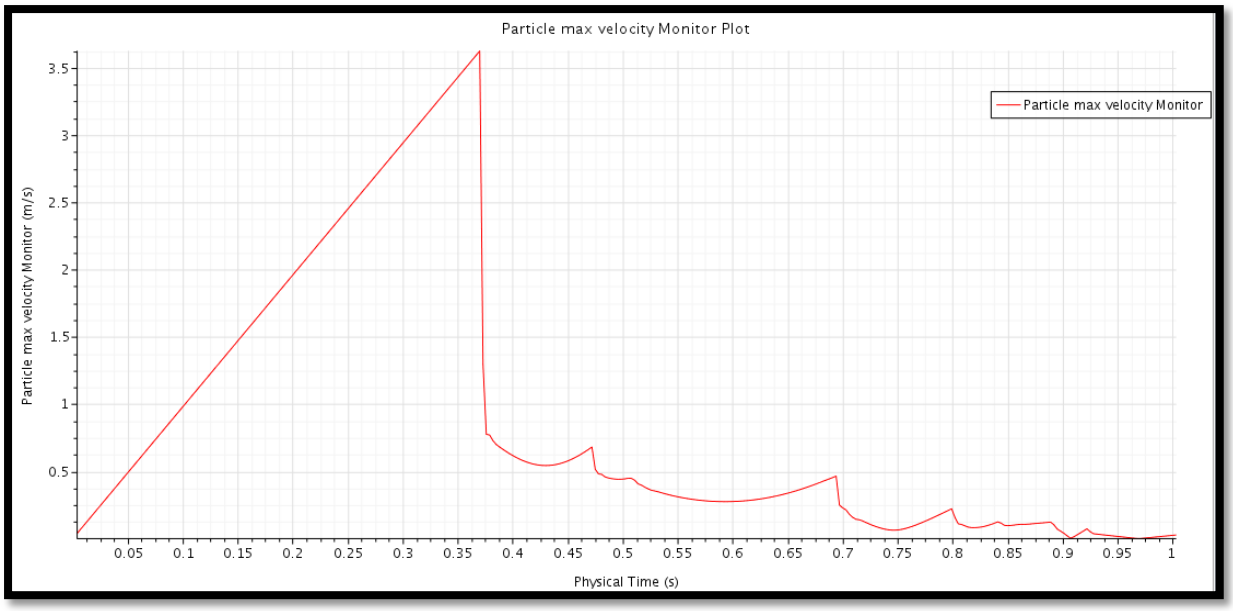

Figure 18 Maximum particle velocity with a coefficient of restitution of 0.2

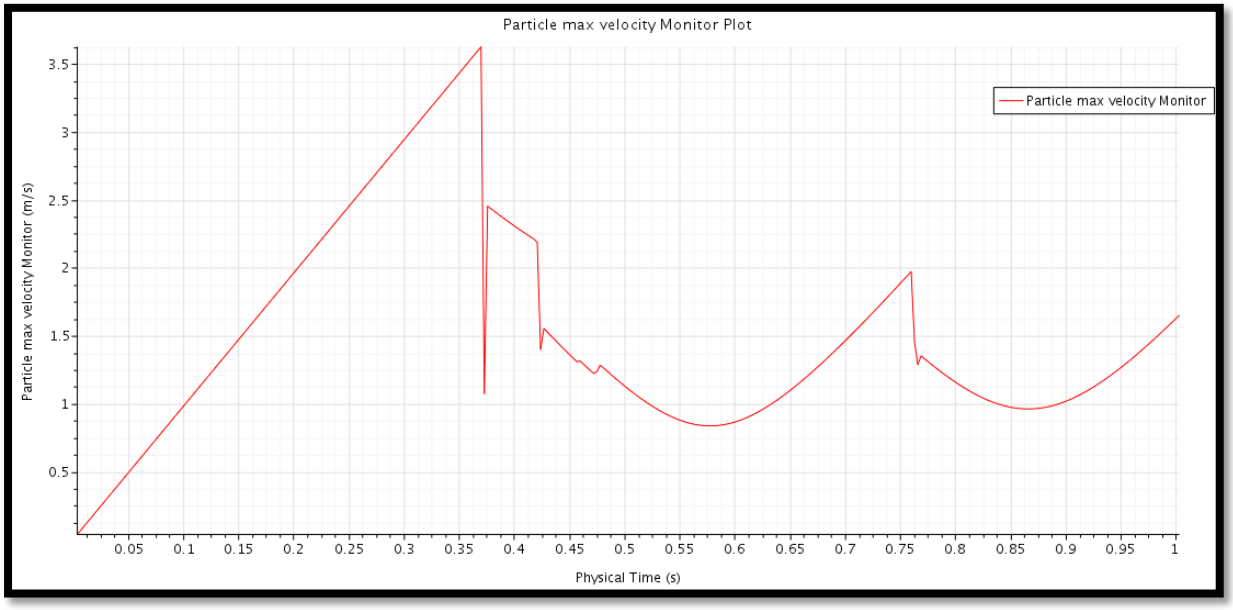

Figure 19 Maximum particle velocity with a coefficient of restitution of 0.8

From the analyses of the simulated particle drop test it was found that a coefficient of restitution of 0.6 would result in a particle velocity after impact of 1.7 m/s. It was therefore decided to use a coefficient of restitution of 0.6 for both the normal and tangential component of the interaction between the coke particle and the conveyor rubber boundary.

For the analyses of the coke-coke interaction restitution coefficient it was realised that a drop test would not be able to provide sufficient results. It was also stated by Thompson (Thompson, 2008) that there has not yet been a test that was able to conclusively calibrate

this parameter. Thompson stated that it is best if typical estimated values be used for the particle-particle coefficient of restitution. According to Thompson a typical value for granular material is 0.3 and it was therefore decided to use 0.3 as the coke-coke normal and tangential coefficient of restitution.

4.7. PARTICLE-PARTICLE FRICTION COEFFICIENT CALIBRATION

The particle-particle friction coefficient (also referred to as the particle-particle static friction coefficient) is an input parameter used by Simcenter STAR-CCM+ to account for the tangential contact force parameter.

4.7.1. METHODOLOGY FOR THE CALIBRATION OF PARTICLE-PARTICLE FRICTION COEFFICIENT

For the particle-particle friction coefficient calibration the bulk calibration approach was followed (level 2 of the V-model). The screened batch of <60mm coke particles (used for the material bulk density validation) was loaded into the material containment hopper and drained though the trap door to assess how the particles interacted with the deflection plate. The entire draining process and deflection plate interaction was recorded with a high speed camera and the angle of repose formed at the bottom of the rig was measured. A simulation model was set up with the calibrated parameters (section 4.2 – 4.6), and the particle-particle friction coefficient was varied until the simulation model matched that of the experimental test. These events are listed in the sequence below.

Experimental test rig procedure

1. Fastened rubber material to the containment hopper walls and to the deflection plate and test rig bottom.
2. Filled experimental test rig containment hopper with <60mm coke particles.
3. Adjusted the deflection plate to an angle of 45 degrees.
4. Switched on the high speed camera and started recording.
5. Released the containment hopper trap door and waited till all of the coke particles were drained and settled at the bottom of the test rig.
6. Stopped the high speed camera recording.
7. Measured the angle of repose formed by the particles at the bottom of the test rig.
8. Removed the particles from the test rig.
9. Reset the containment hopper trap door and loaded the <60mm particles into the test rig containment hopper.
10. Repeated step 4 – 9 for 5 iterations.

Simulation test rig procedure

1. Developed a simulation model to replicate the experimental test setup with the deflection plate at 45 degrees.
2. The Hertz Mindlin contact model was selected and the previously validated parameters were inserted into the model input parameters.
3. Injected the 35mm, 40mm and 60mm particles with a random injector according to the validated porosity and bulk density limit determined in section 4.3. Random particle orientation was selected in the random injector settings in order to ensure that random particle packing was obtained. As soon as the total number of particles (491) was injected and the particles settled, the model was saved so that the following steps could be repeated.
4. The trap door model setting was changed in order to allow the particles to drain from the containment hopper to the deflection plate.
5. A monitor plot was generated to track the particle mass flow rate from the containment hopper.
6. During each time step a snapshot of the simulation model result was captured in order to allow for a simulation video to be compiled. This video thus allowed for a comparison between the simulation and experimental material bulk behaviour.
7. The simulation was continued until all of the particles settled at the bottom of the test rig. When all of the particle motion stopped the simulation was stopped.
8. After the simulation model was stopped, the angle of repose formed by the particles at the bottom of the test rig was measured.
9. The particle-particle friction coefficient was adjusted from 0.1 to 2.4 with incremental steps of 0.1. Steps 4 to 9 were repeated after which the angles of repose and containment hopper draining times were recorded.

4.7.2. EXPERIMENTAL TEST RIG SETUP AND RESULTS

The test rig was set up in such a manner that the maximum amount of light would be available for the high speed camera setup. The high speed camera was also positioned such that the containment hopper draining, the deflection plate interaction and the bottom particle settling could be captured in one shot. Figure 20 illustrates the test setup layout and Figure 21 illustrates a snap shot of the result produced by the high speed camera.

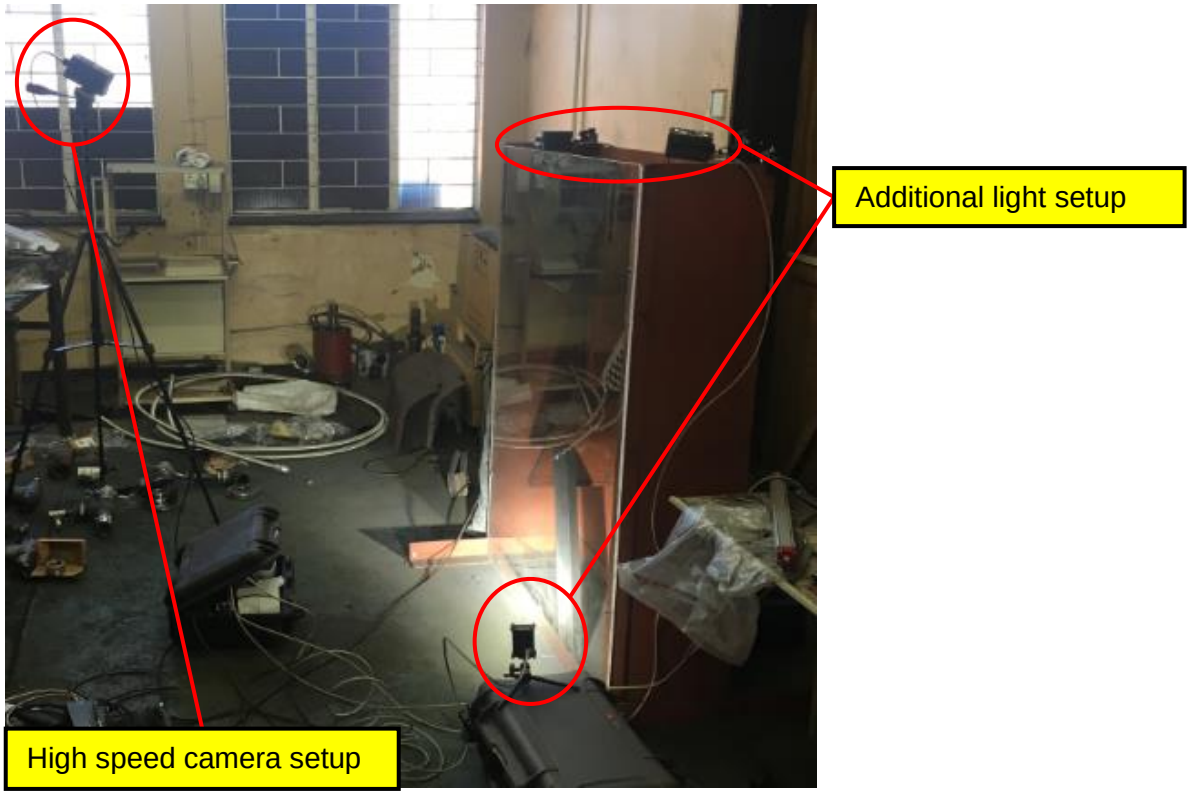

Figure 20 Experimental test setup for particle-particle friction coefficient calibration

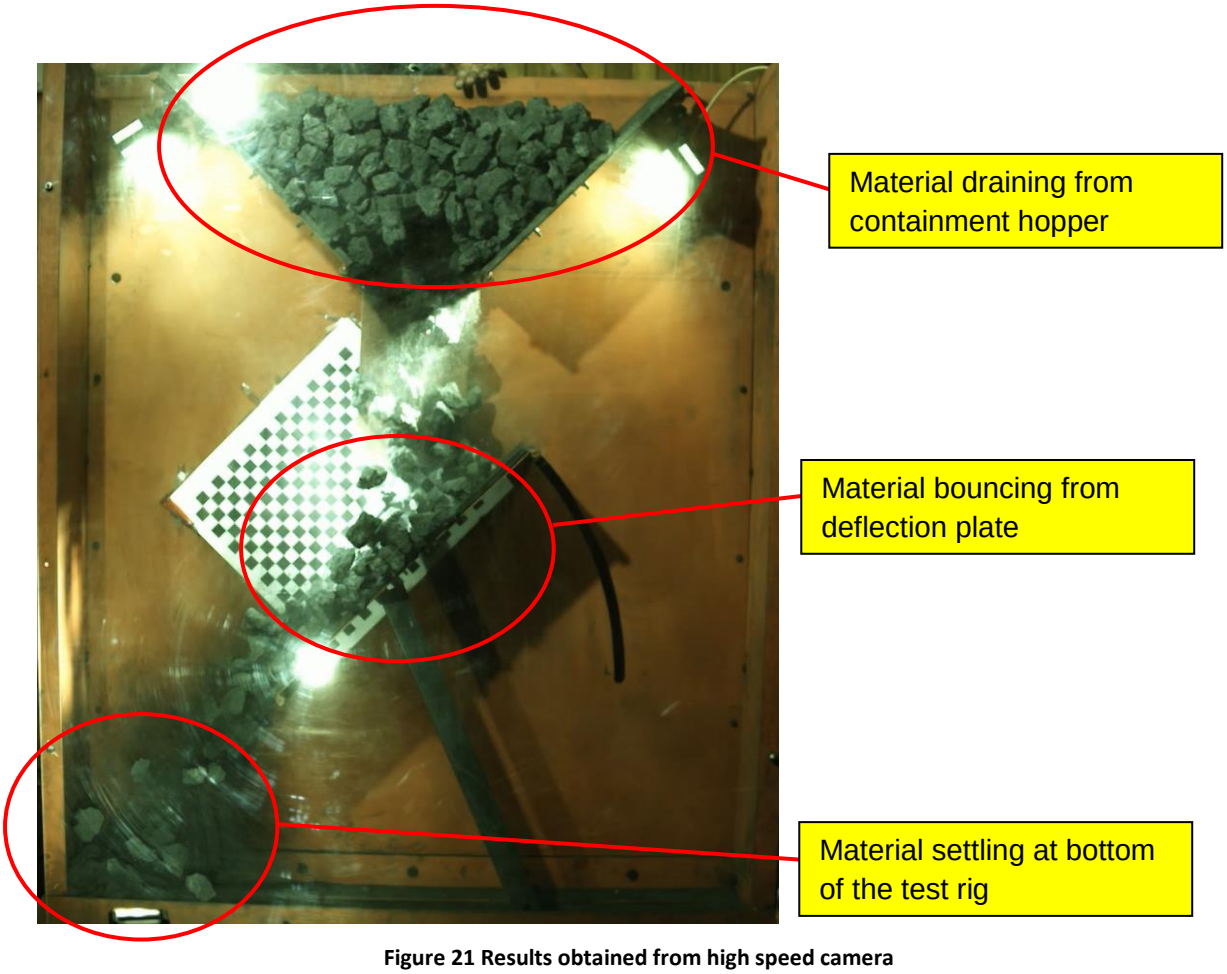

Figure 21 Results obtained from high speed camera

After completing the 5 iterations, the high speed camera videos were analysed in order to calculate the containment hopper draining time for all of the iterations. This was done by evaluating the number of frames it took the hopper to drain and then dividing this value with the frame rate that was used to capture the video. The result obtained would thus provide the actual time (in seconds) it took for the containment hopper to drain. The results for each of the iterations are listed in Table 14.

Table 14 Containment hopper draining duration

Containment hopper draining duration	
Test number	**Time**
1	1.872 s
2	1.920 s
3	2.448 s
4	1.968 s
5	1.750 s

After each of the iterations the material settling angle of repose was also measured and the results are tabulated in Table 15.

Table 15 Material settling angle of repose

Material settling angle of repose	
Test number	**Angle of repose**
1	33 degrees
2	40 degrees
3	31 degrees
4	35 degrees
5	36 degrees

4.7.3. SIMULATED TEST RIG SETUP AND RESULTS

For the setup of the Simcenter STAR-CCM+ simulation model the previously calibrated particle parameters (section 4.2 – 4.6) were used as input values. These values are summarised in Table 16.

Table 16 Simcenter STAR-CCM+ simulation model input parameters

Simcenter STAR-CCM+ model input parameters	
General	
Parameter description	**Value**
Deflection plate inclination angle	45 degrees
Contact model	Hertz Mindlin
Coke particle	
Parameter description	**Value**
Density	1021.54 kg/m^3
Poisson's ratio	0.05
Young's modulus	100 Mpa
Shape	Sphere triangular cluster
Size	35mm, 40mm and 60mm
Particle-particle normal restitution coefficient	0.3
Particle-particle tangential restitution coefficient	0.3
Particle-particle rolling resistance	0.001
Particle-particle static friction coefficient	To be increased incrementally from 0.1 to 2.4
Rubber boundary	
Parameter description	**Value**
Density	1100 kg/m^3
Poisson's ratio	0.45
Young's modulus	1 MPa
Particle-boundary normal restitution coefficient	0.6
Particle-boundary tangential restitution coefficient	0.6
Particle-boundary rolling resistance	0.001
Particle-boundary static friction coefficient	0.852

The simulation model was started off with a particle-particle friction coefficient of 0.1 and it was increased by 0.1 for the first 10 iterations and then it was increased by 0.2 for the following 6 iterations. All of the results generated were saved and used for the verification of the experimental hopper draining test and settling angle of repose test.

Firstly taking a look at the results generated by the hopper draining test. The simulation model was set up such that the particle flow rate passing through the containment hopper could be tracked. Therefore the draining duration could be determined for each of the particle-particle static friction coefficient values. Figure 22 illustrates a typical hopper draining graph that was obtained, and all of the results can be viewed under Appendix 3.

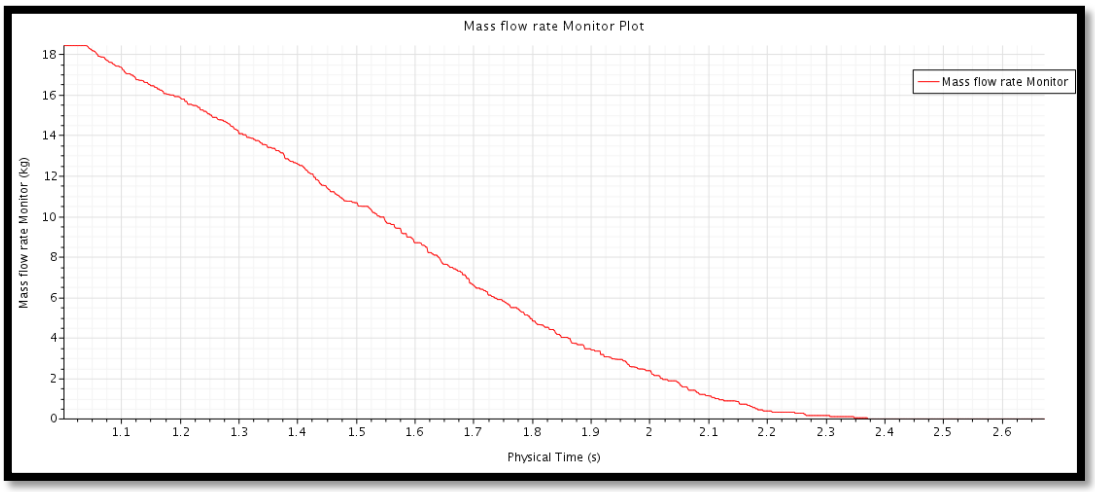

Figure 22 Containment hopper draining rate graph for particle-particle friction coefficient of 0.5

The simulated containment hopper draining times were tabulated and plotted on a graph. The graph also included the range between the minimum and maximum containment hopper draining times obtained from the high speed camera video processing (Table 14). Figure 23 illustrates the results obtained.

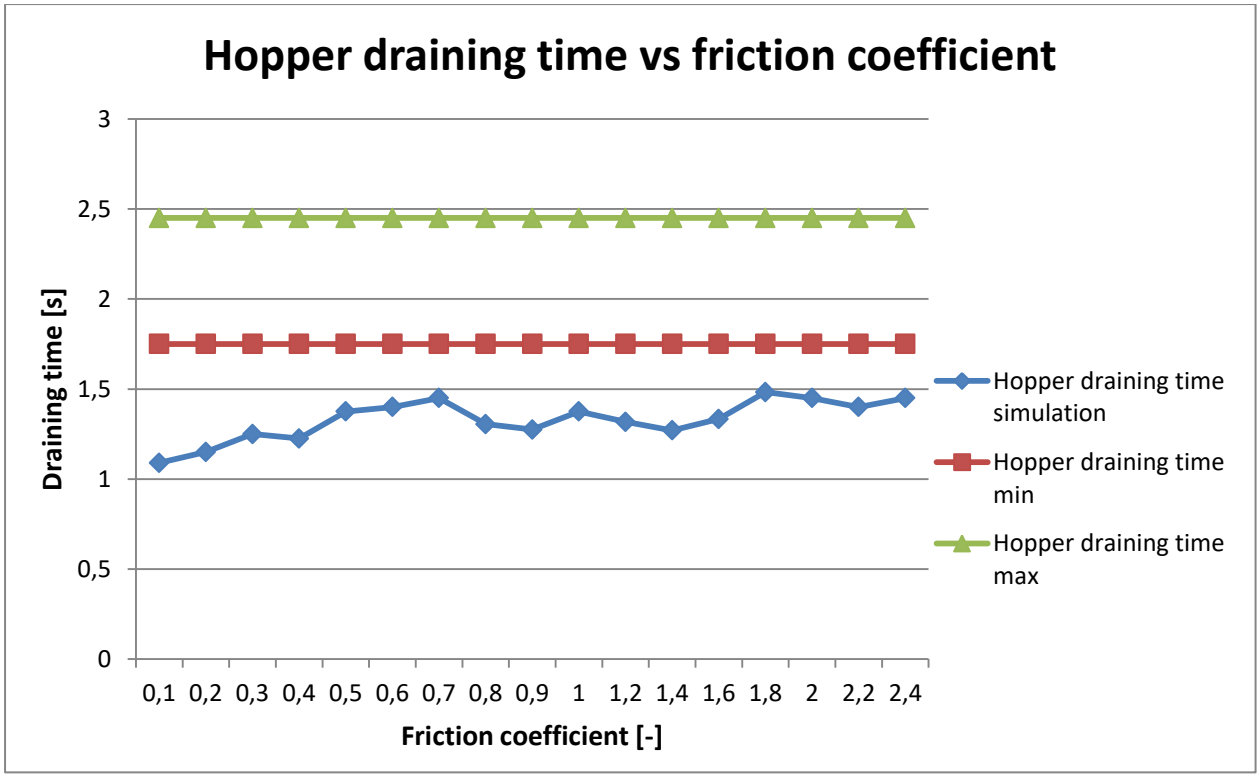

Figure 23 Simulated containment hopper draining time relative to experimental results

From the results illustrated in Figure 23 it is evident that the particle-particle static friction coefficient does have an effect on the hopper draining time. It was found that an increase in the particle-particle static friction coefficient resulted in an increase in the containment hopper draining duration. It was found that even though the draining time increased it did not match the minimum and maximum draining time band determined by the experimental tests. Upon further investigation, based on (Coetzee, 2017) and (Siemens Product Lifecycle Management Software Inc., 2018), it was determined that the hopper draining time could be increased by increasing the Young's modulus and coefficient of particle rolling resistance. It was decided not to adjust the Young's modulus in order to save on computational time, and to not adjust the coefficient of rolling resistance in order to prevent adding too many bulk calibration variables. It was determined by Figure 23 that the draining time predicted by the model matched the experimental tests within 0.3s when using a particle-particle static friction coefficient of 1.8 or 2. From Figure 22 it is evident that the hopper draining rate is almost linear and thus when this simulation is done on a larger scale the hopper draining time will not deviate further. Thus for the purpose of this study the containment hopper draining time deviation was deemed acceptable.

The second portion of the particle-particle static friction coefficient calibration was to analyse the angle of repose that the material formed at the bottom of the simulated test rig. This was

done by importing the image captured at the final time step (of each of the friction coefficient adjustment iterations) into a CAD program which allowed for an angle measurement to be obtained. Figure 24 illustrates a typical result that was obtained, and all of the results can be viewed under Appendix 4.

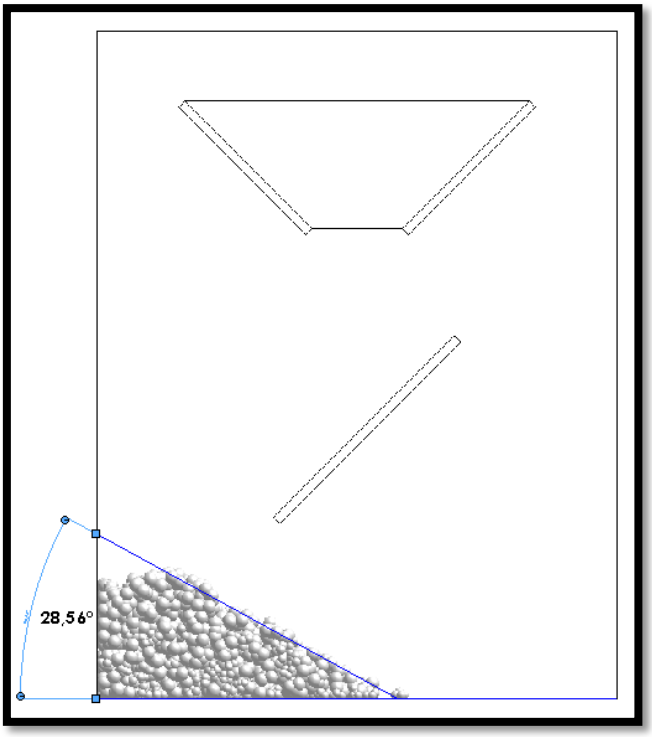

Figure 24 Angle of repose measurement taken from the simulation result of particle-particle static friction coefficient of 0.6

All of the measured angle of repose results were tabulated and plotted onto a graph. The experimental results were also included into the graph by generating a region between the minimum and maximum angle of repose measurements taken from the experimental tests. Figure 25 illustrate the angle of repose results obtained.

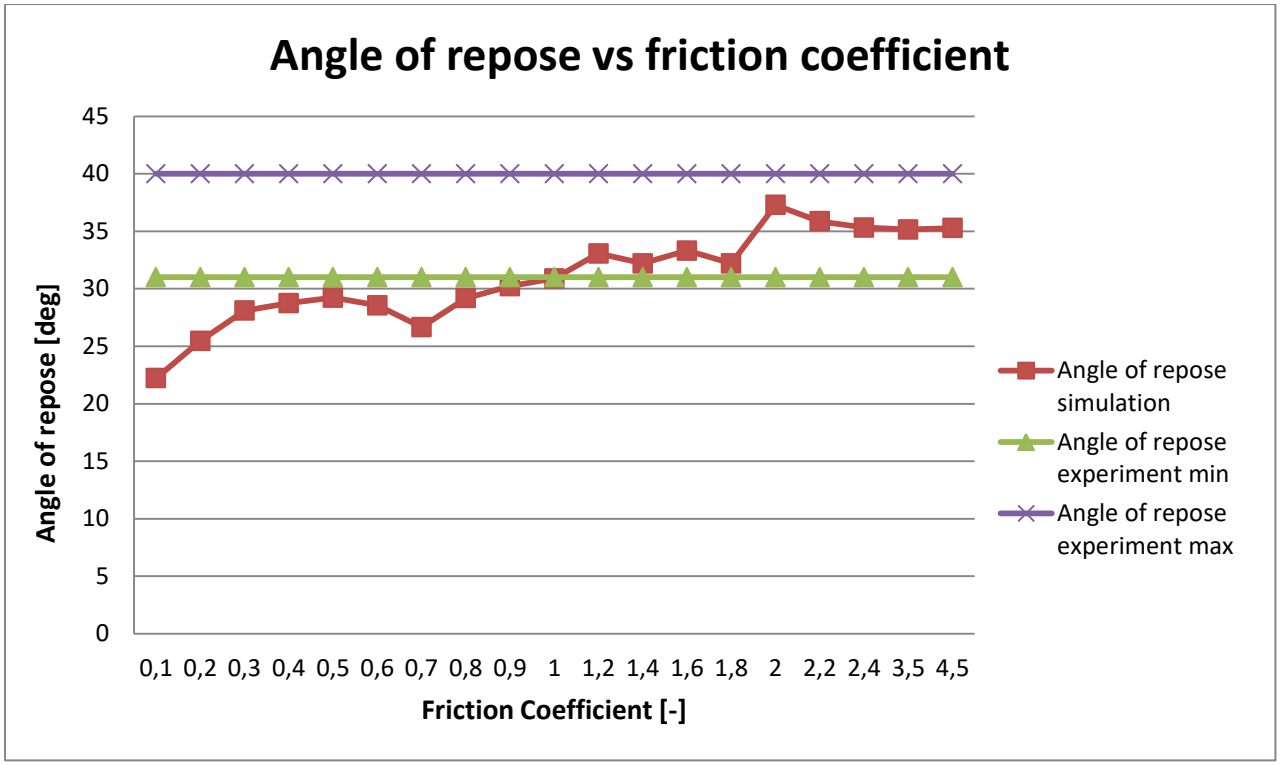

Figure 25 Simulated angle of repose results relative to experimental results

Figure 25 illustrates that the material settling angle of repose increases as the particle-particle static friction coefficient is increased. From literature it was stated that the angle of repose would start to flatten out which means that there is a point that the particle-particle static friction coefficient would have no further effect on the angle of repose (Coetzee, 2016). This statement was investigated further and it was found that this is due to the formulation of the tangential force component. It is evident from Equations 12 and 13 that when the particle-particle static friction coefficient is increased it will reach a point where the tangential contact force component is independent of the static friction coefficient. Therefore a point will eventually be reached where the tangential force stops increasing, resulting in a constant angle of repose. It was suspected that this point had been reached and it was decided to include an arbitrary particle-particle static friction coefficient of 3.5 and 4.5. It is illustrated by Figure 25 that this was indeed true, the trend flattened out after the static friction coefficient of 2. From Figure 25 it is evident that a particle-particle static friction coefficient of 1.2 to 4.5 will provide an angle of repose which matches the experimental results. By comparing the results generated by the hopper draining test and the angle of repose test it is evident that the particle-particle static friction coefficient of 2 matches the experimental results the best.

A further visual validation was done with all of the simulation input parameters set to Table 16's values and the particle-particle static friction coefficient of 2. The comparison between

the experimental high speed camera footage and the simulation model results are illustrated by Figure 26 and 27 respectively.

Figure 26 Experimental high speed camera footage analyses

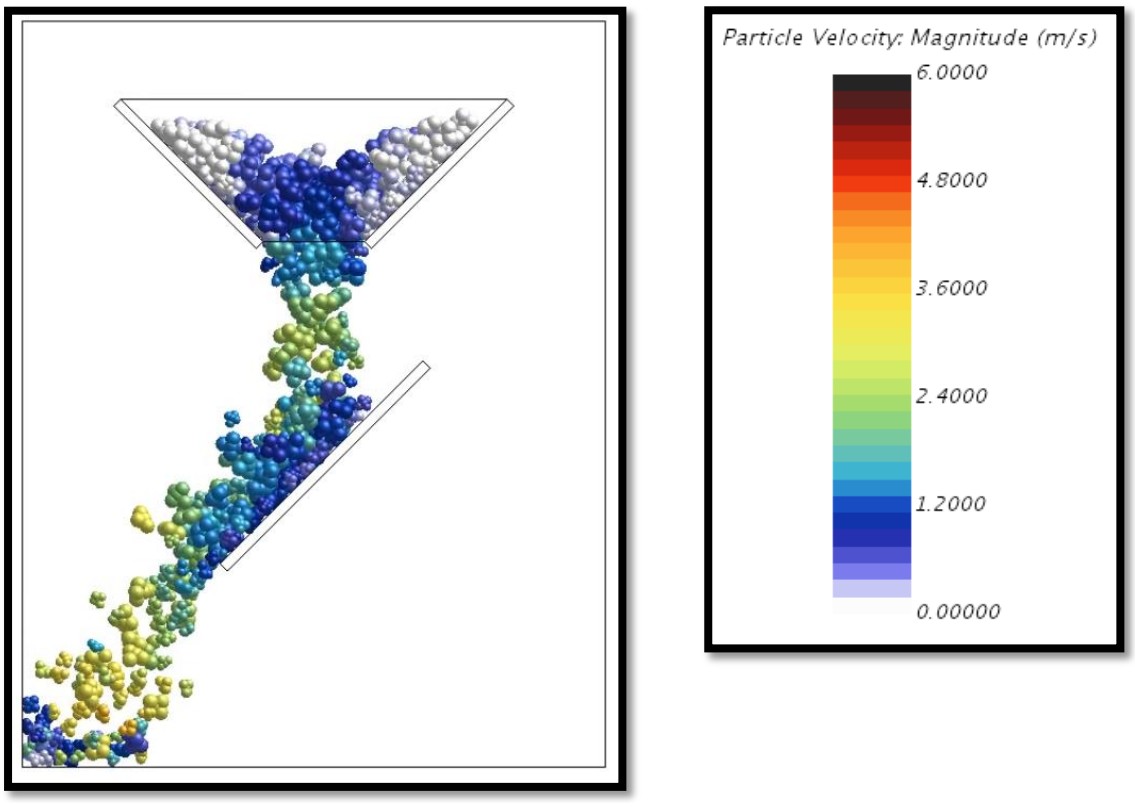

Figure 27 Simulated test rig result for particle-particle static friction coefficient of 2

When comparing Figures 26 and 27 it is evident that the model parameters selected produce a particle behaviour which closely resembles that of the actual material bulk behaviour. Firstly the material profile formed within the containment hopper (while draining) closely matches that of the experimental test. Both Figures 26 and 27 indicate that the material starts to drain from the centre, which is directly in line with the hopper trap door opening, causing a V-like shape in the material profile. Figure 27 illustrates that the V-like material profile is due to the material being stationary at the sides of the containment hopper, which only starts to drain when a sufficient amount of material has drained through the centre. As the material drop towards the deflection plate the particles tend to separate. This behaviour is present in both the experimental test and the simulation model. When the particles come in contact with the deflection plate the particle movement is dampened by the constant impact of particles falling from above. It is evident here that a small stationary zone is formed at the top of the deflection plate, and that the particles tend to roll of one another as they move down the deflection plate. The depth of material stream formed on the deflection plate also correlates between the experimental test and the simulated results. Finally the particles flow down to the test rig left bottom corner. Once again the particles tend to separated and the movement is dampened by the particles falling from above. As the simulation continues the particles settle and an angle of repose is formed which matches the experimental test results. Thus it can be concluded that the simulation parameters determined in Table 16 and a particle-particle static friction coefficient can be used for the subsequent simulations.

4.8. FINAL MODEL PARAMETER VALIDATION

As stated by Quist and Evertsson a final parameter validation has to be done whereby the test rig settings should be adjusted in order to verify if the simulation model still produces a similar result to that of the experimental test. For this validation it was decided to adjust the deflection plate to the extreme scenario of an angle of inclination of zero (deflection plate in the horizontal position). This angle of inclination was used because it is the furthest point from the initial calibration settings used, and would therefore be a clear indication if the model parameters are correct. The input parameters for the Simcenter STAR-CCM+ simulation model are tabulated in Table 17.

Table 17 Final validation Simcenter STAR-CCM+ simulation model input parameters

Simcenter STAR-CCM+ model input parameters	
General	
Parameter description	**Value**
Deflection plate inclination angle	0 degrees
Contact model	Hertz Mindlin
Coke particle	
Parameter description	**Value**
Density	1021.54 kg/m^3
Poisson's ratio	0.05
Young's modulus	100 MPa
Shape	Sphere triangular cluster
Size	35mm, 40mm and 60mm
Particle-particle normal restitution coefficient	0.3
Particle-particle tangential restitution coefficient	0.3
Particle-particle rolling resistance	0.001
Particle-particle static friction coefficient	2
Rubber boundary	
Parameter description	**Value**
Density	1100 kg/m^3
Poisson's ratio	0.45
Young's modulus	1 MPa
Particle-boundary normal restitution coefficient	0.6
Particle-boundary tangential restitution coefficient	0.6
Particle-boundary rolling resistance	0.001
Particle-boundary static friction coefficient	0.852

The experimental test was repeated 3 times and recorder with a high speed camera. The hopper draining time as well as the angle of repose formed on the deflection plate was measured. The results obtained from the experimental tests are tabulated in Table 18 and 19 respectively and the settling angle formed is illustrated by Figure 28.

Table 18 Containment hopper draining duration for final validation

Containment hopper draining duration for final validation	
Test number	**Time**
1	1.588 s
2	1.75 s
3	2.05 s

Table 19 Material settling angle of repose for final validation

Material settling angle of repose for final validation		
Test number	**Left side angle of repose**	**Right side angle of repose**
1	46 degrees	36 degrees
2	45 degrees	34 degrees
3	42.7 degrees	36 degrees

Figure 28 Validation test experimental angle of repose formed

The simulation model run was also repeated three times with the random injector filling the containment hopper for each of the iterations. One of the results obtained in the validation process is illustrated by Figure 29.

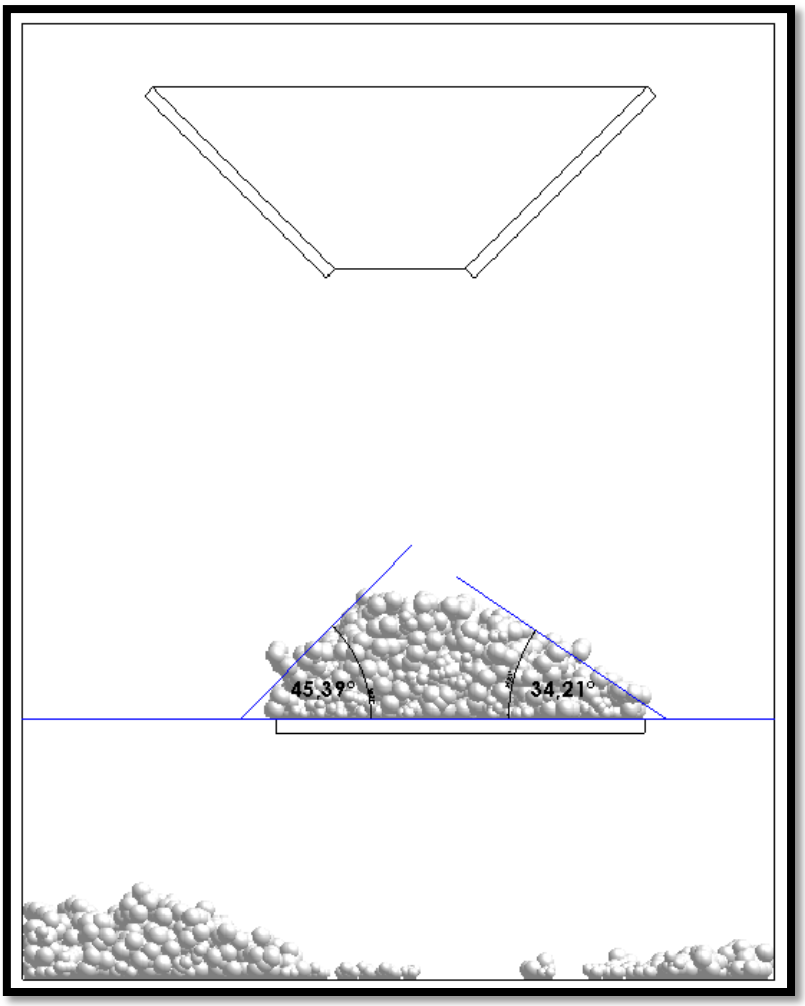

Figure 29 Validation test simulated angle of repose formed

The simulated hopper draining time was plotted against the region between the minimum and maximum hopper draining time obtained from the experimental tests, and is illustrated by Figure 30. The simulated settling angle of repose (for the left and right side of the deflection plate) was also plotted against the region between the minimum and maximum settling angle of repose obtained from the experimental tests, and is illustrated by Figure 31 and 32.

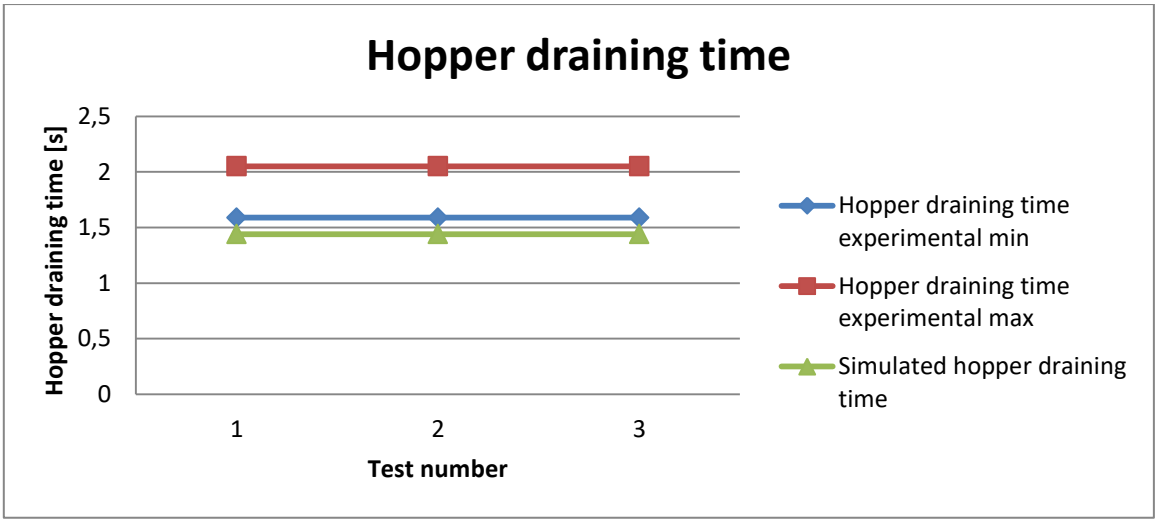

Figure 30 Final validation hopper draining time evaluation

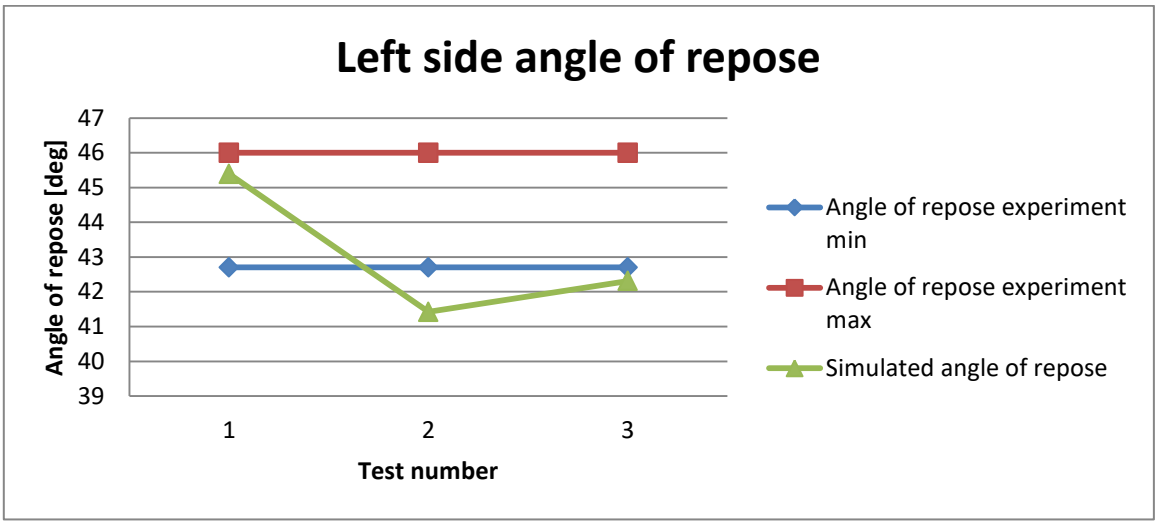

Figure 31 Final validation left side angle of repose evaluation

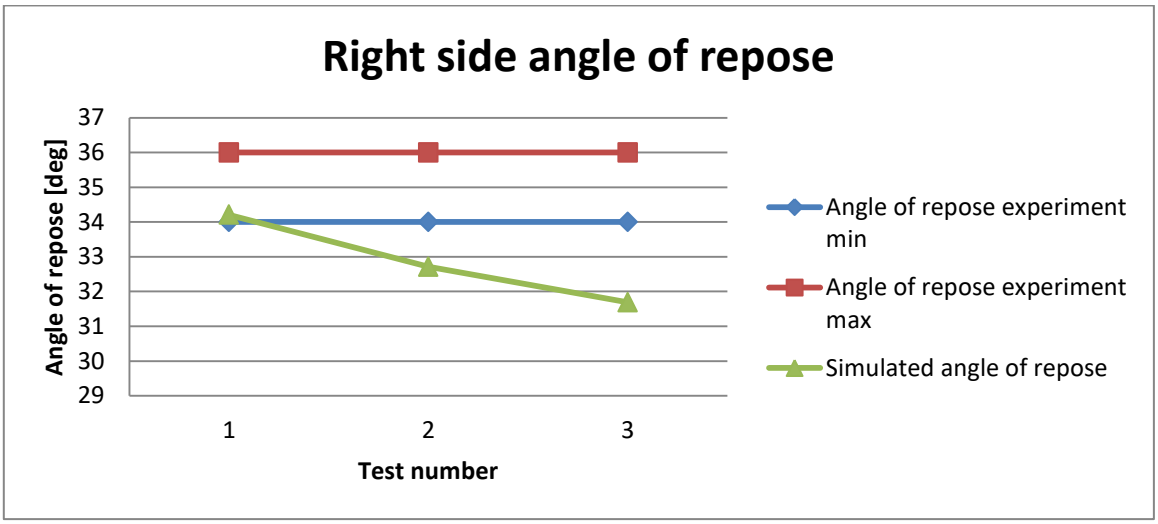

Figure 32 Final validation right side angle of repose evaluation

An average value was calculated for the experimental and simulated hopper draining and angle of repose results. The deviation between these results was then calculated in order to determine if the simulation parameters are acceptable for the next phase of simulation. These results are tabulated in Table 20.

Table 20 Validation test results assessment

Validation test results assessment	
Angle of repose experiment left side avg.	44.57 degrees
Simulated left side angle of repose avg.	43.04 degrees
Deviation between experimental and simulated	-3.55%
Angle of repose experiment right side avg.	35.33 degrees
Simulated right side angle of repose avg.	32.87degrees
Deviation between experimental and simulated	-7.49%
Hopper draining time experimental avg.	1.80 s
Hopper draining time simulated avg.	1.44 s
Deviation between experimental and simulated	0.36 s

It is clearly illustrated by Figure 28 and 29 that the simulation model produced a similar material settling angle of repose to that of the experimental tests. The material profile on top of the deflection plate as well as the material on the test rig bottom plate corresponds well with the experimental results. The results tabulated in Table 20 also illustrate that the simulation model produced and angle of repose which is only 3.55% lower on the left side and 7.49% lower on the right side of the experimental results. The hopper draining time deviation was calculated at 0.36 s which corresponds with the findings in section 4.7.3 and was deemed acceptable. It was therefore decided that the simulation parameters determined by the calibration process are acceptable for the next step in the simulation process.

4.9. CONCLUSION

In this chapter a combination of the direct calibration and bulk calibration approaches were used to calibrate the material parameters for the Hertz Mindlin contact model. The direct measuring approach was used for the calibration of particle size, shape, density and boundary friction coefficients. Some of the parameters (Young's modulus, Poisson's ratio, particle coefficient of restitution and rolling resistance) of the contact model were obtained from research articles and some were used as default values from Simcenter STAR-CCM+.

This was done due to the testing facilities available. A test rig was built for the bulk calibration approach according to the calibration work done by Quist and Evertsson. The test rig was used for the calibration of the particle-particle static friction coefficient and the boundary coefficient of restitution. The test rig was also used for the final parameter validation and it was determined that the calibration process was applicable in producing a simulation result, which matched the experimental result (obtained from high speed camera footage). The next chapter will focus on the development of a steep incline sidewall conveyor simulation model.

5. STEEP INCLINE SIDEWALL CONVEYOR SIMULATION

Chapter 4 reported on the required material parameters for the DEM simulation. The focus now will be on the development of the steep incline sidewall conveyor simulation. The plant equipment geometry and layout are assessed along with the plant operational sequence. Simulation meshing requirements are also discussed in order to allow for the required equipment movement. The validation between the actual steep incline sidewall conveyor loading and the DEM simulation model was done with the use of high speed camera footage. The layout requirements and results obtained from the high speed camera footage are discussed in this chapter. The final validation between the simulation results and the high speed camera footage is also discussed, and furthermore, to determine if the DEM simulation is capable of simulating the loading of a steep incline sidewall conveyor.

5.1. PLANT LAYOUT AND OPERATIONAL ANALYSES

The steep incline sidewall conveyor loading section consists of two conveyors build in a mirror image of one another. This is evident from Figure 33 which is a section view of the two conveyors from the as built drawings. When taking a look at Figure 33 it has to be noted that the top portion is the loading portion and moves into the page while the bottom portion is the return side of the belt which is moving out of the page. There are also side skirting structures installed between the discharge chute and the sidewall of the steep incline conveyor. The purpose of these side skirting structures are to contain as much of the material particles at the loading interface when particles jump from the belt. It was determined that these side skirting plates were not effective, because material spillages were still reported at the loading points of the steep incline sidewall conveyor. It should be noted that the side skirting structures were not included in the simulation model due to the high speed camera setup constraints and will be discussed further in later sections.

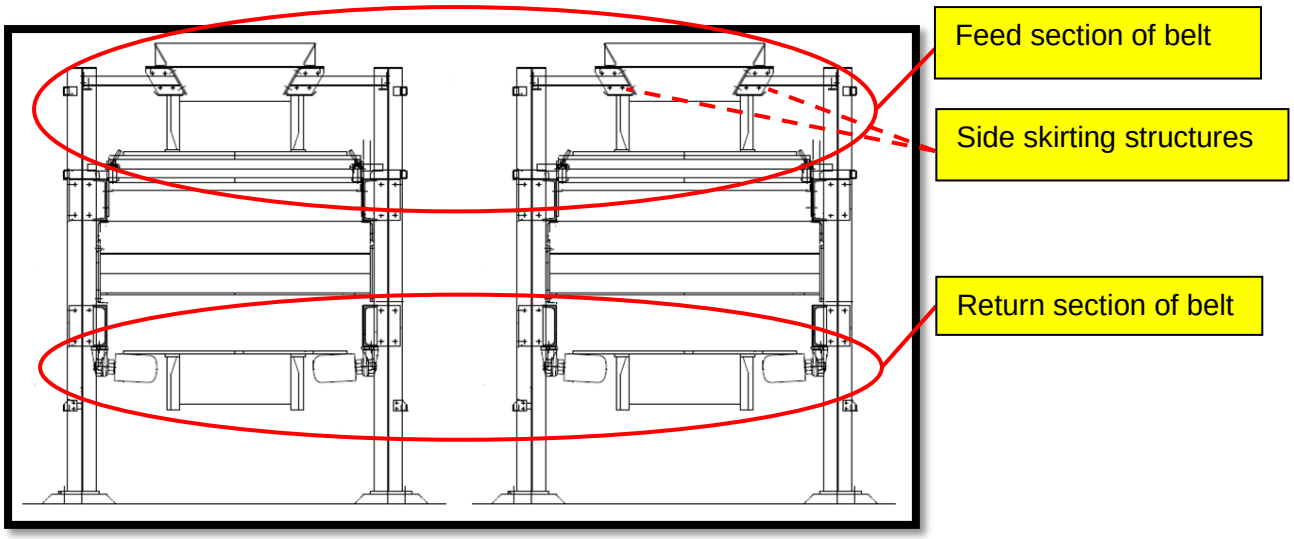

Figure 33 Section view of the two steep incline sidewall conveyors

The operational strategy between the two belts is such that one belt operates while the other belt is isolated. This is done so that the plant can do maintenance on one belt while the plant is still in operation. It is due to this reason that it was decided to only include one belt into the simulation model.

The loading is done on the steep incline sidewall conveyor via three surcharge hoppers. The surcharge hopper closest to the tail pulley is designated for the ore and additive material. Following the moving direction of the belt the next surcharge hopper would be the coke surcharge hopper followed by the sinter surcharge hopper. These sections are illustrated by Figure 34.

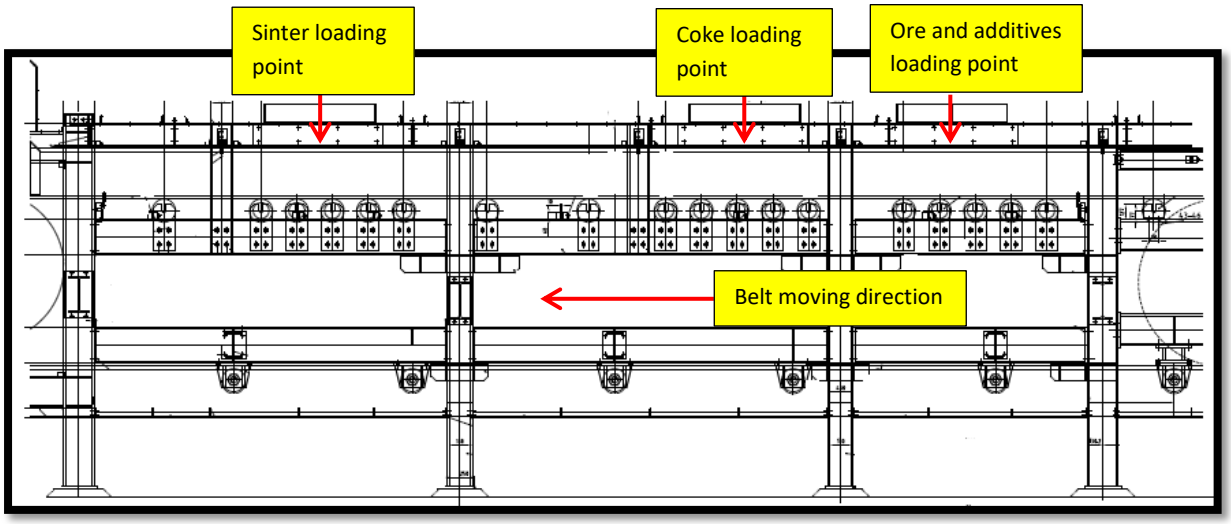

Figure 34 Surcharge hopper layout of the steep incline sidewall conveyor loading point

The charging sequence that is followed by the plant is as follow:

1. Coke material is loaded into the coke surcharge hopper from the raw material bunkers while the surcharge hopper discharge gate is in the closed position.
2. The furnace top would then send a command for the coke surcharge hopper to start discharging.
3. The coke surcharge hopper discharge gate would then be moved via a hydraulic cylinder to the charging position which is controlled via a limit switch. As the discharge gate opens the coke material would start to flow and the coke is discharged onto the moving steep incline sidewall conveyor.
4. While the coke is discharging from the coke surcharge hopper, the sinter surcharge hopper is filled from the raw material bunkers.
5. After the coke surcharge hopper has been drained completely (and the scale reads zero for a few seconds) the discharge gate will move back to the closed position.
6. The furnace top would then send a command to the sinter surcharge hopper to start discharging.
7. The sinter surcharge hopper discharge gate would then be moved via a hydraulic cylinder to the charging position which is controlled via a limit switch. As the discharge gate opens the sinter material would start to flow and the sinter is discharged onto the moving steep incline sidewall conveyor.
8. At a specific time during the sinter material discharge, the command is given for the ore and additive material to discharge.
9. The ore and additives surcharge hopper discharge gate is opened and the ore and additive are discharged directly from the raw material bunkers without first filling up the ore and additive surcharge hopper.
10. At this point it should be noted that the ore and additives and sinter material are discharged simultaneously.
11. While the sinter and the ore and additives are discharged the coke surcharge hopper is once again filled from the raw material bunkers.
12. After the sinter surcharge hopper has been drained completely (and the scale reads zero for a few seconds) the discharge gate will move back to the closed position. The ore and additives would still continue to discharge until all of the necessary charging weights have been met. The ore and additive discharge gate would then also move back to the closed position.
13. As the stock line level drops in the furnace the furnace top would send a signal for the coke material to discharge and the entire sequence is repeated.

From the charging sequence discussed above it is evident that the sinter and ore and additive discharge mechanism is complex due to the fact that these materials not only interact with the steep incline sidewall conveyor but also interact with each other. Due to this it was decided to only evaluate the coke material discharging mechanism, and if successful, the simulation of the sinter and ore and additives can be included in later studies.

Taking a closer look at the coke surcharge hopper layout it was found that the coke surcharge hopper was divided into three main segments. The total volume obtained by the coke surcharge hopper installation (adding the three segments together) is 39 m^3. It was noticed here that the total hopper discharge flow was controlled via the discharge gate, which meant that when the gate is in the fully open position a steady state discharge condition would be obtained. It was due to this observation that it was decided to not include the entire surcharge hopper into the simulation. This was done because the total volume of material would not have an influence on the discharge result just as long as there is sufficient material simulated so that the steady state condition can be maintained. Figure 35 illustrates the coke surcharge hopper segment that would be included into the simulation.

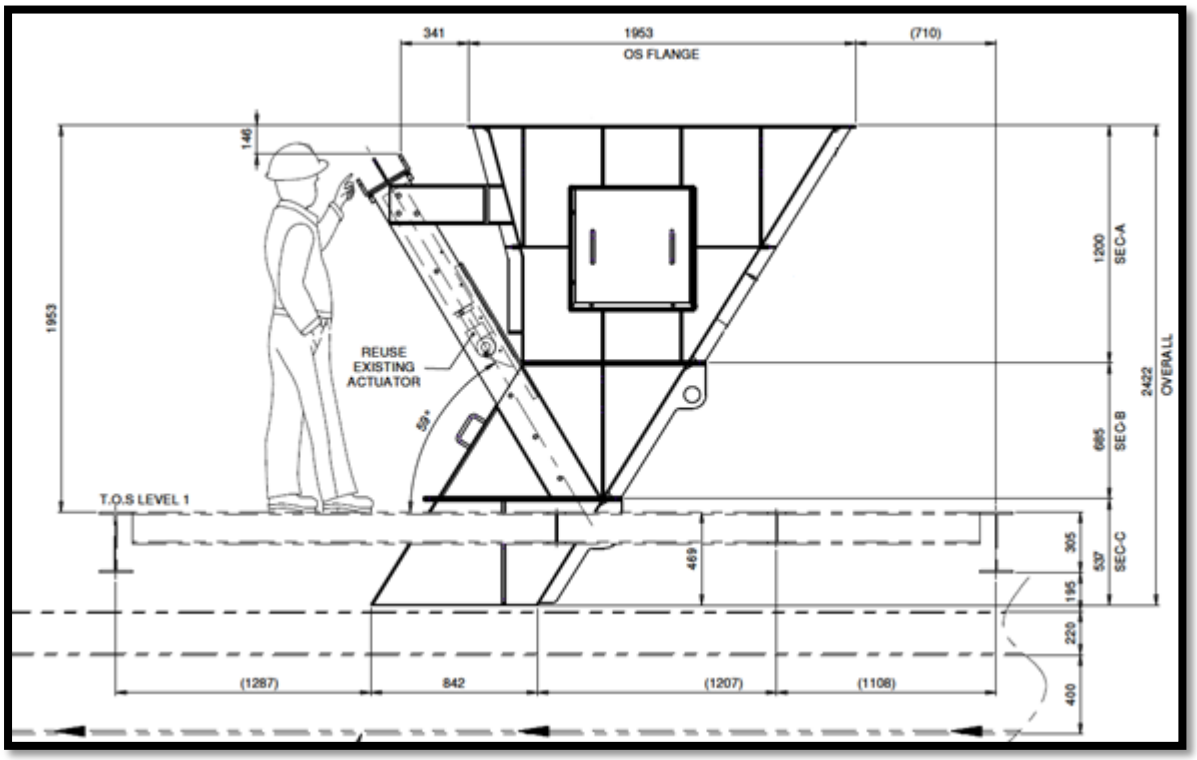

Figure 35 Drawing of coke surcharge hopper included into the simulation model

5.2. GEOMETRY MODELLING

After the plant operation and general equipment layout was assessed the individual equipment geometry could be analysed. This had to be done in order to determine how the geometry will be simulated and how many different regions will be required for the model. It is therefore necessary to understand how Simcenter STAR-CCM+ defines regions and how the geometry is represented within a region.

A region within Simcenter STAR-CCM+ is defined as a volume domain in space which is completely surrounded by boundaries as illustrated by Figure 36.

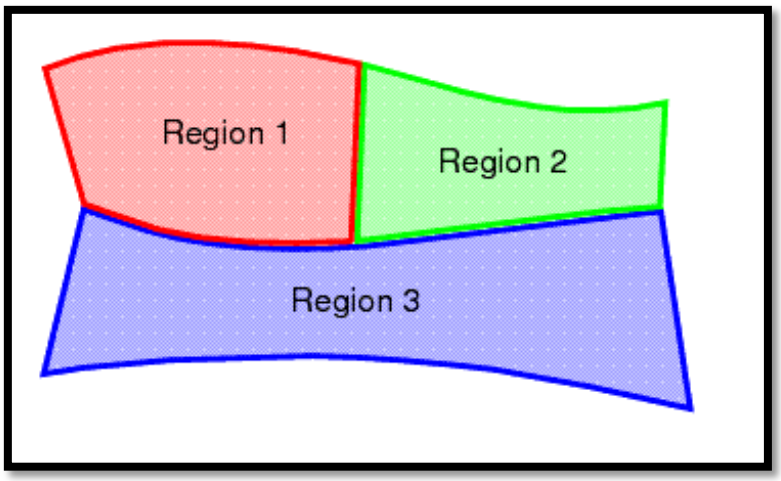

Figure 36 Illustration of a region layout (Siemens Product Lifecycle Management Software Inc., 2018)

The boundaries surrounding the regions can either be part related (pipe wall surrounding internal flow) or user related (volume of air surrounding a building). For example if the flow around a car is analysed the car body will not be the boundary of the region but rather the outside limits of the volume of air surrounding it. Therefore it can already be seen that for the simulation of the steep incline sidewall conveyor there will be three distinct regions:

1. The region surrounding the steep incline sidewall conveyor.
2. The region within the surcharge hopper where particles will be injected.
3. The region enveloping all of the parts which will represent the atmosphere surrounding all of the equipment.

The parts (hoppers, chute and conveyor) form part of the regions and are also surrounded by the regions. Simcenter STAR-CCM+ subtracts the geometry of a simulated part from a region in order to form a cavity within the region. This is done because the simulation is based on the interaction between the volume surrounding the part and the walls generated

by the part and not necessarily the part structure itself. It is evident here that the geometry of the part has to be simulated accurately, because if there are discrepancies between the simulated geometry and the actual geometry an accurate result generated from the interaction calculations will not be obtained. Therefore as built drawings and plant measurements were taken of the equipment and the layout of the equipment in order to ensure an accurate representation of the plant layout.

5.2.1. STEEP INCLINE SIDEWALL CONVEYOR BELT GEOMETRY MODELLING

Firstly taking a look at the geometry of the steep incline sidewall conveyor it can be noted from Figure 37 that there are three main elements of detail that have to be included into the simulation. These are the sidewalls, cleats (buckets) and base belt.

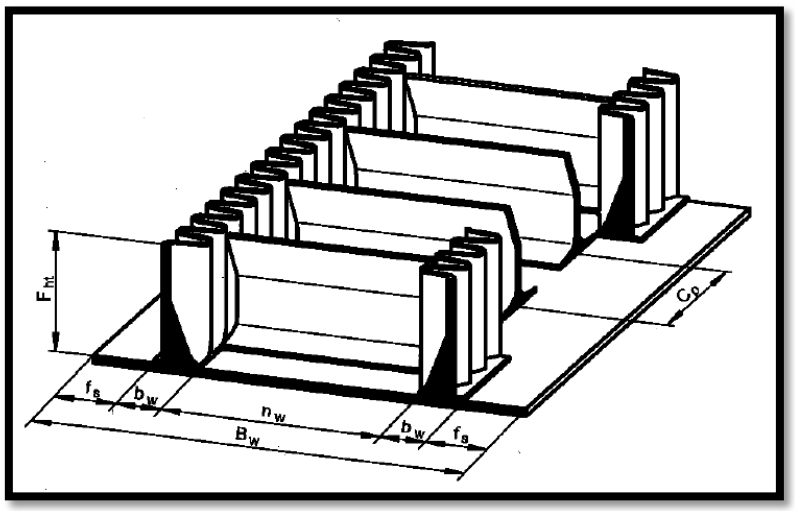

Figure 37 Section view of steep incline sidewall conveyor detail

The sidewall section of the belt is made up of convoluted rubber. It was decided to include these convolutes into the geometry because these convolutes increase the contact surface area of the sidewalls. This means that there is a greater surface for the particles to come in contact with if the particles were to move over the top portion of the sidewall.

The cleat portion of the belt (also referred to as the buckets) has a distinctive angle associated with it. This angle is designed such that when the steep incline sidewall conveyor starts rotating from a horizontal position to a vertical position, the material on the belt will not slide or spill form the belt. Therefore these angles were measured so that an accurate representation of the cleats could be included into the model.

It was also decided to only simulate the horizontal section of the belt. This was done because the aim of the simulation was to evaluate the loading interface of the steep incline sidewall conveyor. Due to the fact that the loading only takes place while the belt is in the horizontal position, there was no need to simulate the rotation of the belt to the vertical position.

The steep incline sidewall conveyor belt had to be simulated such that each of the cleats were to translate individually through the loading interface, which meant that an overset mesh had to be generated (which will be discussed in a later section of this report). The overset mesh required a fine mesh due to the small clearances associated with the equipment, which meant that a limitation had to be placed on the simulated conveyor length. The limitation was required here because if the length of the belt were to be increased, the number of cells within the mesh would increase which would result in additional computational time required. Therefore in order to reduce computational time the belt length was limited to a length which would just be able to contain the simulated material. This means as soon as the hopper has finished discharging the material, the belt length would be finished.

With all of the above mentioned factors in consideration a 12,7m section of belt was simulated in a 3D CAD environment. Figure 38 illustrates the result obtained.

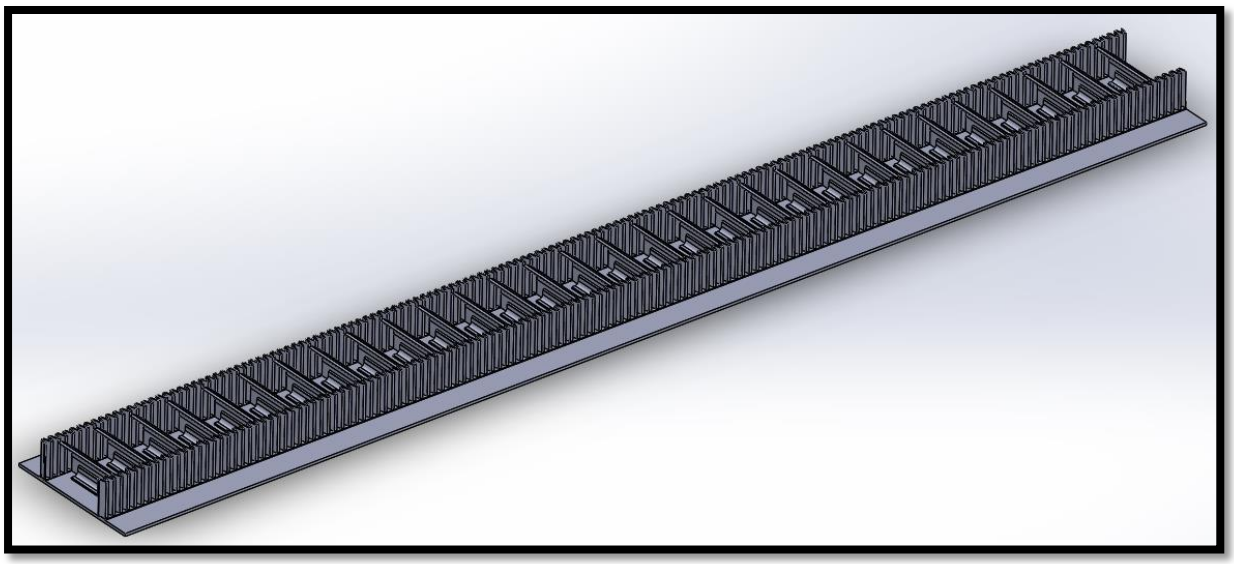

Figure 38 Steep incline sidewall conveyor simulated geometry

5.2.2. COKE SURCHARGE HOPPER AND GATE GEOMETRY MODELLING

In section 5.1 it was stated that it is not necessary to simulate the entire surcharge hopper volume due to the fact that a steady state material flow condition is reached when discharging. This meant that a size limitation could be placed on the surcharge hopper like it was done with the steep incline sidewall conveyor.

It was stated in section 5.1 that only the bottom third of the surcharge hopper would be included into the simulation as illustrated by Figure 35. This was validated by firstly calculating the internal volume of the bottom third of the coke surcharge hopper. The maximum hopper discharge rate was stated to be 450 t/h worth of coke. This material flow rate was converted from tons per hour to cubic meters per hour with the use of the bulk density calculated in section 4.3.2 and then converted to cubic meters per second. The hopper draining time (in seconds) could then be calculated by dividing the simulated hopper volume with the volumetric material flow rate. The results of this analysis are tabulated in Table 21.

Table 21 Bottom third of surcharge hopper geometry size validation

Hopper geometry size validation	
Bottom third of surcharge hopper volume	1.415 m^3
Maximum hopper draining rate	450 t/h
Bulk density of coke	0.428 t/m^3
Maximum hopper volumetric draining rate	0.292 m^3/s
Duration of bottom third of surcharge hopper draining	4.85 s

From Table 21 it was calculated that an approximate 4.85s of coke discharge time would be simulated if only the bottom third of the surcharge hopper were to be used. This amount of time does not seem like much but taking into consideration that the steep incline sidewall conveyor moves at a speed of 2.2m/s a total length of 10.67m of conveyor will be filled with material. This also means that a total of 26 cleats (buckets) will pass through the loading interface. It was therefore concluded that the bottom third of the surcharge hopper would be sufficient for the simulation model.

After determining the size of the simulated surcharge hopper the next point of evaluation was done on the detail that would be included into the geometry. There are three main areas of detail associated with the surcharge hopper, one being the inclination angles of the

hopper, two being the liner material on the inside of the hopper and the third being the discharge gate mechanism.

The inclination angles were taken from the as build drawings and verified on site. A representation of the hopper was simulated with the use of 3D CAD software for the hopper as depicted in Figure 35.

The liner material of the surcharge hoppers are individual tiles that are glued to the hopper steel. From an internal inspection it was noted that the tiles are placed so close against each other that there are no cavities formed. This meant that the individual tiles did not have to be simulated, but that a continuous surface could be used to simulate the increase in hopper thickness caused by the liner material. It was thus decided that the hopper wall thickness could be simulated as one material which included the hopper steel plates and liners.

It was stated in section 5.1 that the flow of the coke from the surcharge hopper is controlled via a hydraulically operated discharge gate. This gate installation is illustrated by Figure 39.

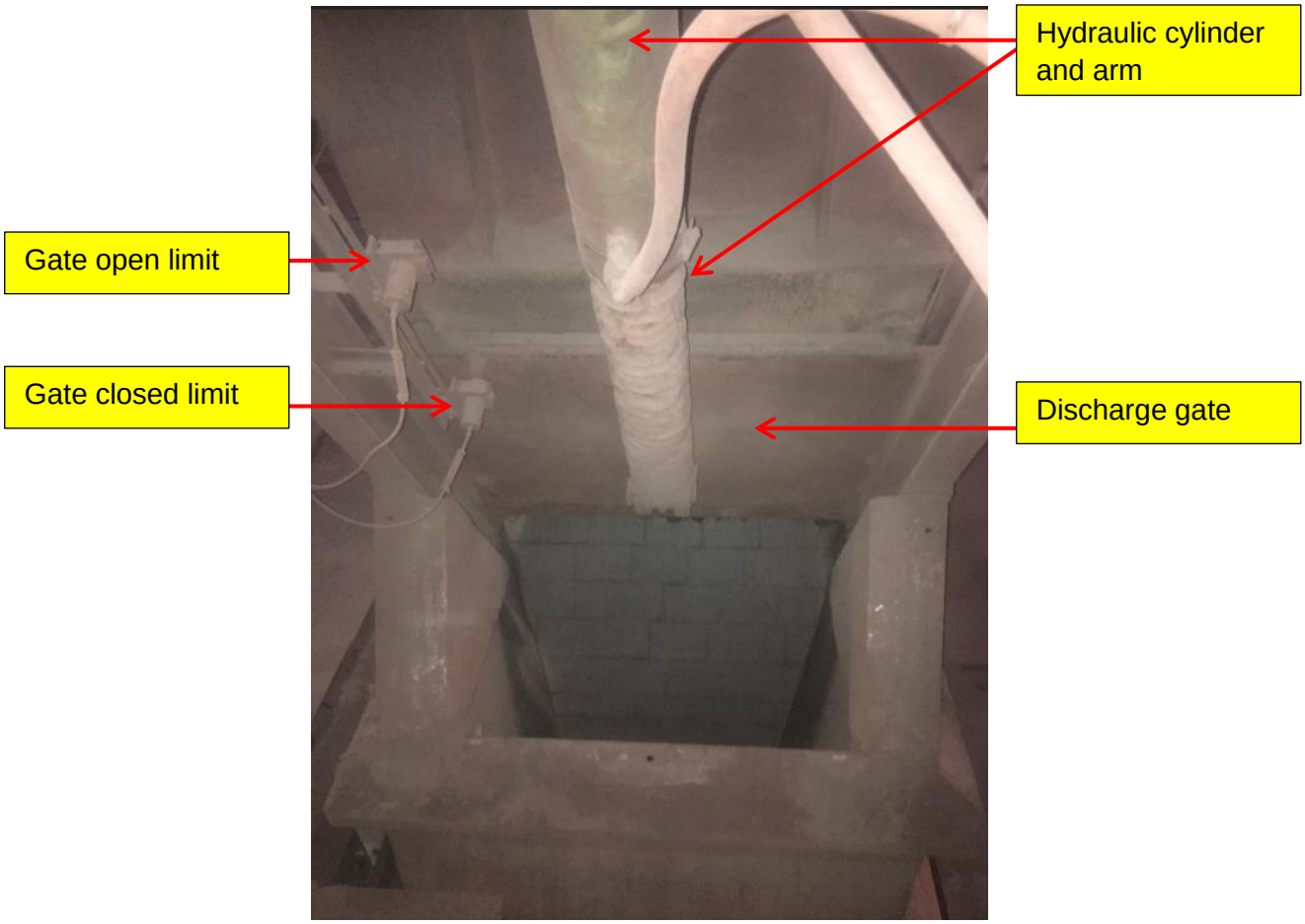

Figure 39 Coke discharge gate installation

The detail associated with the opening and closing of the gate was deemed irrelevant. In order to simulate this movement an additional overset mesh had to be included in the simulation which would result in greater computational time. This was excluded because the statement of the steady state material flow still holds. When the gate reaches the fully open position it remains in this position until all of the material is drained. Therefore a constant discharge rate is maintained (if no material property deviations are experienced). Thus for the geometry simulation only the gate angle and the distance of the gate opening (when in the fully open position) was of concern. Figure 40 illustrates the final coke surcharge hopper arrangement which was included into the simulation model.

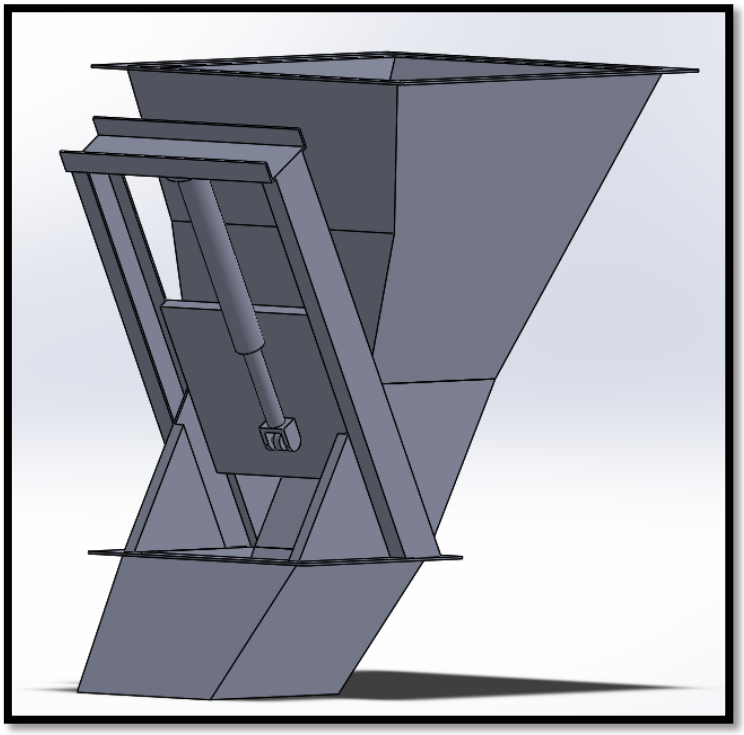

Figure 40 Coke surcharge hopper simulated geometry

5.2.3. REGION SELECTION

With all of the part geometries and layout completed the next step was to set up the simulation regions. It was previously stated that three separate regions would be required.

1. The region surrounding the steep incline sidewall conveyor.
2. The region within the surcharge hopper where particles will be injected.
3. The region enveloping all of the parts which will represent the atmosphere surrounding all of the equipment.

The first region was set up as a block surrounding the steep incline sidewall conveyor. This region can be seen as the section of atmosphere surrounding the steep incline sidewall conveyor which will be used to simulate the motion of the conveyor. This means that with each time step taken in the simulation model this region will move in the belt direction in order to simulate the belt movement. The pink highlighted section in Figure 41 illustrates this region.

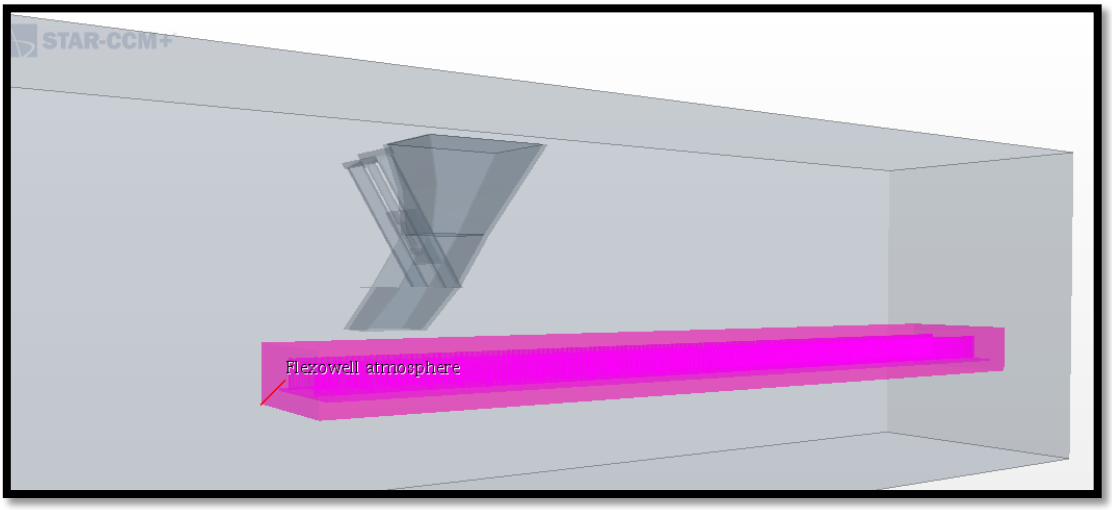

Figure 41 Illustration of the region surrounding the steep incline sidewall conveyor

The second region was set up as a volume inside the coke surcharge hopper. This region was required in order to provide a specific volume within which particles could be injected. Therefore this region allowed for a random injector to be set up so that the coke particles could be injected according to the size distribution and porosity required. The pink highlighted section in Figure 42 illustrates the region associated with the particle injection.

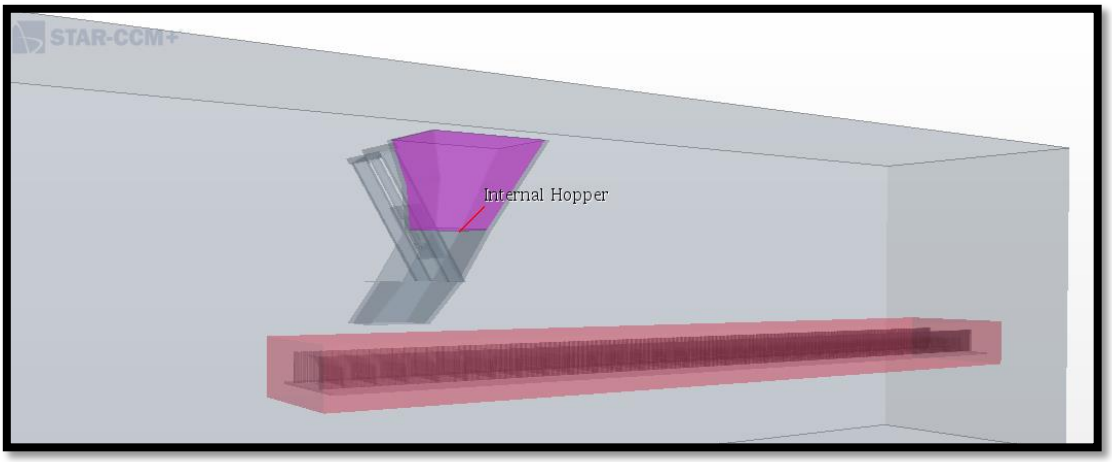

Figure 42 Illustration of particle injector region

The final region required was for the total simulation boundary. This region is required in order to contain all of the separate elements within the simulation model. It could also be seen as the atmosphere surrounding all of the simulated components. The size of this region was determined by the size of the steep incline sidewall conveyor that was simulated. This means that this region had to be a minimum of two times bigger than the steep incline sidewall conveyor in order to allow for the full length of conveyor to move through the loading interface. This region is illustrated by the grey block surrounding all of the other equipment in Figure 43.

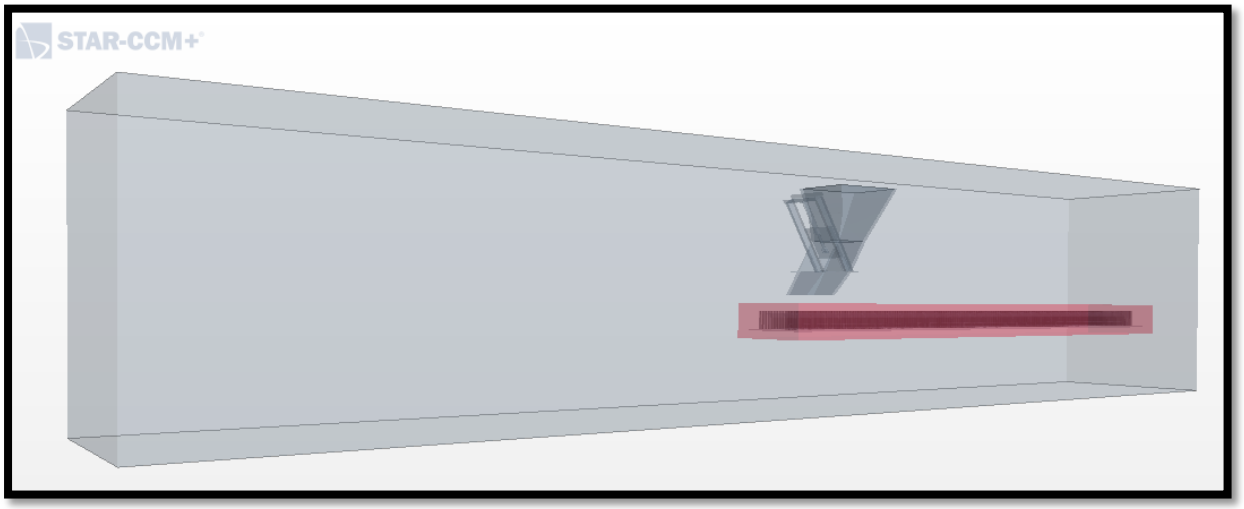

Figure 43 illustration of the atmosphere region

5.3. MESHING

The mesh generation for the steep incline sidewall conveyor was an important section of the modelling process. This is due to the fact that there would be movement associated with the steep incline sidewall conveyor cleats. Normally conveyors are simulated by assigning a velocity to a flat plane which would result in a velocity transfer to a simulated particle when it comes in contact with the plane. By following this approach there is no physical movement of the parts within the model and the particles react when interacting with the boundaries (conveyor surface). If this approach were to be used for the steep incline sidewall conveyor the cleats would not move and the material particles would only interact with one cleat and would possibly start to build up. This would not be an accurate representation of the loading interface of the steep incline sidewall conveyor, and movement is thus critical to the result.

Simcenter STAR-CCM+ has an option that allows the user to generate a mesh that would move through the background mesh (at a specific user defined velocity) with every time step. This is known as an overset mesh. The overset mesh is assigned to a specific region that

will be assigned to a specific movement. In order for the overset mesh region to pass through the background region an interaction has to take place between the two neighbouring cells (new cell associated with the moving region and old cell associated with the background mesh). Simcenter STAR-CCM+ conducts a hole cutting process where a hole is cut in the background region at the overset interface in order to allow for the overset region coupling. For the coupling to occur there has to be donor cells as well as acceptor cells. Donor cells are normally associated with the background mesh and the acceptor cells are associated with the overset mesh. The set of donor cells depends on the interpolation option that is chosen and on the number of active cells in the donor region around the acceptor cell centroid. There are three interpolation options that can be chosen:

1. Distance-weighted interpolation.
2. Linear interpolation.
3. Least squares interpolation.

For the simulation of the steep incline sidewall conveyor belt it was decided to choose the linear interpolation option. This was done due to the fact that it is described as the most accurate with regards to moving meshes (Siemens Product Lifecycle Management Software Inc., 2018). A typical example of testing if the overset mesh is correctly coupled to the background region is to determine if there is an interaction between the two. It is stated in the Simcenter STAR-CCM+ user guide that there has to be a section of cells surrounding the overset mesh which is the acceptor cells. It is not allowed for the donor cells to be directly in contact with the inactive cells (overset region cells). Figure 44 illustrates a typical example of the distinction between the active cells (background), acceptor cells and the inactive cells (overset region cells).

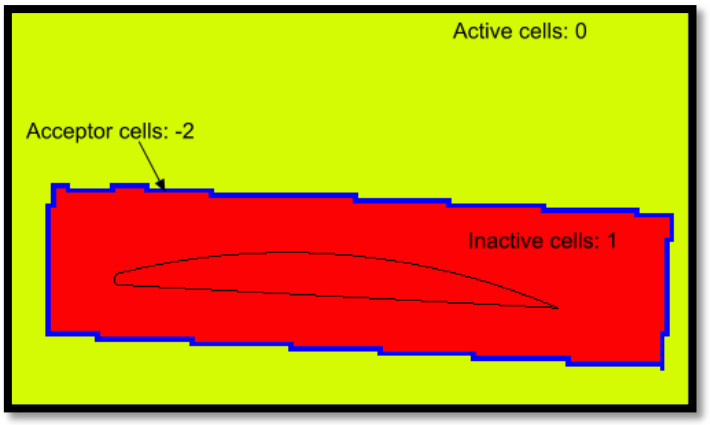

Figure 44 Overset mesh cell coupling illustration (Siemens Product Lifecycle Management Software Inc., 2018)

Simcenter STAR-CCM+ provides some guidelines in order to assist with the type of mesh that has to be chosen as well as the cell size selection when using the overset mesh option. Firstly the maximum cell size is determined by how close a wall (part surface) is to the boundary of the overset mesh region. It is recommended by Simcenter STAR-CCM+ that there should be a minimum of 4 cells between a wall and the overset region boundary in both the overset region as well as the background region. This means that if the overset region boundary is drawn close to a specific part wall, the cell size will be small to allow for 4 cells to fit between the region boundary and the part wall. Thus the bigger the distance between the part wall and the overset mesh boundary the bigger the cell size can be.

Another recommendation that is made by the Simcenter STAR-CCM+ user guide is that the size and shape of the mesh should be the same in the overlapping region of the overset mesh. This means that the size of the mesh in the background region should match the size of the mesh on the overset region for at least the overlapping portion (blue cells in Figure 44) at the overset interface.

Taking these recommendations into consideration it was decided to use the trimmer mesh for the simulation of the steep incline sidewall conveyor model. The trimmer mesh is based on a square shape which is sub divided as it is required to decrease the mesh cell size. The trimmer mesh also allows for the cells to line up which would allow for accurate interpolation of the overset mesh movement. Figure 45 illustrates the trimmer mesh layout.

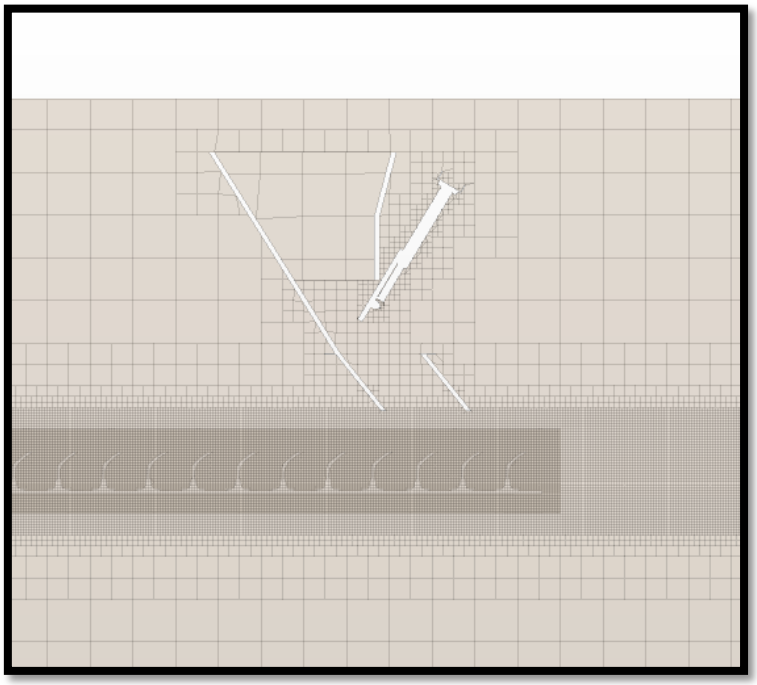

Figure 45 Illustration of the trimmer mesh selected for the steep incline sidewall conveyor simulation

The cell size of the trimmer mesh was determined by the distance between the top of the sidewall (of the steep incline sidewall conveyor) and the bottom of the coke surcharge hopper chute. Following the guideline of maintaining a minimum of 4 cells in both the overset and background regions an additional mesh criteria was assigned to the volume around the overset mesh and the bottom of the discharge chute. The cell size in this volume was made sufficiently small in order to allow for the minimum cell number required. Figure 46 illustrates this cell refinement.

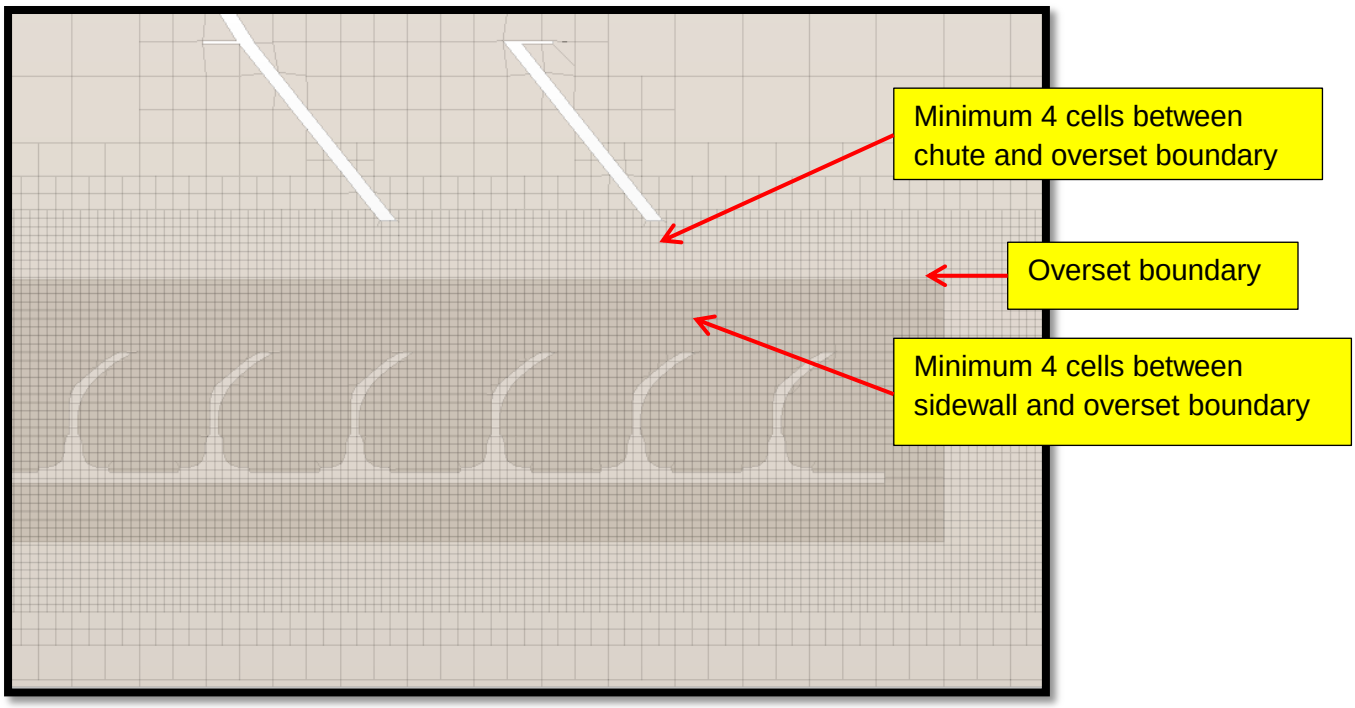

Figure 46 Illustration of mesh cell size refinement

The final check done on the overset mesh was to determine if the coupling between the overset mesh region and the background region was done correctly. This was done in a similar manner as described by Figure 44 to determine if there is an overlapping section of acceptor cells between the background region and the overset region. Figure 47 and 48 illustrate the result obtained. It can be seen that the donor cells are not in direct contact with the inactive cells and that there is a section of acceptor cells surrounding the inactive cells. Figure 47 and 48 correspond with the guideline stipulated by Figure 44 and the coupling was therefore deemed correct.

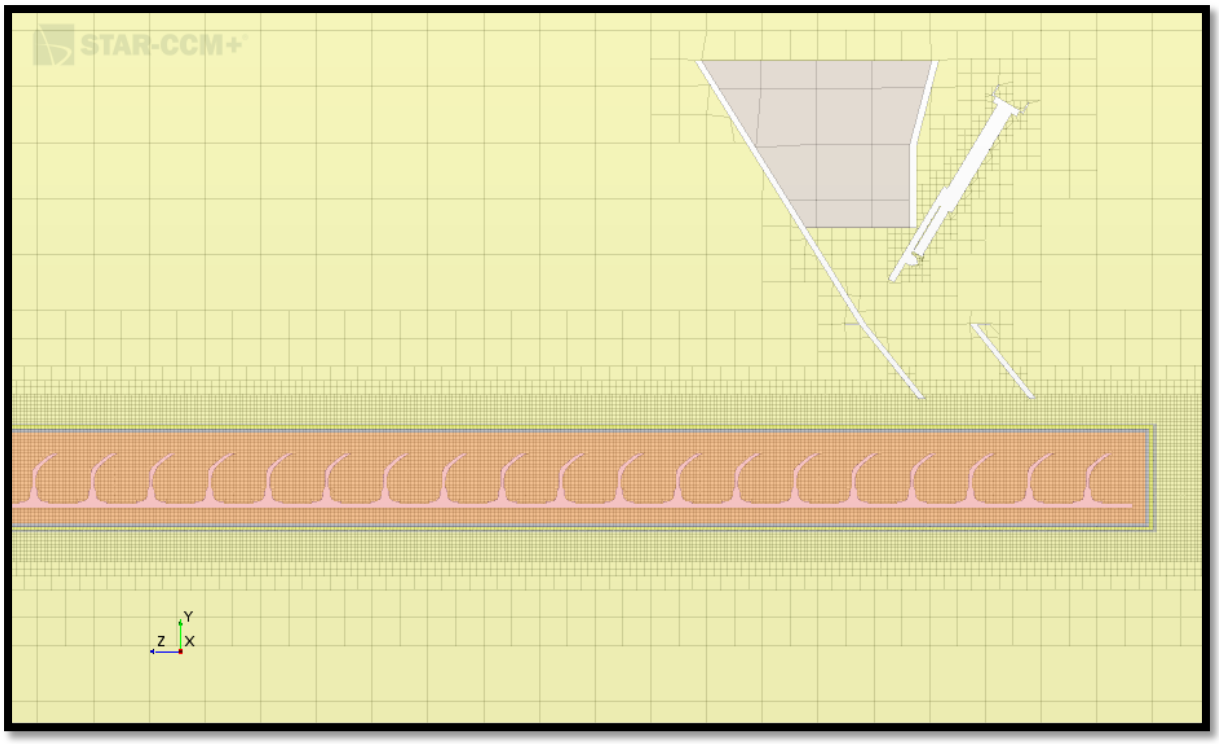

Figure 47 Illustration of the distinction between the overset region, background region and overlapping

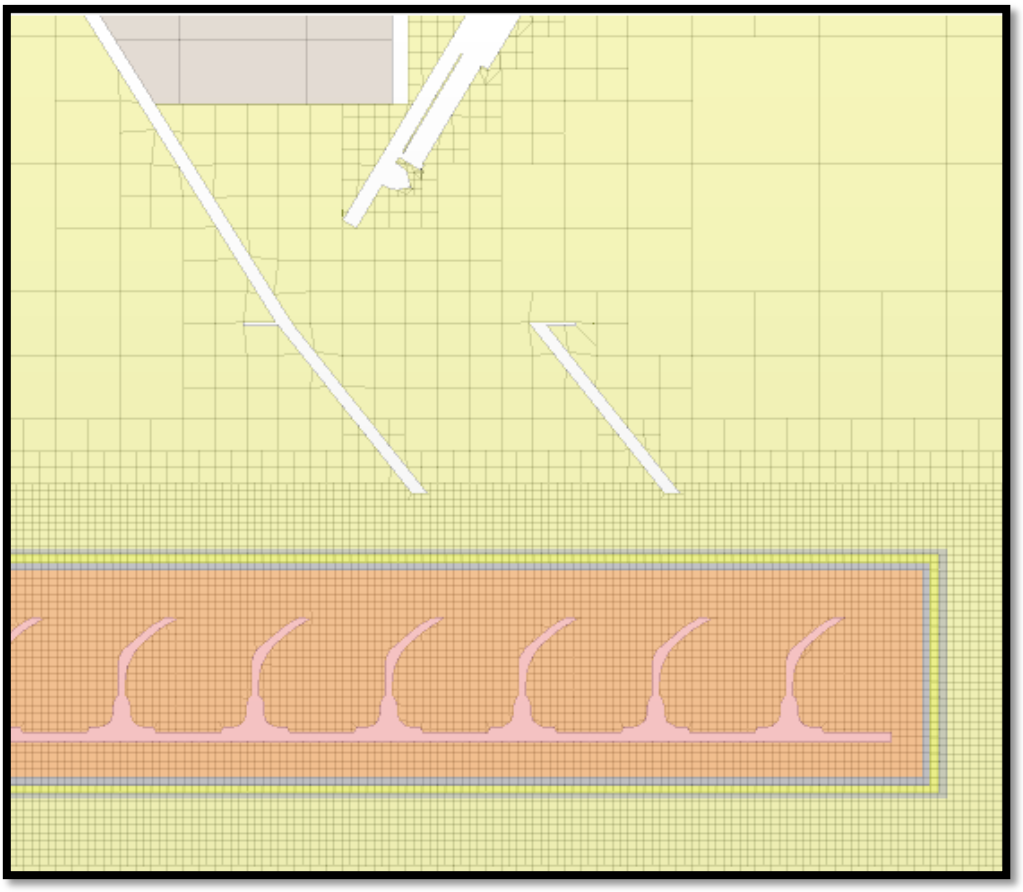

Figure 48 Illustration of acceptor cell section

5.4. PARTICLE INJECTOR

The particle injector for the steep incline sidewall conveyor simulation was set up in a similar fashion as with the test rig simulation. The injector type used was the random injector. As specified in chapter 4 the random injector allows for a specific particle size to be injected to a specific porosity limit within a designated region volume. This meant that the exact particle size distribution could be achieved and therefore allows the model to replicate the actual charging operation.

For the simulation of the steep incline sidewall conveyor an additional particle size was added. This particle size would include the >60mm particles that were not included in the test rig simulation due to the test rig size constraints. It was decided to include the >60mm particle percentage as an 80mm particle. The particle injection criteria are tabulated in Table 22.

Table 22 Steep incline sidewall conveyor particle size distribution

Steep incline sidewall conveyor particle size distribution						
	>100 Average	80 -100 Average	60 - 80 Average	40 - 60 Average	35 - 40 Average	30 - 35 Average
	0%	30%		56%	7%	7%
Plant hopper particles porosity limit division	0	0,126		0,235	0,029	0,029
Modelled particle size		80mm		60mm	40mm	35mm
Number of particles	0	1372		6070	2561	3823

After injecting all of the particles into the coke surcharge hopper a bulk density validation was once again done in order to ensure that the simulated bulk density matched the actual bulk density. The results obtained are tabulated in Table 23.

Table 23 Simulated material bulk density validation for steep incline sidewall conveyor simulation

Plant hopper filled with 35, 40, 60, 80mm particles with Simcenter STAR-CCM+ particle count that matches the total porosity limit of 0,4194		
Hopper weight	606,436	kg
Particle count	13826	-
Hopper volume	1,415	m^3
Bulk density	428,453	kg/m^3

From the results obtained in Table 23 it is evident that the simulated bulk density matched the calibration values within 2% and was therefore deemed correct.

5.5. DISCRETE ELEMENT MODEL PARAMETER SETUP

The final section of the model set up was to define the physics encapsulated in the simulation and to define discrete element model parameters. This was done according to the calibrated parameters obtained from the test rig material validation process. Table 24 lists all of the input parameters used for the steep incline sidewall conveyor simulation.

Table 24 Steep incline sidewall conveyor DEM parameters used

Simcenter STAR-CCM+ model input parameters	
General	
Parameter description	**Value**
Gravity active	-9.81 m/s^2 in y axis
Overset mesh motion selected	Translation
Overset mesh motion value	-2.2 m/s in the z axis (belt movement direction)
Discharge chute angle	38 degrees
Contact model	Hertz Mindlin
Coke particle	
Parameter description	**Value**
Density	1021.54 kg/m^3
Poisson's ratio	0.05
Young's modulus	100 Mpa
Shape	Spherical cluster
Size	35mm, 40mm, 60mm and 80mm
Particle-particle normal restitution coefficient	0.3

Particle-particle tangential restitution coefficient	0.3
Particle-particle rolling resistance	0.001
Particle-particle static friction coefficient	2
Rubber boundary	
Parameter description	**Value**
Density	1100 kg/m^3
Poisson's ratio	0.45
Young's modulus	1 MPa
Particle-rubber normal restitution coefficient	0.6
Particle-rubber tangential restitution coefficient	0.6
Particle-rubber rolling resistance	0.001
Particle-rubber static friction coefficient	0.852
Liner boundary	
Parameter description	**Value**
Density	7832 kg/m^3
Poisson's ratio	0.285
Young's modulus	200 GPa
Particle-hopper liner normal restitution coefficient	0.5
Particle-hopper liner tangential restitution coefficient	0.5
Particle-hopper liner rolling resistance	0.001
Particle-hopper liner static friction coefficient	0.24

5.6. HIGH SPEED CAMERA SETUP AND RESULTS

It was required to capture the footage in such a way that the full loading interface was in view while also allowing for post processing to be done. The position that was chosen was the eastern side of the eastern steep incline sidewall conveyor. This was mainly due to the fact that the eastern steep incline sidewall conveyor just finished its maintenance cycle and was not yet started for operation. This meant that the necessary cover structures could be removed (while keeping the belt isolated) to allow for the camera setup. A scaffold was built on the side of the steep incline sidewall conveyor in order to provide access for the high speed camera and additional lights to be installed. It was mentioned in section 5.1 that the side skirting structures were not included in the analyses. This was done due to the fact that the only area which allowed access for the high speed camera was directly from the side. If the side skirting structure were not removed the loading interface would not be recorded. This setup was replicated in the simulation model in order to be able to compare the high speed footage with the simulation result. Figure 49 illustrates the final camera setup.

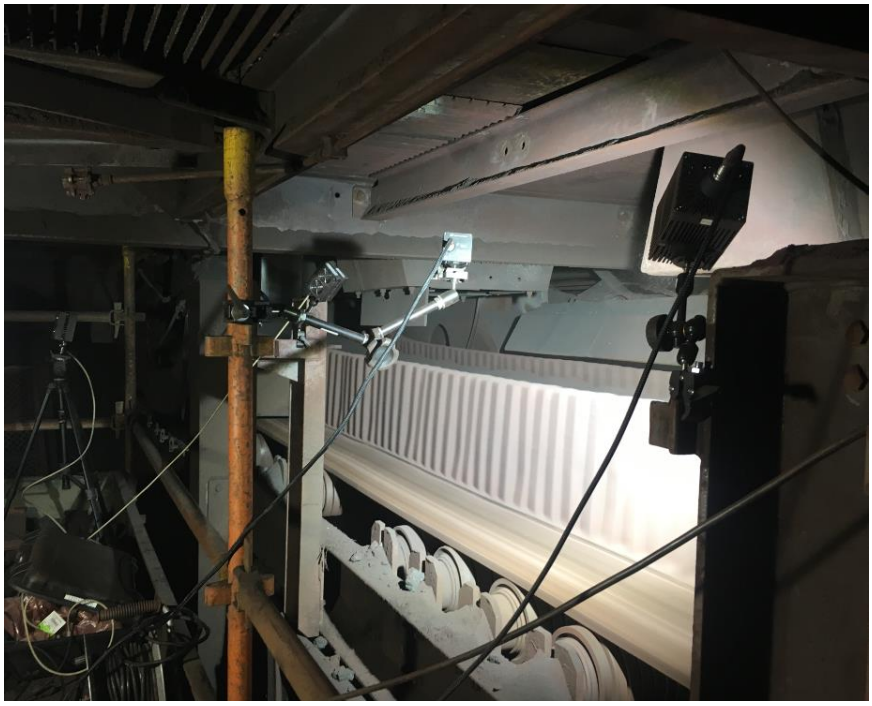

Figure 49 High speed camera setup for the steep incline sidewall conveyor

After the camera setup was completed, the eastern steep incline sidewall conveyor was de-isolated and the production team used it to charge a few rounds of coke material. These charging rounds were captured with the high speed camera according to the following sequence of events.

1. High speed camera ready for recording.
2. As soon as the hydraulic gate started to open the recording started.
3. A 9 second (actual time) video was recorder while the material charged.
4. The raw video files were downloaded to the computer.
5. Step 1 to 4 were repeated for 5 rounds.

For the first two iterations a video capturing frame rate had to be selected. The camera that was used was capable of capturing images at a maximum frame rate of 2000 frames per second. A quick calculation was done in order to determine what the belt displacement would be for each frame when selecting a different frame rate. Table 25 illustrates the results obtained.

Table 25 Frame rate selection calculation

Frame rate selection	
Belt velocity [m/s]	2,2
Possible frame rate [frame/s]	**Belt travel distance per frame [mm/frame]**
2000	1,100
1500	1,467
1000	2,200
500	4,400
200	11,000
100	22,000

From Table 25 it is evident that if the maximum frame rate of 2000fps were to be selected the belt would displace 1.1mm per frame which was deemed unnecessarily small. On the other hand if a frame rate of 200fps were to be chosen the belt would displace 11mm which meant that possible information between frames would be lost and was deemed too big. Therefore a middle ground had to be reached and was thus decided to choose a frame rate of either 1000fps or 500fps. The first two iterations of the video revealed that a frame rate of 1000fps was too high and also revealed that due to the limitation in storage space a higher frame rate would result in a shorter (actual time) video captured. Therefore the 500fps was chosen because it provided a sufficiently small belt displacement with sufficiently long video capture duration. Figures 50 and 51 illustrate the result of the high speed camera footage for just as the hydraulic door opened and for when fully opened.

Figure 50 High speed camera footage of coke charging at start of gate opening

Figure 51 High speed camera footage of coke charging with gate in fully open position

It was also decided to calculate the average velocity of the particles from exiting the chute until contact with the top of the steep incline sidewall conveyor cleat. This was done in a similar fashion as with the coefficient of restitution calculation done in chapter 4.6. Particle tracking was used in order to determine the number of frames it took for a particle to move from the outlet of the chute until contact with the belt cleat (bucket). Table 26 illustrates the results obtained.

Table 26 Average particle velocity calculation results

Coke steep incline sidewall conveyor analyses		
FPS of captured video	500	fps
Plant coke belt loading		
Total frames	4500	frames
Video actual time	9	s
Video playback fps	24	fps
Average frames via particle tracking	55	frames
Average velocity of particles before belt contact	4,102	m/s

From Table 26 it is evident that the average velocity obtained by the particles was 4.102 m/s. One point of note is that this velocity is the velocity of the particle in the direction of travel as it leaves the discharge chute. Due to the plant limitations it was not possible to obtain a camera setup that would allow for the particle motion to distinguish between the horizontal and vertical direction. Therefore the velocity in the direction of travel (estimated as the chute outlet angle) was obtained.

5.7. SIMULATION POST PROCESSING SETUP

The setup for the post processing of the simulation model was done such that the high speed camera footage could be compared with the simulation result. A scalar scene was generated in Simcenter STAR-CCM+ that would replicate the view obtained from the high speed camera footage. A function was selected which would illustrate the velocity of the particles in the direction of motion similar to the result obtained from Table 26. A colour bar was also assigned to the function which would colour the particles according to the velocity obtained. This colour bar was set up such that particles matching the velocity of the high speed footage would be coloured green and yellow. Therefore with this scalar scene the particle interaction with the belt could be assessed along with the particle velocity. Figure 52 illustrates the scalar scene that was generated.

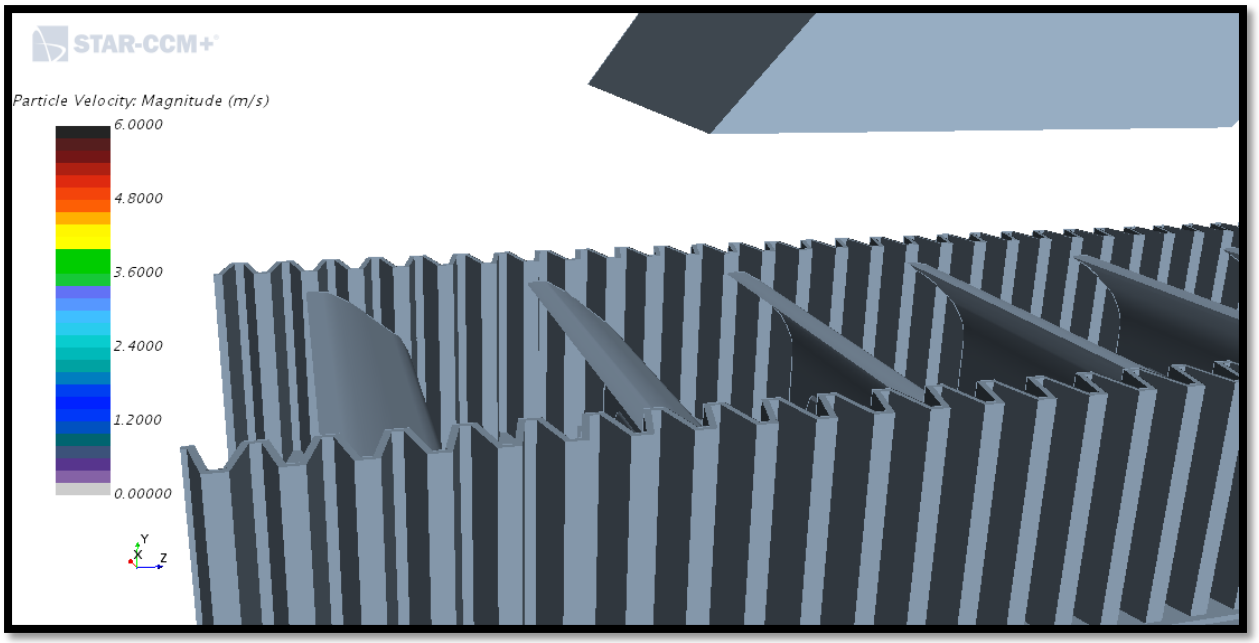

Figure 52 Scalar scene for high speed camera view

It was also decided to generate a scalar scene which would provide a more holistic view of the charging process. This view would include the entire simulated coke surcharge hopper with a section of the steep incline sidewall conveyor. The opacity of the parts would be lowered in order to allow for the internals of the hopper and the steep incline sidewall conveyor belt to be visible. This view would determine if the steady state material discharge is obtained and what the total displacement is achieved when particles interact with the steep incline sidewall conveyor. A function was once again chosen for the velocity of the particle but in this case it was set up to illustrate the velocity of the particle in the direction of belt motion. Therefore if the particle were to match the belt velocity the particle would be coloured green. Figure 53 illustrates the scalar scene generated.

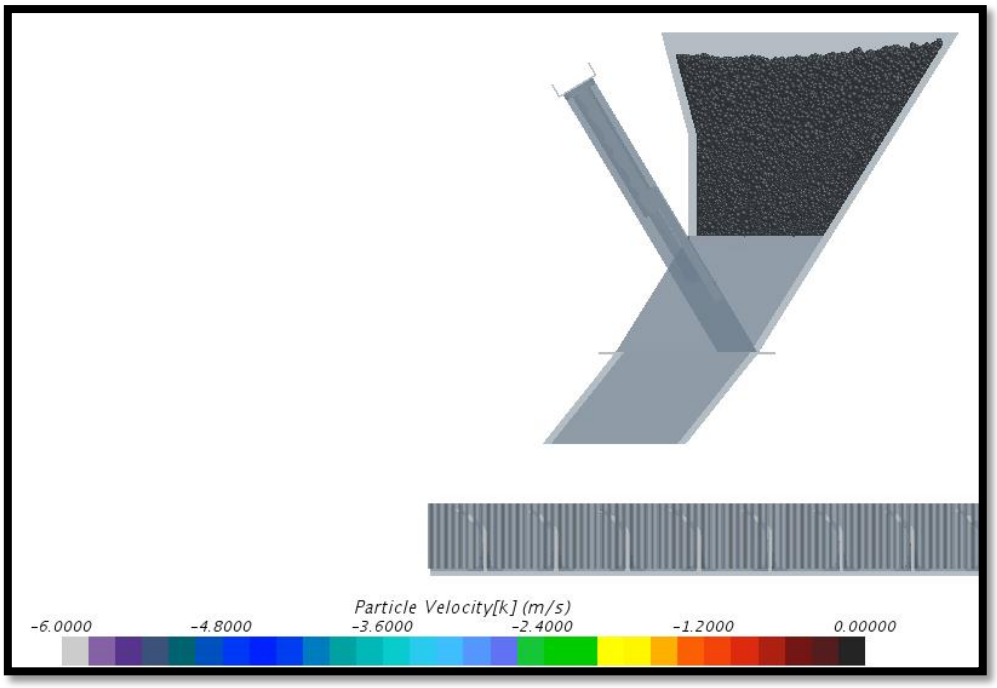

Figure 53 Scalar scene for particle velocity in the belt direction

5.8. RESULTS

The simulation model results were compared to the high speed camera footage with regards to three main criteria. Firstly the velocity of the particles at discharge was compared to the velocity of the particles on the high speed footage. Secondly the material trajectory profile was evaluated to determine if the particle-hopper liner interactions were correct. Thirdly the particle belt interaction was evaluated in order to determine if the particle-conveyor interaction and particle-particle interaction was modelled correctly. These three criteria are discussed with regards to images taken from the simulation and high speed videos.

5.8.1. SIMULATED AND EXPERIMENTAL PARTICLE VELOCITY COMPARISON

When analysing the high speed camera footage, an average particle velocity was calculated as 4.102 m/s as illustrated by Table 26. From a visual inspection it was also noted that the material would build up for each frequency of a cleat (bucket) passing. This meant that a type of surge effect was present on the surface of the belt cleat. It was evident that as the particles exit the chute it would increase to a maximum velocity and then would experience a decrease in velocity as it comes in contact with other particles and the belt cleat surface. Figures 54 and 55 illustrate this occurrence.

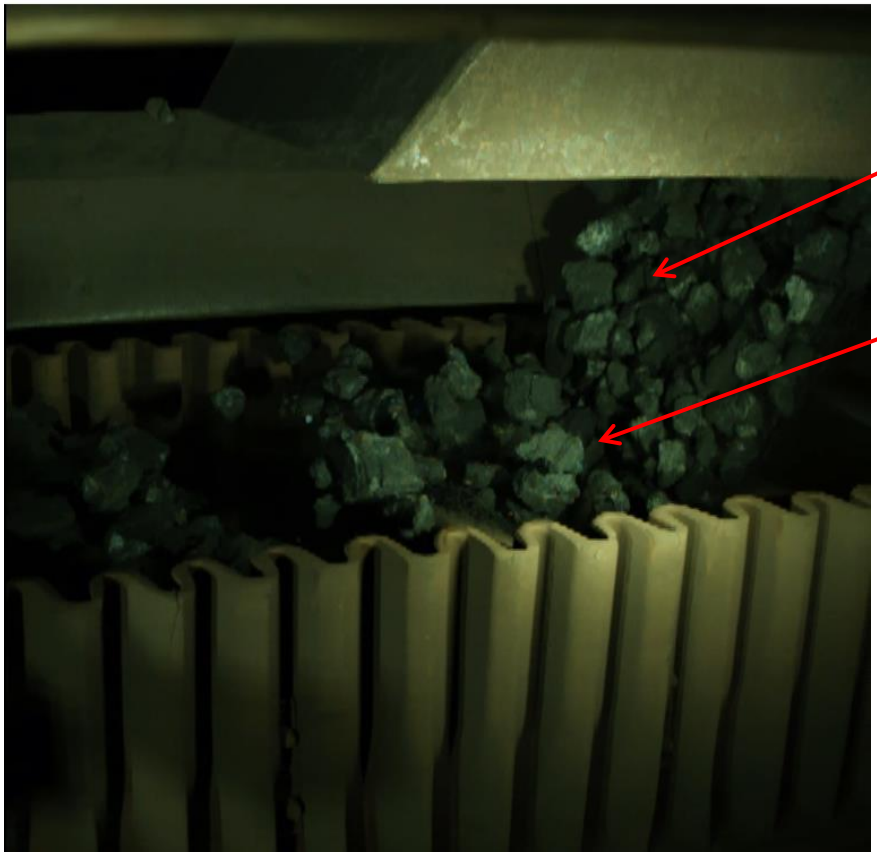

Figure 54 Experimental particle velocity evaluation

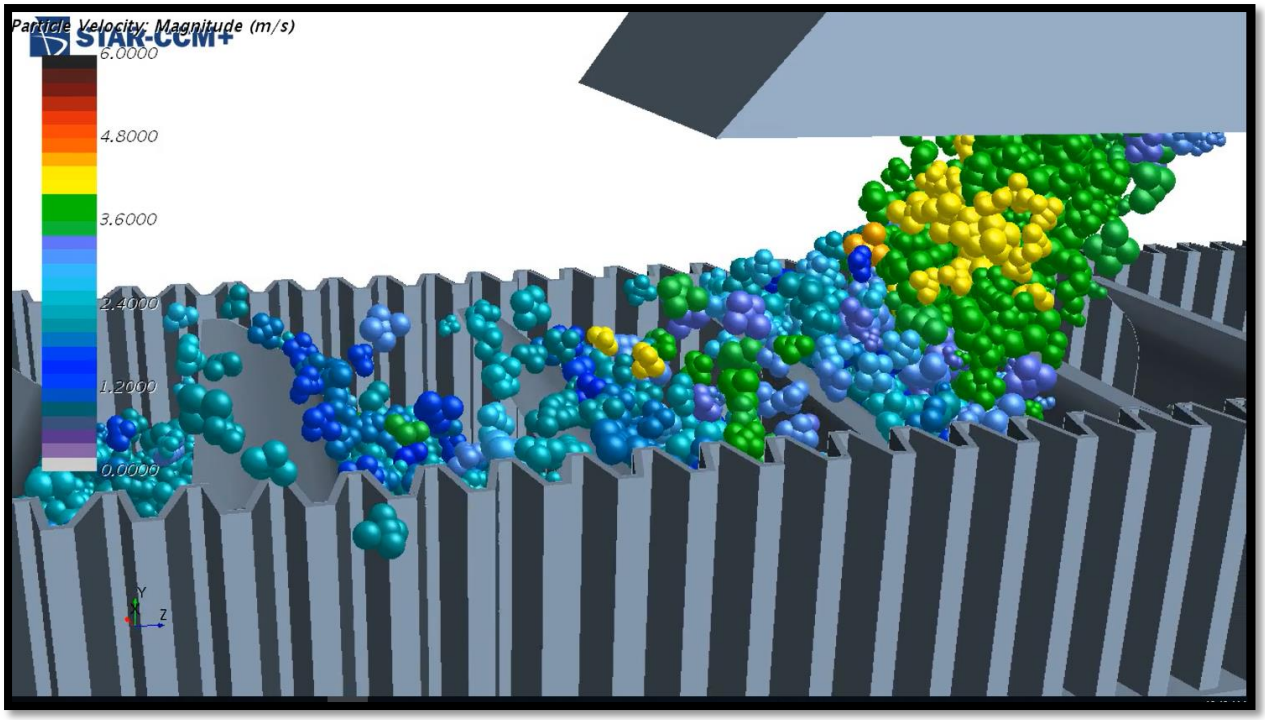

Figure 55 Simulated particle velocity evaluation

By comparing Figure 54 and 55 it is evident that the simulation model was capable of replicating the surge and build-up effect that was noticed with the frequency of cleat passing. The high velocity particles are seen leaving the chute outlet and then decrease in velocity as the particles come in contact with cleats and other particles. It is also evident that the particle simulated chute exit velocity was between 3.6 m/s and 4.2 m/s which is close to the average of 4.102 m/s. It could therefore be concluded that the particle simulated velocity was a good match to the experimental velocity.

5.8.2. SIMULATED AND EXPERIMENTAL PARTICLE TRAJECTORY COMPARISON

The material trajectory was analysed to determine if the simulation model could accurately replicate the trajectory witnessed from the high speed camera footage. An image was taken from a different angle which only illustrates the trajectory that the material follows after exiting the chute.

It is evident from Figure 56 that the material continues at an angle similar to the chute inclination angle. It can also be seen that there is not much separation between the particles after exiting the chute. This indicates that the particles have close to the same velocity within the trajectory profile. It can be concluded that there is not much friction between the chute liners and the material and that there is only a slight loss in velocity.

Comparing Figure 56 and 57 it can be seen that the simulation model was capable of replicating the material trajectory angle as well as the trajectory profile. Looking at the velocity profile of the material it is also evident that the material in contact with the chute has a lower velocity than the top material. This correlates with the high speed footage taken and can therefore be concluded that the simulation model accurately represents the actual plant process. Thus the parameter set up for the particle-chute liner interaction was done correctly.

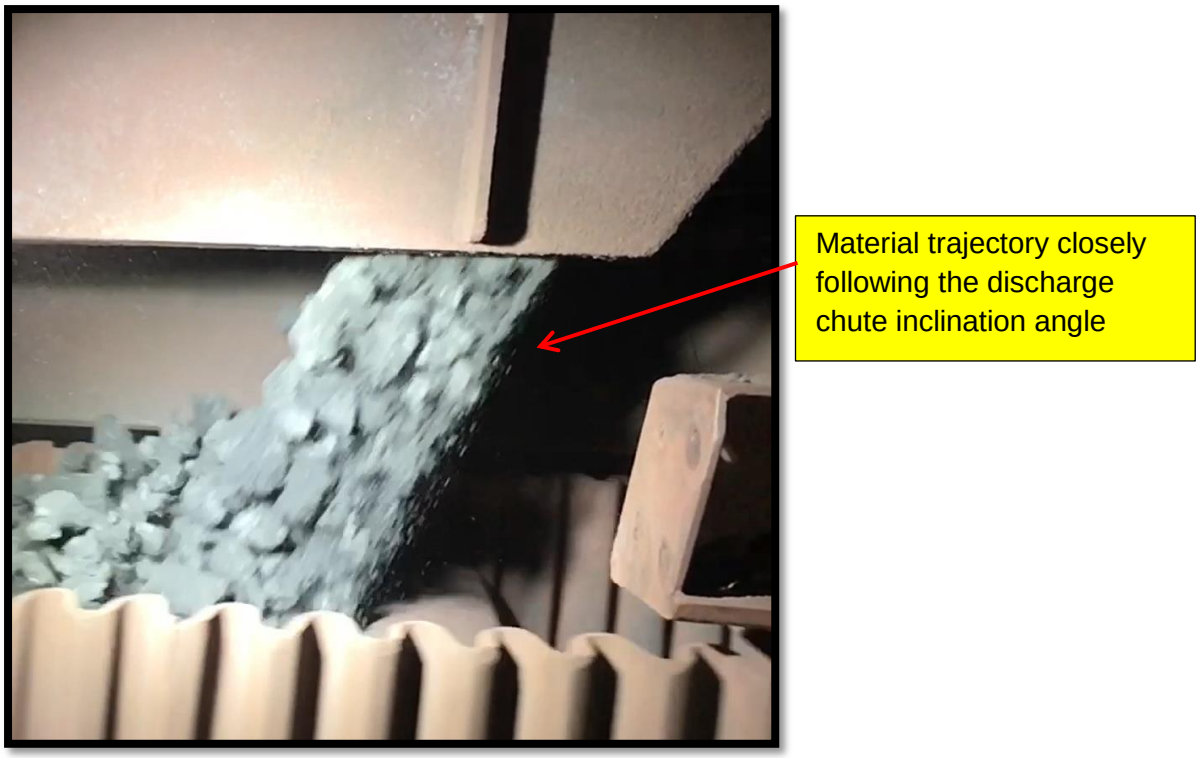

Figure 56 Experimental particle trajectory evaluation

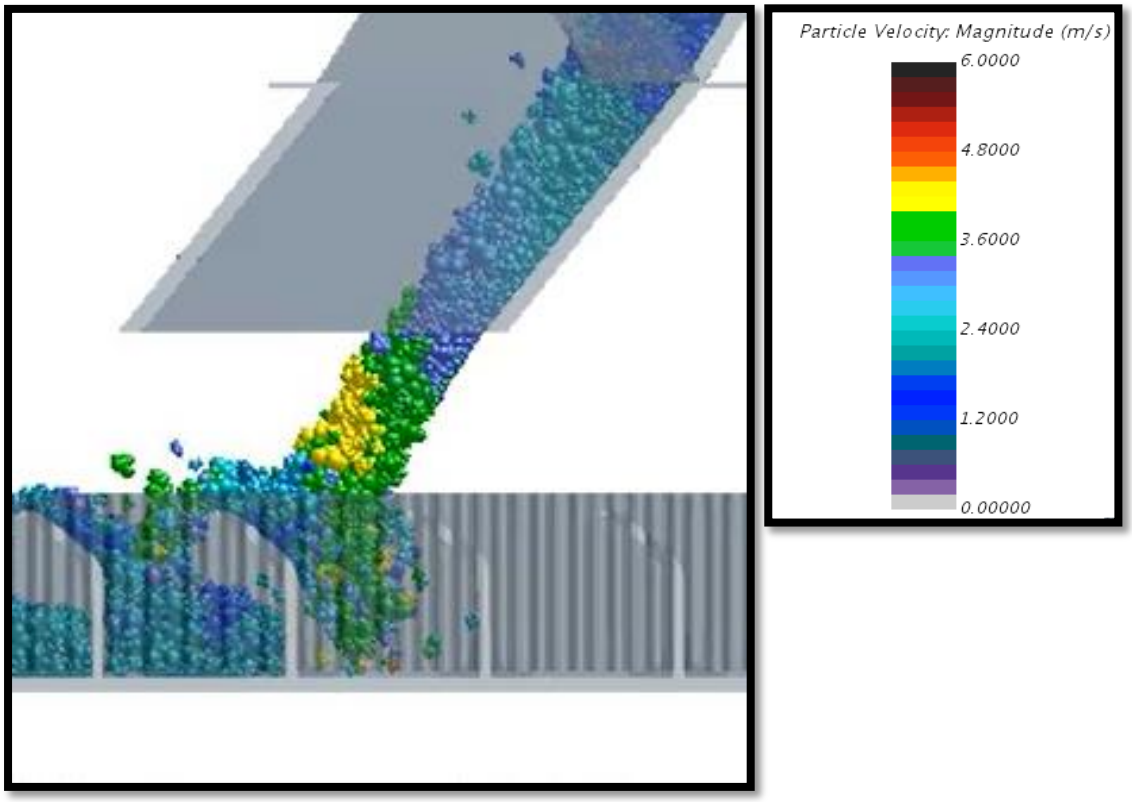

Figure 57 Simulated particle trajectory evaluation

5.8.3. SIMULATED AND EXPERIMENTAL PARTICLE-PARTICLE AND PARTICLE-CONVEYOR INTERACTION COMPARISON

The comparison for the particle-particle and particle-conveyor interaction was done via visual inspection (illustrated by Figure 58 and 59). First of all the material build up effect mentioned in section 5.8.1 has to be mentioned here as well. From the high speed camera footage it can be seen that this material build-up effect causes a slight damping effect for the interaction between the particles. It was also noticed that the particles tend to stay on top of the belt cleats and then slowly slide down as the belt moved on.

When comparing the simulation model results with the high speed camera footage it is evident that the material build-up effect is also obtained. It is also evident that the simulation model has the same damping effect due to the particle-particle interaction. Taking a look at the cleats that have passed the loading zone it is evident that the particles also tend to stay on the cleat surface and then slowly slide down as the belt moves on.

It can therefore be concluded that the simulated particle-particle and particle-conveyor interaction closely resemble that of the actual plant operation. This means that the parameters selected for the simulation model was sufficient for the steep incline sidewall conveyor.

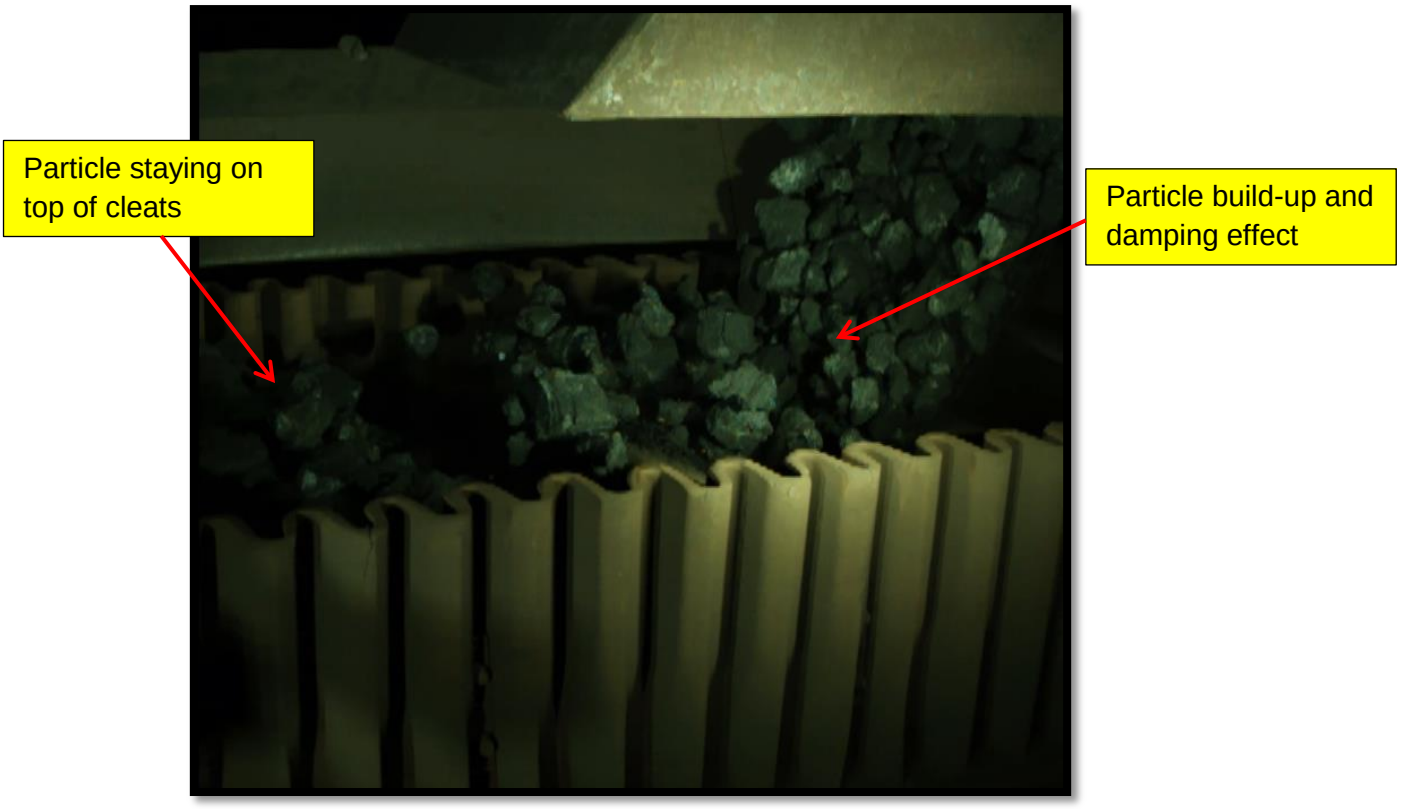

Figure 58 Experimental particle-particle and particle-conveyor interaction evaluation

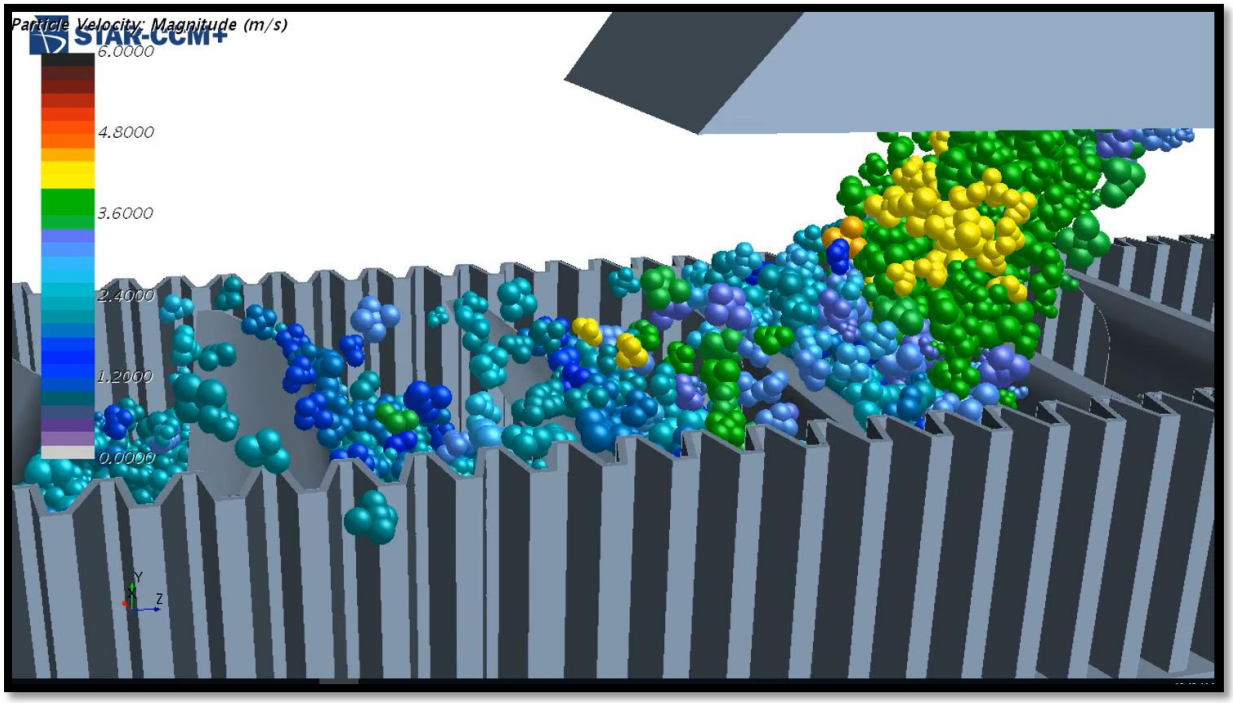

Figure 59 Simulated particle-particle and particle-conveyor interaction evaluation

5.9. CONCLUSION

In this chapter a steep incline sidewall conveyor was simulated. The equipment geometry and layout was accurately simulated with the use of as built drawings and plant measurements. The movement of the conveyor was replicated with the use of the overset mesh tool within Simcenter STAR-CCM+. Simulated coke particles were injected into the simulation domain with a parameter setup as determined in Chapter 4. The validation between the actual steep incline sidewall conveyor loading and the simulation result was done with the use of a high speed camera. After comparing the simulation results with the high speed camera footage it was found that the simulation model was capable of replicating the material bulk flow behaviour. It was found that all three of the validation criteria were met and it was thus concluded that the DEM simulation for the steep incline sidewall conveyor passed the final validation test. Therefore the DEM simulation is capable of simulating the loading of a steep incline sidewall conveyor.

The aim of this study can now be addressed, which is to determine how the material spillage will be affected by a change in conveyor velocity or material velocity. This will be addressed in the next chapter.

6. DESIGN MODIFICATION ASSESSMENT

In Chapter 5 it was shown that the DEM simulation was applicable in modelling the loading of the steep incline sidewall conveyor. This chapter will now evaluate different plant design changes with the aim to minimise spillages and therefore increasing belt life. The design modifications to be evaluated are the alteration of the belt velocity vs. the alteration of the discharge chute angle. For this evaluation a report was set up in the calibrated steep incline sidewall conveyor simulation that would monitor the coke particle count for the entire simulation duration. The atmosphere bottom boundary was also modified to allow for particles to escape the model boundaries which would be an indication of the quantity of material spilled from the belt. This meant that the existing plant design and suggested design modifications could be evaluated based on spilled material percentage, particle velocity vs. belt velocity comparison and the material loading profile and settling result.

6.1. EXISTING PLANT DESIGN EVALUATION

The existing plant design was simulated according to the evaluation criteria. For this simulation the belt velocity and chute discharge angle was set according to current plant conditions (values used in Table 24). The results obtained from this simulation was then used as a baseline for the evaluation of the subsequent design changes. Table 27 lists the current design criteria.

Table 27 Existing plant design values

Existing plant design values	
Belt speed	2.2 m/s
Chute discharge angle	38 degrees

Firstly taking a look at the quantity of particles spilled from the belt, the particle count report revealed that a total of 27 particles spilled from the belt which resulted in a spilled percentage of 0.195%. This value does not seem like much but that is because only the bottom cone of the surcharge hopper is included into the simulation. If the total material volume is taken into consideration (based on the plant operation specifications that the surcharge hopper is filled to 80% of design capacity) and it is assumed that the rate of spillage is constant it can be calculated that 597 particles spill from the belt with each charging round. This means that if the side skirting structures are removed a spillage of 597 particles per round can be expected. The plant production personnel stated that per day an average of 120 rounds of coke material are charged which pushes the spillage amount up to

71640 particles. This means that if the side skirting structures are to be removed a spillage of 5 times the size of the simulated hopper volume can be expected each day.

Focusing on the particle velocity relative to the belts velocity (in the direction of belt travel) it is evident that with the current design setup the particles are slightly slower than the belt. Within Figure 60 a colour scale was set up which coloured all particles green when a particle velocity between 2,0 and 2,4 m/s was reached. From Figure 60 it can be seen that the majority of the particles are coloured yellow which corresponds to a velocity in the region of 1,8m/s. It can therefore be estimated that the average particle velocity is 18% slower that the belt velocity in the direction of belt travel.

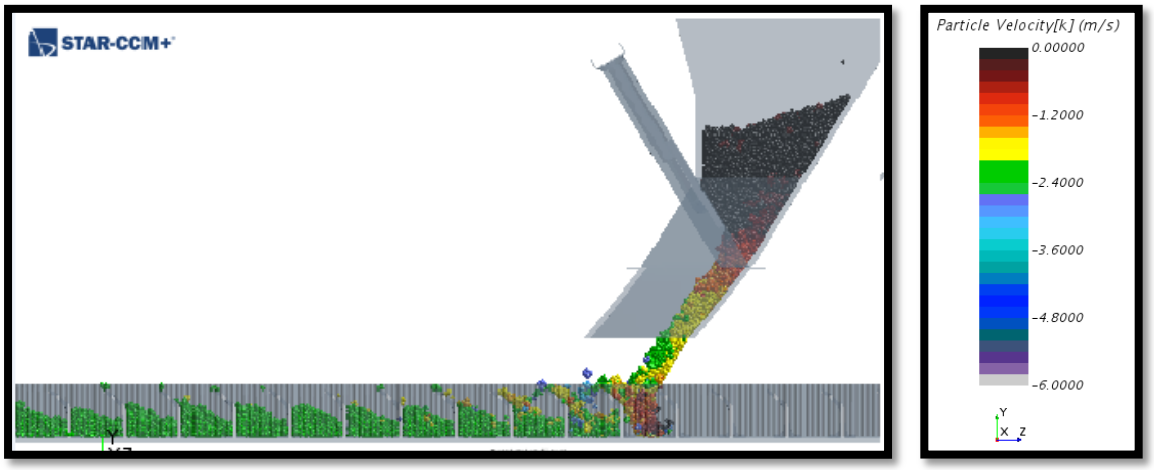

Figure 60 Particle velocity relative to belt velocity assessment

The last section of evaluation was the material loading profile and settling results. The material surging effect at the loading interface was assessed (similar to section 5.8). The duration before particles settled and the volume of material within each of the cleat compartments were also evaluated. From Figure 61 it is evident that a surging effect is present with the current plant design. As determined in Chapter 5 this is the mechanism that causes the majority of the spillage. Figures 60 and 61 also reveal that it takes the material approximately three cleat lengths beyond the chute discharge point to settle and become stationary. It is also evident that the cleat compartments are filled to approximately 50% of the volume. This allows room for the material to shift when the steep incline conveyor rotates to the vertical direction and thus prevents material to spill from the cleat compartment.

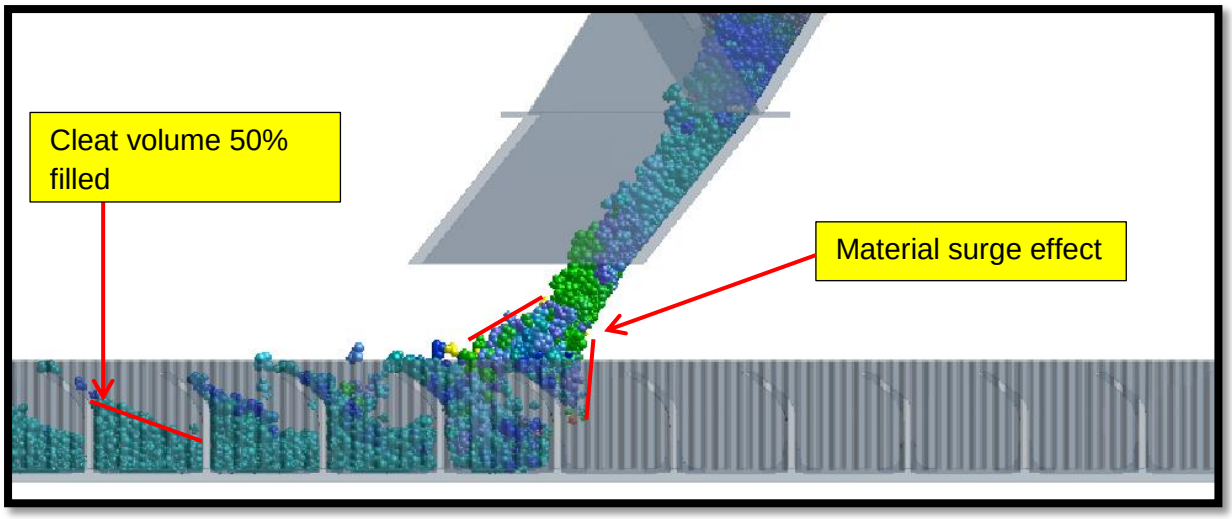

Figure 61 Material loading profile and settling result for current plant design

6.2. BELT VELOCITY ADJUSTMENT EVALUATION

The belt velocity was evaluated by simulating velocities of 50% higher and lower than the current design specification. This was done to investigate the possibility of a variable speed drive installation on the steep incline sidewall conveyor motor, and what effect the velocity change would have on the material bulk behaviour.

6.2.1. BELT VELOCITY REDUCTION EVALUATION

The steep incline sidewall conveyor simulation model was modified by reducing the translation value of the over set mesh region while maintaining the same chute outlet angle. The values used are tabulated in Table 28.

Table 28 Steep incline sidewall conveyor velocity reduction values

Velocity reduction simulation values	
Belt speed	1.1 m/s
Chute discharge angle	38 degrees

After completing the belt velocity reduction simulation the particle count report revealed that a total of 35 particles would be spilled. This equates to 0.253% of the material charged, which is greater than the existing design. Evaluating the material discharge velocity relative to the belt velocity, it is evident from Figure 62 that the material velocity still remained at 1.8m/s, and the belt velocity was reduced to 1.1m/s. This resulted in the material velocity being 63.63% higher than the belt velocity.

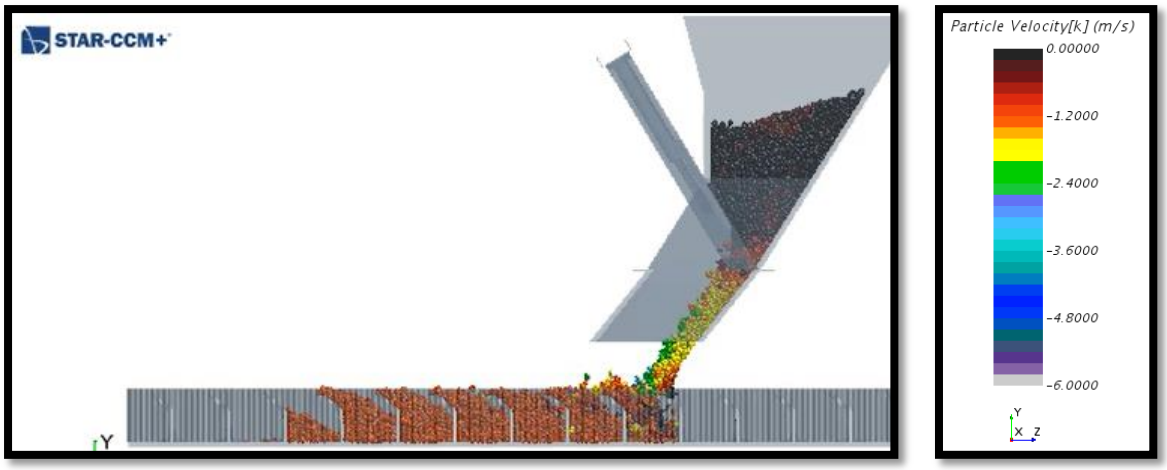

Figure 62 Particle velocity relative to belt velocity with 50% belt velocity reduction

Figure 63 revealed that the surge effect would be greater if the belt velocity were to be reduced by 50%. This is mainly due to the material velocity being greater than the belt velocity, which results in a material build-up on the belt. Evaluating the material settling time, Figures 62 and 63 reveal that the material settles out to match belt speed at one cleat (bucket) interval from the chute discharge point. Figure 63 also reveals that if the belt speed was to be reduced by 50%, the cleat volume would be almost fully filled (estimated to be greater than 90% of the volume). This would not be acceptable for plant operation because the belt is required to rotate to approximately 62 degrees which would result in the material spilling from the cleats.

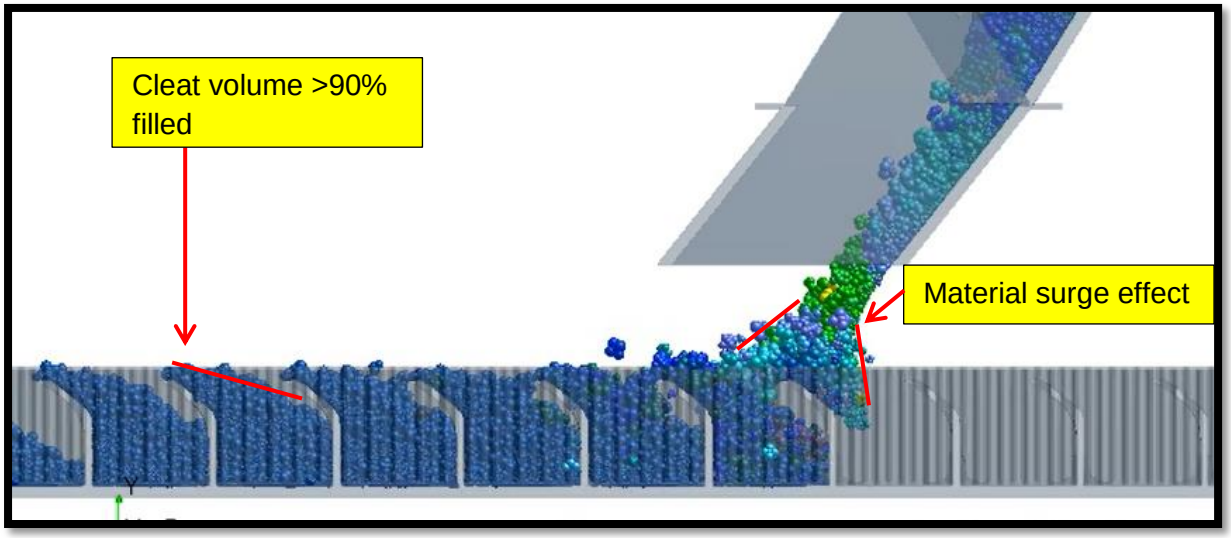

Figure 63 Material loading profile and settling result for 50% belt velocity reduction

6.2.2. BELT VELOCITY INCREASE EVALUATION

For the belt velocity increase evaluation the overset mesh translation value was increased by 50% while still maintaining a constant chute outlet angle. The values used are tabulated in Table 29.

Table 29 Steep incline sidewall conveyor velocity increase values

Velocity increase simulation values	
Belt speed	3.3 m/s
Chute discharge angle	38 degrees

After completing the belt velocity increase simulation the particle count report revealed that a total of 25 particles would be spilled. This equates to 0.181% of the material charged, which is lower than the existing design. Evaluating the material discharge velocity relative to the belt velocity it is evident from Figure 64 that the material velocity still remained at 1.8m/s, and the belt velocity was increased to 3.3m/s. This resulted in the material velocity being 45.45% lower than the belt velocity.

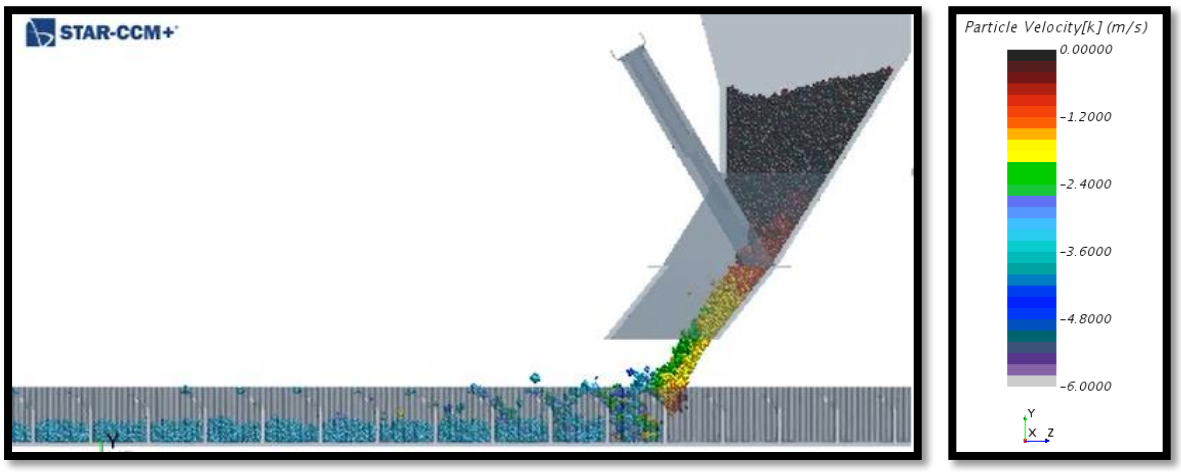

Figure 64 Particle velocity relative to belt velocity with 50% belt velocity increase

Figure 65 revealed that the surge effect would be less if the belt velocity were to be increased by 50%. This is mainly due to the material velocity being lower than the belt velocity, which results in less of a material build-up. An additional observation was made when increasing the belt velocity, which was a material impact effect. This effect can be seen in Figure 65 where the cleat has almost fully past the loading point. This impact effect is due to the belt velocity being so high that the material does not build up on the cleat but rather interact with the leading edge of the cleat. Evaluating the material settling time,

Figures 64 and 65 reveal that the material settles out to match belt speed at six cleat intervals from the chute discharge point. Figure 65 illustrates that if the belt speed were to be increased by 50%, the cleats would be filled less than 50% of the volume, which would allow the belt to rotate without spilling material.

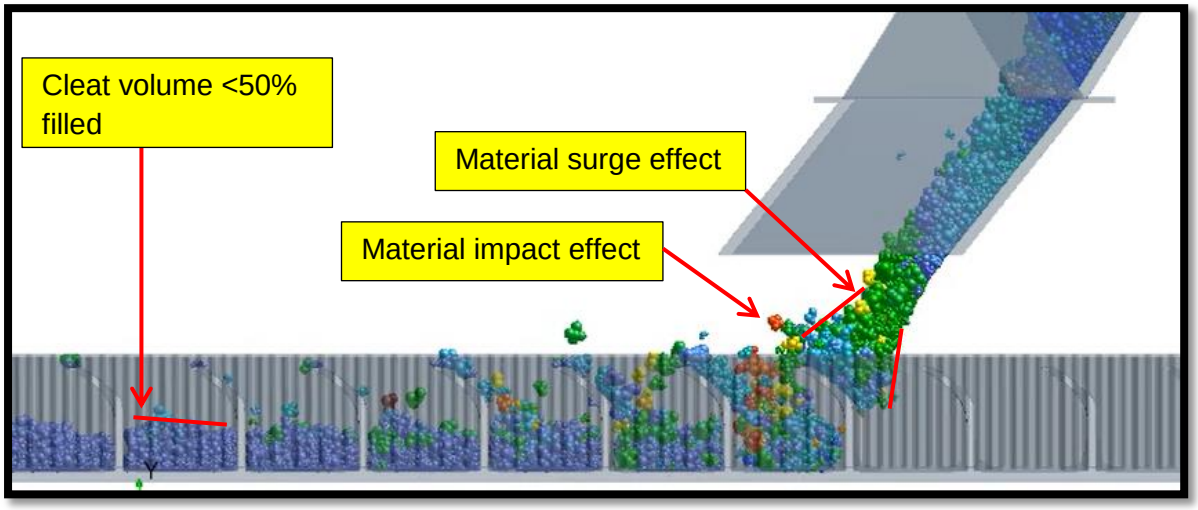

Figure 65 Material loading profile and settling result for 50% belt velocity reduction

6.3. DISCHARGE CHUTE ANGLE ADJUSTMENT EVALUATION

The discharge chute angle was evaluated by simulating a chute angle of respectively 10 degrees higher and lower than the existing design specification. This was done to investigate the possibility of improving the material trajectory to better match the current belt velocity.

6.3.1. CHUTE ANGLE REDUCTION EVALUATION

The steep incline sidewall conveyor simulation model was modified by reducing the chute angle of the bottom section of the discharge chute while keeping the belt velocity the same. The values used are tabulated in Table 30.

Table 30 Steep incline sidewall conveyor discharge chute angle reduction

Chute angle reduction simulation values	
Belt speed	2.2 m/s
Chute discharge angle	28 degrees

After completing the discharge chute reduction simulation the particle count report revealed that a total of 32 particles would be spilled. This equates to 0.231% of the material charged, which is greater than the existing design.

Evaluating the material discharge velocity relative to the belt velocity it is evident from Figure 66 that the material velocity reduced with a reduction in the discharge chute angle. From Figure 66 it can be seen that the majority of the material particles have a velocity of about 1.6m/s. This resulted in the material velocity being 27.27% lower than the belt velocity.

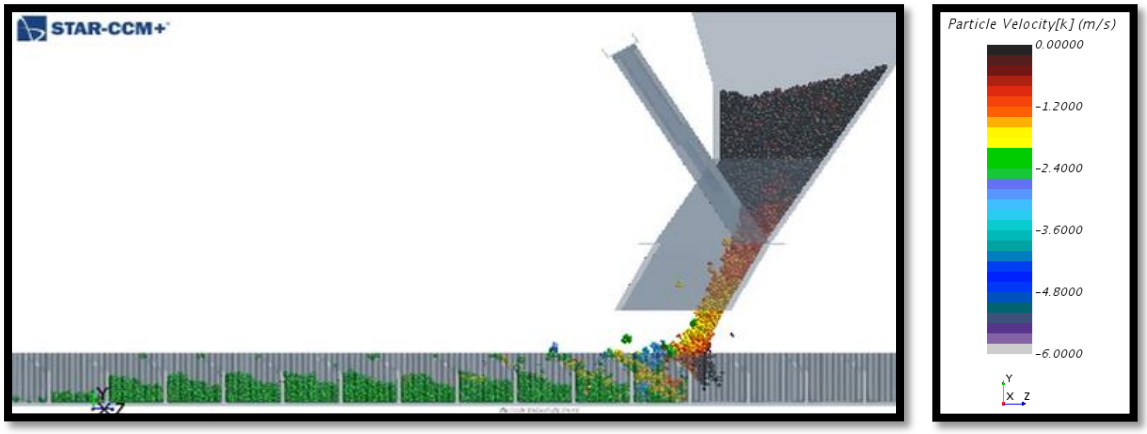

Figure 66 Particle velocity relative to belt velocity with 10 degree chute reduction

Figure 67 revealed that the surge effect was less when the discharge chute angle was reduced with 10 degrees. This is mainly due to the fact that the reduction in the chute angle caused a material trajectory change. With this reduction a more vertical material trajectory was obtained, which reduced the material surge or build up effect. Figure 67 also illustrates that due to the more vertical trajectory of material, the material did tend to separate from the flow stream, which resulted in a more erratic flow when coming into contact with the cleats. It is this erratic flow that contributed to more spilled particles, even though the surge effect was less. The material settling time was the same as with the base line simulation in section 6.1, which is three cleat intervals from the discharge chute point. It can also be noted from Figure 67 that the cleat volume is filled to approximately 50%, which is acceptable for belt rotation.

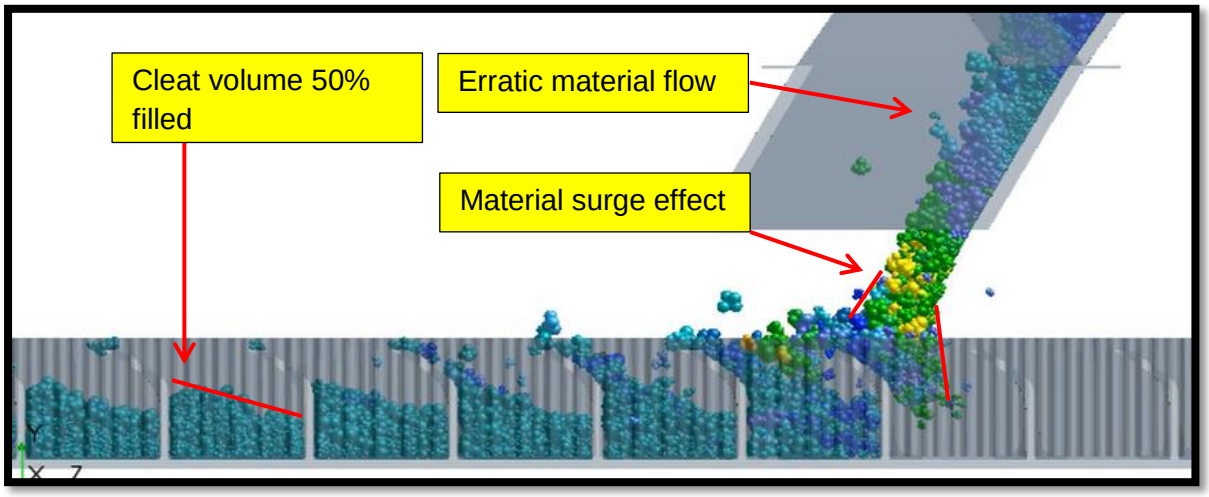

Figure 67 Material loading profile and settling result for 10 degree chute reduction

6.3.2. CHUTE ANGLE INCREASE EVALUATION

The steep incline sidewall conveyor simulation model was modified by increasing the chute angle of the bottom section of the discharge chute while keeping the belt velocity the same. The values used are tabulated in Table 31.

Table 31 Steep incline sidewall conveyor discharge chute angle increase

Chute angle increase simulation values	
Belt speed	2.2 m/s
Chute discharge angle	48 degrees

After completing the discharge chute reduction simulation the particle count report revealed that a total of 9 particles would be spilled. This equates to 0.065% of the material charged, which is substantially lower than the existing design.

Evaluating the material discharge velocity relative to the belt velocity it is evident from Figure 68 that the material velocity increased with an increase in the discharge chute angle. From Figure 68 it can be seen that the majority of the material particles have a velocity of about 2m/s. This resulted in the material velocity being 10% lower than the belt velocity.

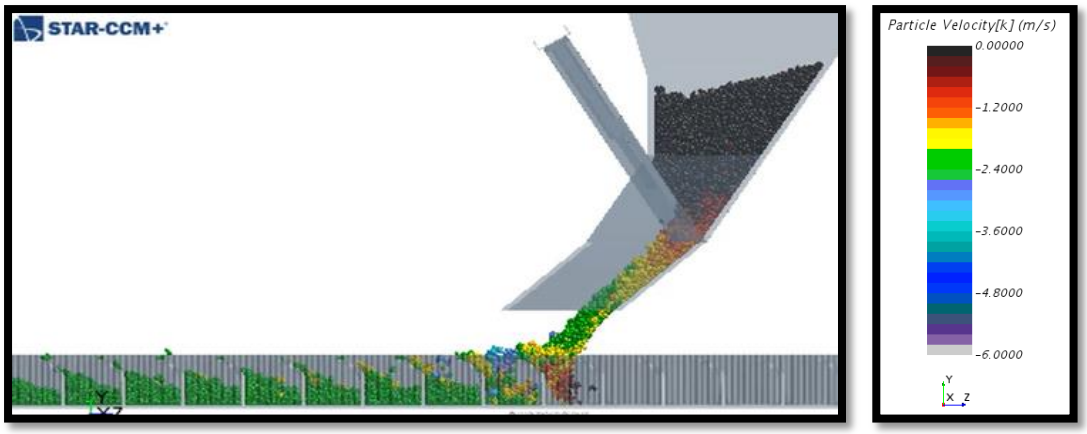

Figure 68 Particle velocity relative to belt velocity with 10 degree chute increase

Figure 69 revealed that the surge effect was less when the discharge chute angle was increased with 10 degrees. This was due to the material trajectory change that resulted from the chute angle change. It is also evident from Figures 68 and 69 that the material velocity closely matched the belt velocity which resulted in a less erratic material behaviour when the particles came into contact with the cleats. The material flow stream within and at the outlet of the chute remained closely pact and less separated compared to section 6.3.1. The material settling time was once again very similar to that of the base line case, which resulted in the material settling out at three to four cleat intervals from the chute discharge point. The cleat volume was filled to approximately 50%, which is acceptable for the belt rotation.

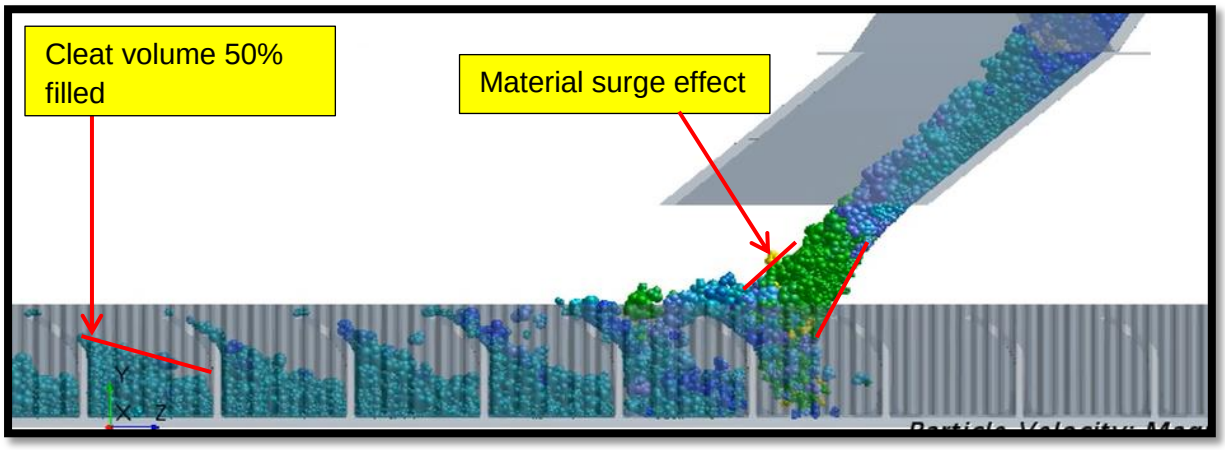

Figure 69 Material loading profile and settling result for 10 degree chute reduction

6.4. CONCLUSION

In this chapter the steep incline sidewall conveyor simulation was modified so that the particle spillage and material trajectory could be analysed. It was determined that the current belt setup resulted in a spillage percentage of 0.195% with a 50% bucket filling volume. The belt velocity was assessed by increasing and decreasing the translation velocity with 50%. It was determined that increasing the belt velocity would reduce the spillage percentage to 0.181%, but the impact on the cleats would result in higher cleat wear. A reduction in the belt velocity resulted in an increase in spilled material percentage to 0.253% with the cleat buckets being overfilled to more than 90% of the volume. The material velocity was assessed by increasing and decreasing the bottom chute section angle with 10 degrees. It was determined that if the chute angle were to be reduced, the material spillage percentage would increase to 0.231% and the bucket filling percentage would remain at 50%. The chute angle increase resulted in a material spillage percentage reduction to 0.065% with a bucket filling percentage of 50%. It can therefore be concluded that the material spillage percentage would be reduced the most (66.7% reduction) if the material relative velocity is matched as close as possible to the belt velocity. This would be achieved by increasing the bottom chute angle to approximately 48 degrees.

7. CONCLUSION AND RECOMMENDATIONS

This chapter outlines the conclusions drawn throughout the study of the DEM simulation of the loading of a steep incline sidewall conveyor. Recommendations are also made with regards to possible improvements in the calibration process, and the simulation of sinter, ore and additive material loading onto the steep incline sidewall conveyor.

7.1. CONCLUSION

The aim of this study was to determine if a DEM simulation model could replicate the loading of coke material onto a steep incline sidewall conveyor. Thereafter it had to be determined which of the suggested design changes would have the greatest effect on reducing the material spillages.

The study was started by conducting a literature study in order to determine what software packages are available, what material properties to consider, what calibration tests are available and how DEM has been used in the industry. The findings made and calibration strategies used by various researchers were incorporated into this study.

An analysis of the DEM formulation was also conducted in order to determine how the software uses different material parameters within the contact model equations. It was also evaluated how the contact model is incorporated into the conservation equations and what parameters influence the computational time of the simulation model.

The material parameters were determined with a combination of Coetzee's (Coetzee, 2017) direct and bulk calibration approaches. The selection of which parameters would be calibrated with the direct or bulk calibration approaches was made based on the availability of testing facilities. Some of the material parameters could not be calibrated with either of the two methods and it was decided to use research and theory based values. A test rig was built based on the design presented by Quist and Evertsson (Quist & Evertsson, 2015) to assist with the bulk calibration approach, and the final material parameter validation. The test rig was used to calibrate the particle-boundary static friction coefficient, particle-boundary coefficient of restitution and the particle-particle static friction coefficient. A high speed camera was used to capture footage of a screened coke sample draining trough the test rig setup. Three points of validation was determined namely: hopper draining time, deflection plate material depth, and material setting angle of repose. It was determined that with the direct and theory based calibrated material parameters, and a particle-particle friction coefficient of 2 the simulation model and the experimental tests correlated. With these

material parameters it was determined that the model was capable of predicting the settling angle of repose within the min to max range established by the experimental tests. The model slightly under predicted the hopper draining time with 0.3s, but this was deemed acceptable for this study. A final validation test was done where the deflection plate angle within the test rig was changed to 0 degrees. The comparison between the experimental results and the simulated results revealed that the model was capable of predicting the settling angle of repose and under predicted the hopper draining time with 0.36s. Upon successfully replicating the results for two different test rig setups the material parameters were deemed calibrated.

The steep incline sidewall conveyor simulation was started by evaluating the equipment geometry, layout and plant operational sequence. The steep incline sidewall conveyor movement was incorporated into the simulation with the use of the Simcenter STAR-CCM+ overset mesh tool. This tool allowed the conveyor cleat buckets to move as the actual plant conveyor moves. A high speed camera was used to capture footage of the coke loading point of the steep incline sidewall conveyor. This footage was used to validate the DEM simulation model with regards to three categories. Firstly the coke particle velocity was compared as it exits the chute until it reaches the belt cleats. It was determined that the DEM simulation model was capable of predicting this velocity within 10 percent. The second comparison was the material trajectory from the chute. It was determined here that the model was capable of visually replicating the material trajectory. The third comparison was the material build-up and settling analyses. It was determined that the simulation model did replicate the actual belt material interaction and settling. Due to the DEM simulation capable of replicating all three of the evaluation criteria, it was concluded that the DEM simulation was capable of simulating the steep incline sidewall conveyor loading interface.

Finally it was determined if plant modifications could be made in order to reduce the material spillage percentage. Here the simulation model was altered so that the particles spilled from the belt would escape the computational boundaries and therefore illustrate a material spilled percentage. The two main plant modifications evaluated were the alteration of the belt velocity and the discharge chute angle, i.e. material velocity. It was concluded that a 10 degree discharge chute angle increase would reduce the material spillage with 66.67%.

Thus in conclusion the combination of the direct and bulk calibration approach yielded calibrated material parameters. With the use of high speed camera footage it was established that the DEM simulation model was capable of replicating the coke loading on a steep incline sidewall conveyor, and that a 10 degree increase in discharge chute angle was

the best of the suggested modification options resulting in the greatest reduction of material spillages.

7.2. RECOMMENDATIONS

During the course of this study a few elements were highlighted which required further investigation form future studies.

The bulk calibration approach used in this study evaluated the angle of repose measurement as a basis of determining the particle-particle static friction coefficient. It was stated by Coetzee that when the angle of repose is used as a measure of particle static friction coefficient, there is a risk that this value might be lower than the actual value (Coetzee, 2016). For the purpose of this study this was mitigated by also analysing the hopper draining duration, but a more accurate method was suggested by Coetzee. It is recommended that a large shear box test setup be used and the bulk test rig built be used as a validation tool.

For the purpose of this study the hopper draining duration did not correlate to the experimental draining duration band. It was determined that this was due to under estimating the coefficient of rolling resistance and Young's modulus. For future studies it is recommended that this value be assessed and calibrated with the use of the large shear box test setup and validated with the hopper draining test setup as built in this study. This would ensure that the DEM simulation more accurately predicts the material flow rate.

The loading of the sinter, ore and additive materials were excluded from this study. It is recommended that later DEM studies include these two loading points in order to obtain a more complete perspective on the material spilled percentage.

It was concluded that the material spillage percentage was reduced the most by increasing the discharge chute angle with 10 degrees. It was determined that the deterioration of material spillage was mainly due to the material relative velocity matching the belt velocity. This resulted in a reduced material build-up effect which led to the reduction in material spillage percentage. It is recommended that this angle be investigated further in order to determine the discharge chute angle which would match the relative velocity even closer. This same analysis can be done for the sinter, ore and additive chutes in order to minimize the material spillage percentage.

APPENDIX 1 – STATIC FRICTION COEFFICIENT RESULTS FOR PARTICLE-CONVEYOR INTERACTION AND PARTICLE-CERAMIC LINER INTERACTION

Particle-Conveyor coefficient of friction		
Test number	Degrees	Static Friction Coefficient
1	40	0,839
2	40	0,839
3	36	0,727
4	37	0,754
5	40	0,839
6	42	0,900
7	45	1,000
8	45	1,000
9	46	1,036
10	34	0,675
11	34	0,675
12	40	0,839
13	40	0,839
14	41	0,869
15	48	1,111
16	35	0,700
17	39	0,810
18	41	0,869
19	41	0,869
20	40,5	0,854
Average	40,2	0,852

Particle-Ceramic liner coefficient of friction		
Test number	Degrees	Static Friction Coefficient
1	12	0,213
2	12	0,213
3	14	0,249
4	14	0,249
5	15	0,268
6	14	0,249
7	14	0,249
8	11	0,194
9	14	0,249
10	15	0,268
11	10	0,176
12	15	0,268
13	14	0,249
14	12	0,213
15	12	0,213
16	13	0,231
17	15	0,268
18	15	0,268
19	15	0,268
20	14	0,249
Average	13,5	0,240

APPENDIX 2 – PARTICLE-BOUNDARY COEFFICIENT OF RESTITUTION CALIBRATION RESULTS

Normal and Tangential coefficient of restitution	0,2
Max velocity	3,626
Second peak	0,688

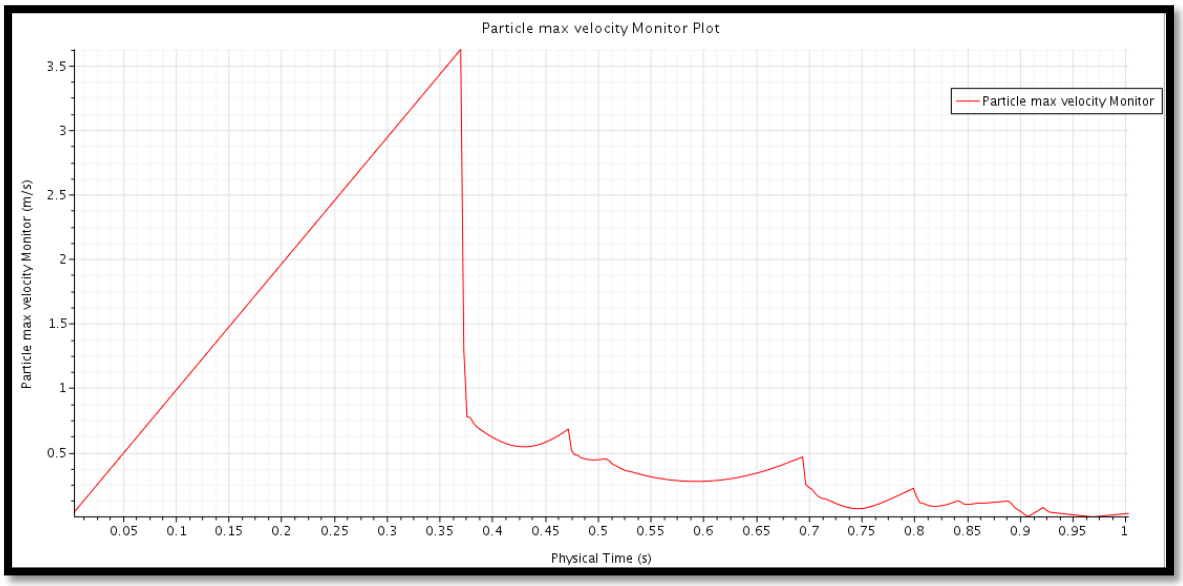

Normal and Tangential coefficient of restitution	0,4
Max velocity	3,626
Second peak	1,024

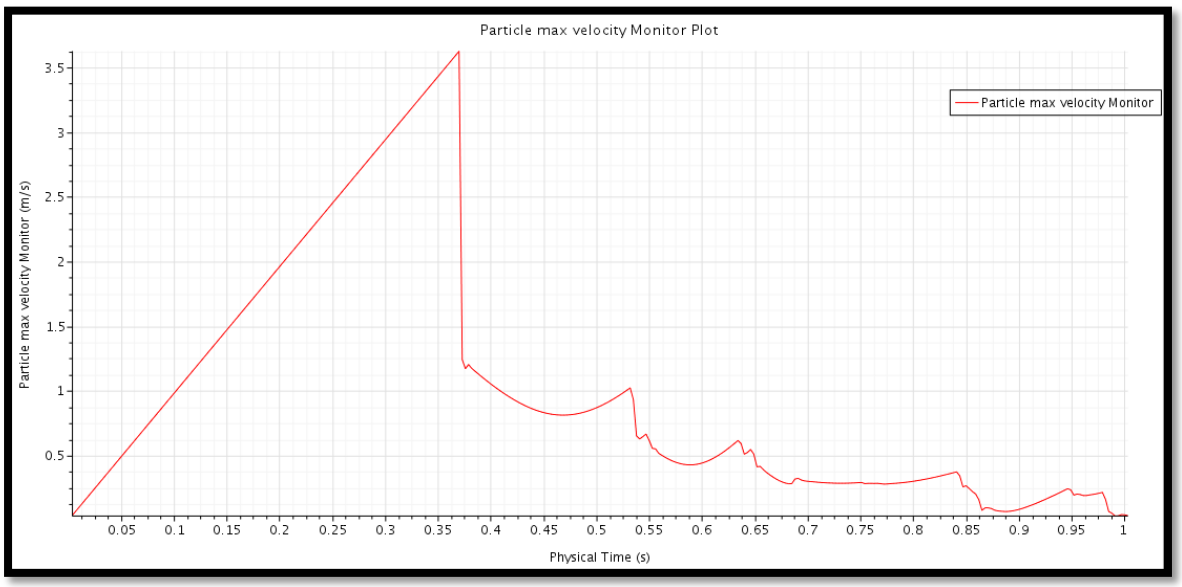

Normal and Tangential coefficient of restitution	0,6
Max velocity	3,626
Second peak	1,726

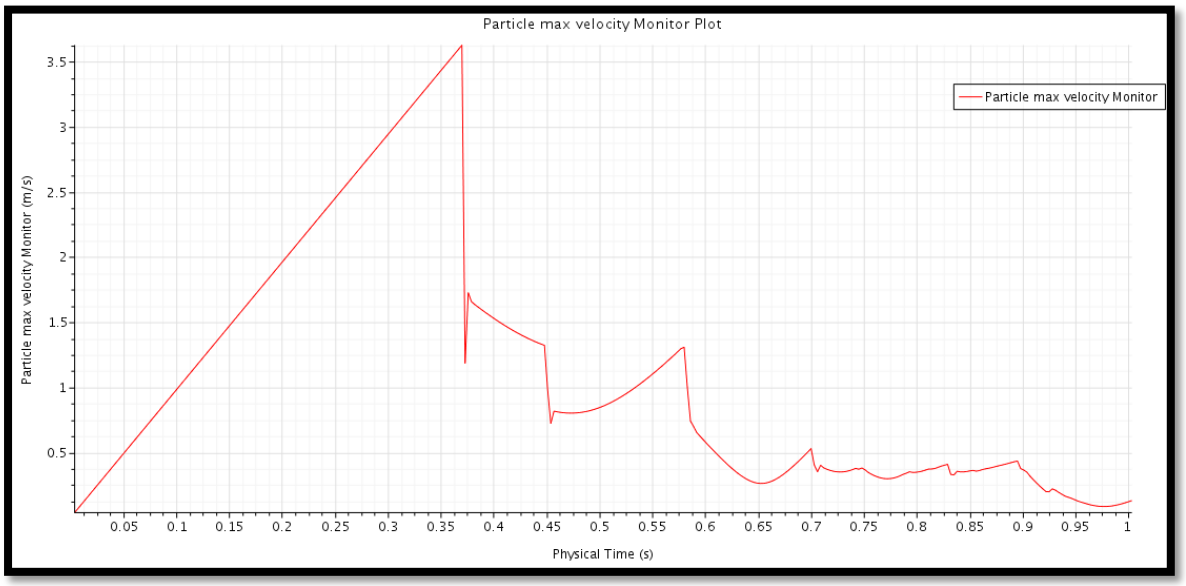

Normal and Tangential coefficient of restitution	0,8
Max velocity	3,626
Second peak	2,454

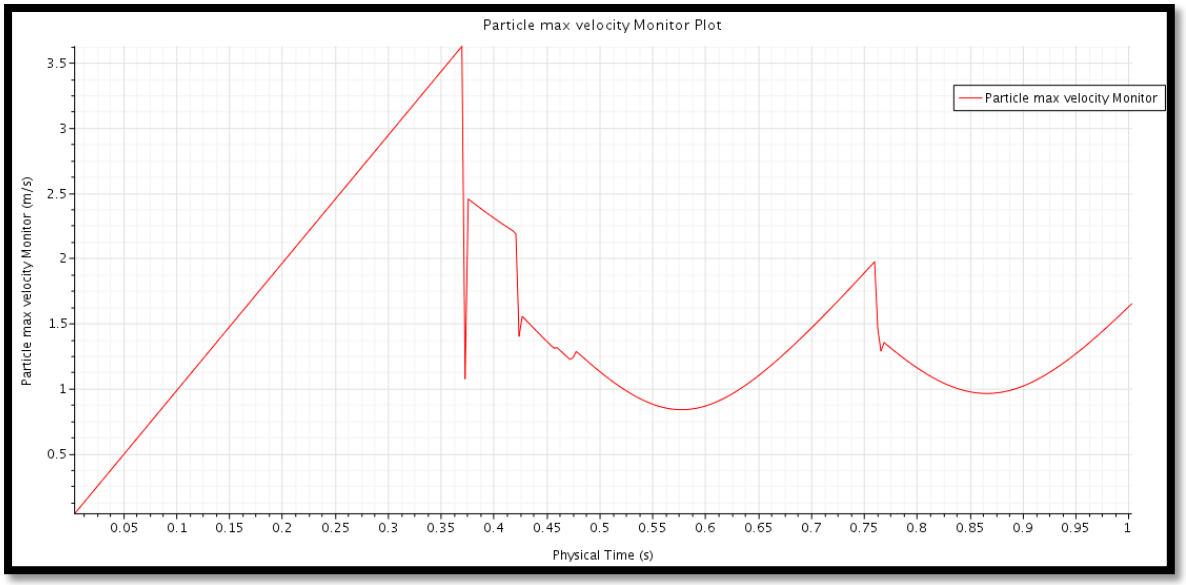

Normal and Tangential coefficient of restitution	1
Max velocity	3,626
Second peak	3,32

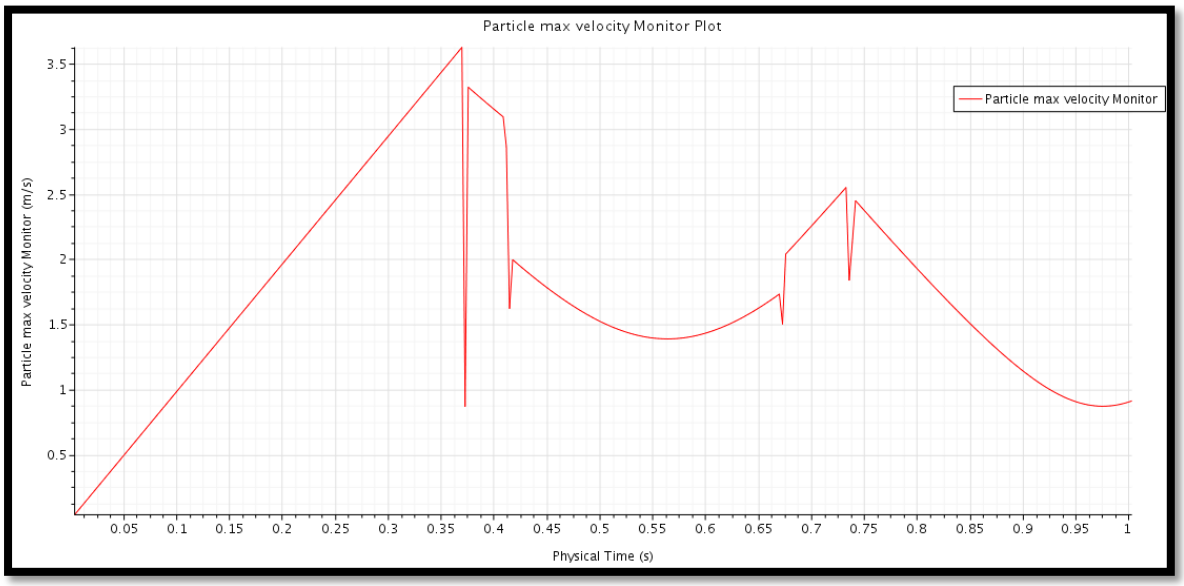

APPENDIX 3 – PARTICLE-PARTICLE STATIC FRICTION COEFFICIENT CALIBRATION SIMULATED HOPPER DRAINING TEST RESULTS

Hopper draining time vs particle-particle static friction coefficient			
Particle-Particle friction coefficient	Hopper draining time simulation	Hopper draining time min	Hopper draining time max
0,1	1,09	1,75	2,45
0,2	1,15	1,75	2,45
0,3	1,25	1,75	2,45
0,4	1,225	1,75	2,45
0,5	1,375	1,75	2,45
0,6	1,4	1,75	2,45
0,7	1,45	1,75	2,45
0,8	1,305	1,75	2,45
0,9	1,275	1,75	2,45
1	1,375	1,75	2,45
1,2	1,317	1,75	2,45
1,4	1,27	1,75	2,45
1,6	1,333	1,75	2,45
1,8	1,483	1,75	2,45
2	1,45	1,75	2,45
2,2	1,4	1,75	2,45
2,4	1,45	1,75	2,45

Static Friction Coefficient	0,1

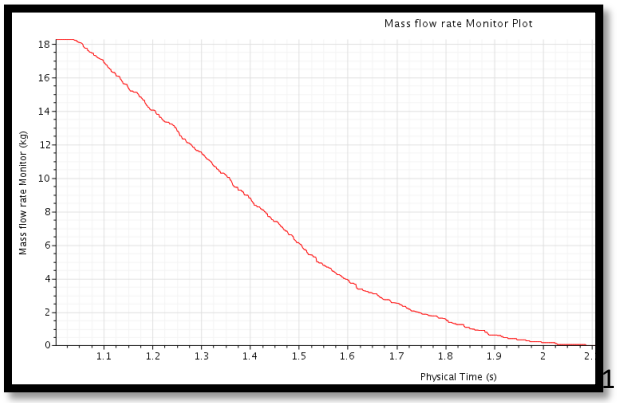

Static Friction Coefficient	0,2

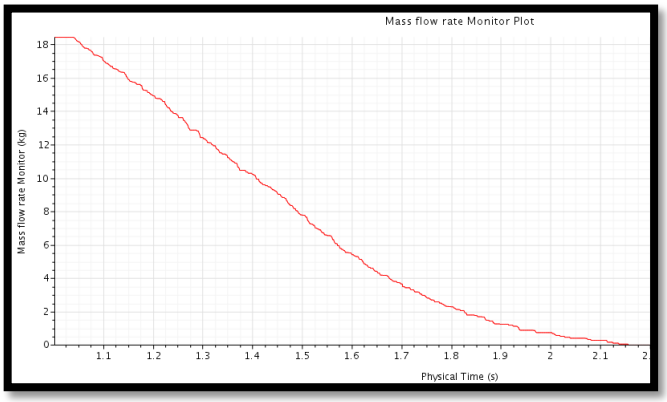

Static Friction Coefficient	0,3

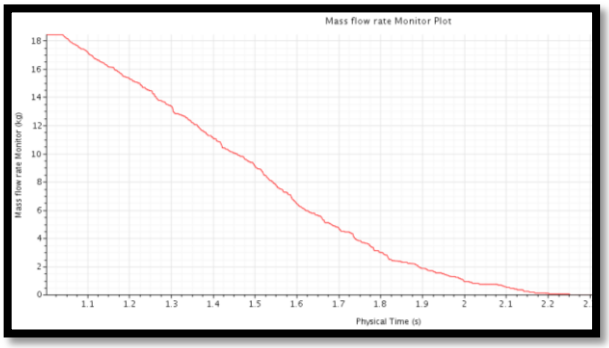

Static Friction Coefficient	0,4

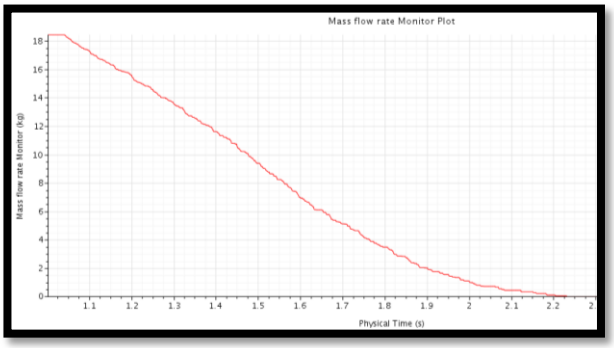

Static Friction Coefficient	0,5

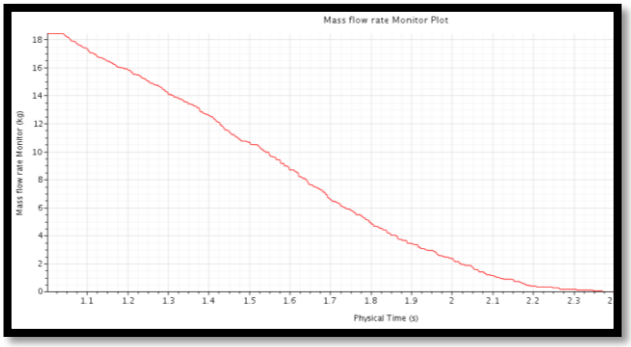

Static Friction Coefficient	0,6

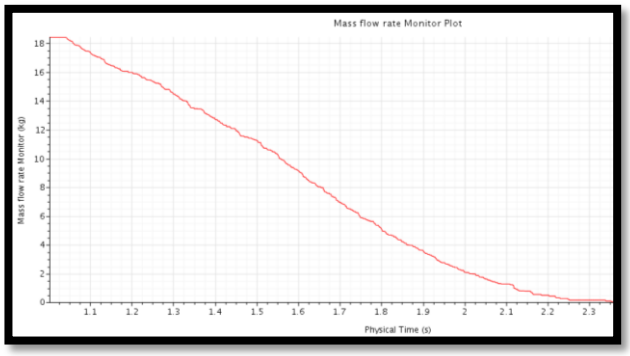

Static Friction Coefficient	0,7

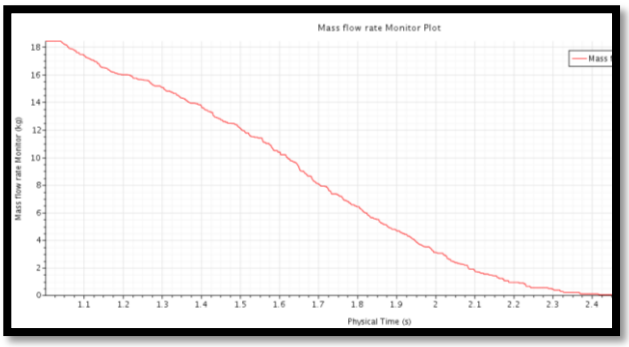

Static Friction Coefficient	0,8

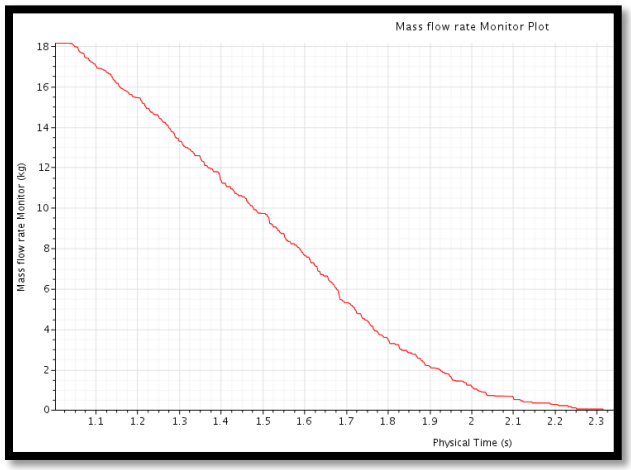

Static Friction Coefficient	0,9

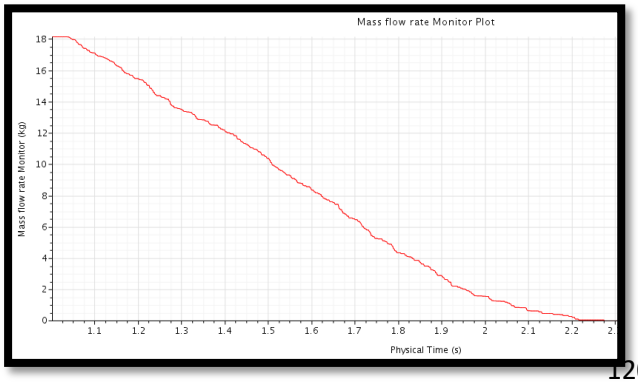

Static Friction Coefficient	1,0

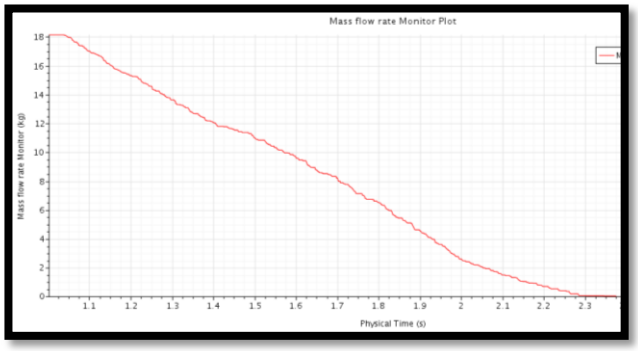

Static Friction Coefficient	1,2

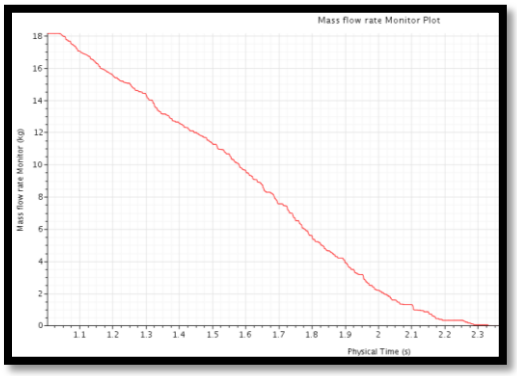

Static Friction Coefficient	1,4

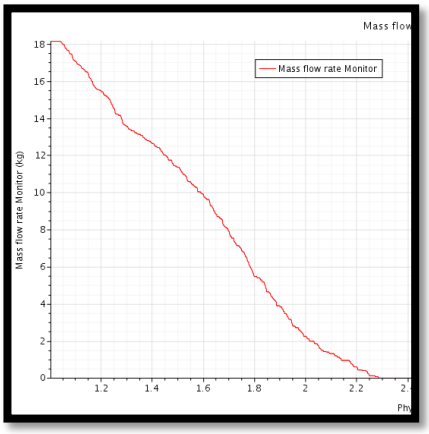

Static Friction Coefficient	1,6

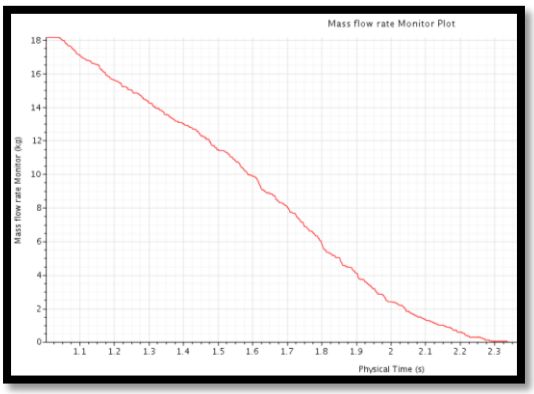

Static Friction Coefficient	1,8

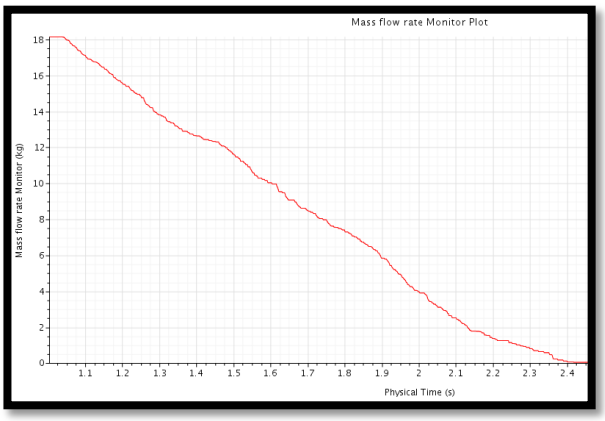

Static Friction Coefficient	2,0

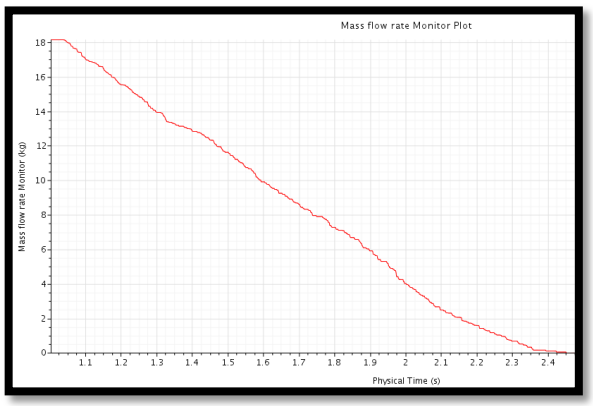

Static Friction Coefficient	2,2

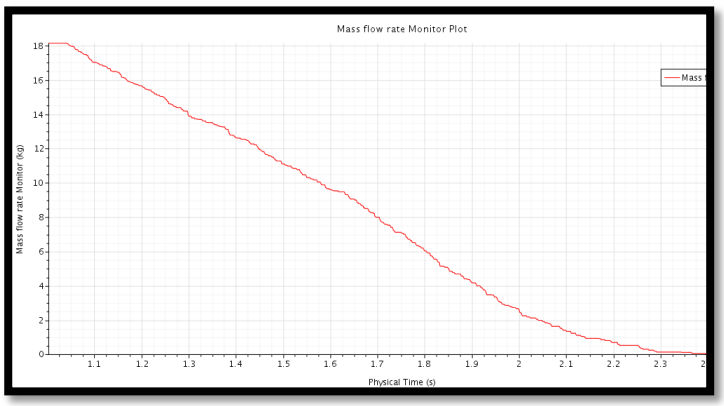

Static Friction Coefficient	2,4

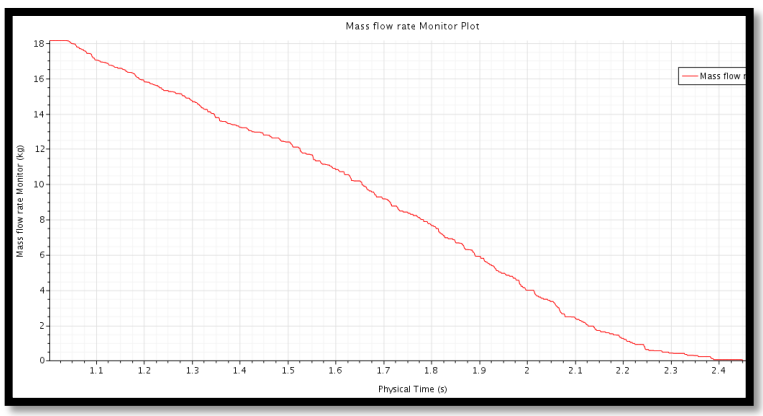

APPENDIX 4 - PARTICLE-PARTICLE STATIC FRICTION COEFFICIENT CALIBRATION SIMULATED ANGLE OF REPOSE TEST RESULTS

Angle of repose test			
Particle-Particle friction coefficient	Angle of repose simulation	Angle of repose experiment min	Angle of repose experiment max
0,1	22,22	31	40
0,2	25,46	31	40
0,3	28,09	31	40
0,4	28,75	31	40
0,5	29,23	31	40
0,6	28,56	31	40
0,7	26,66	31	40
0,8	29,18	31	40
0,9	30,22	31	40
1	30,9	31	40
1,2	33,06	31	40
1,4	32,2	31	40
1,6	33,32	31	40
1,8	32,2	31	40
2	37,28	31	40
2,2	35,87	31	40
2,4	35,32	31	40
3,5	35,16	31	40
4,5	35,28	31	40

Static Friction Coefficient	0.1

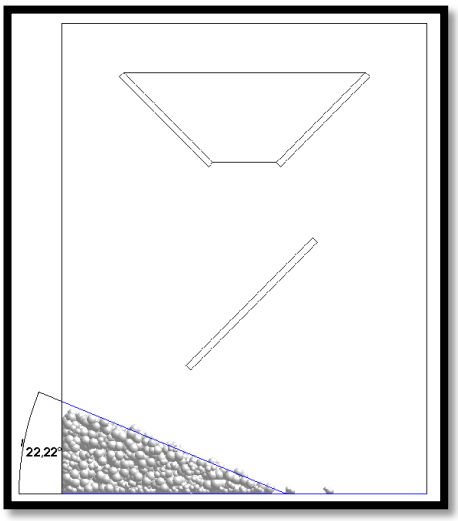

Static Friction Coefficient	0.2

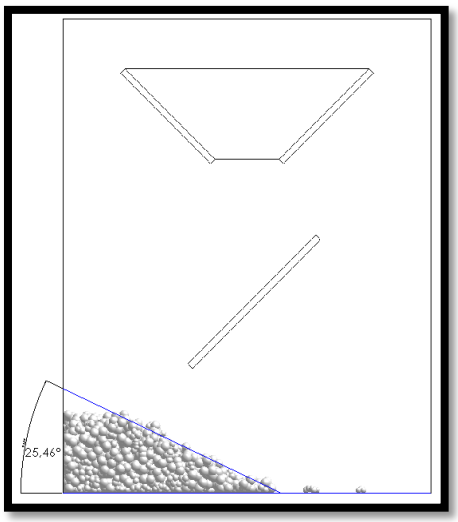

Static Friction Coefficient	0.3

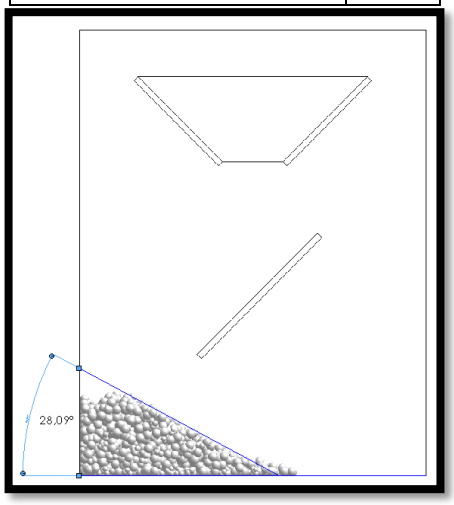

Static Friction Coefficient	0.4

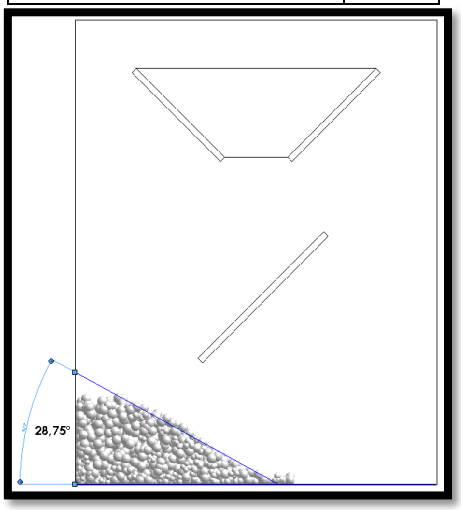

Static Friction Coefficient	0.5

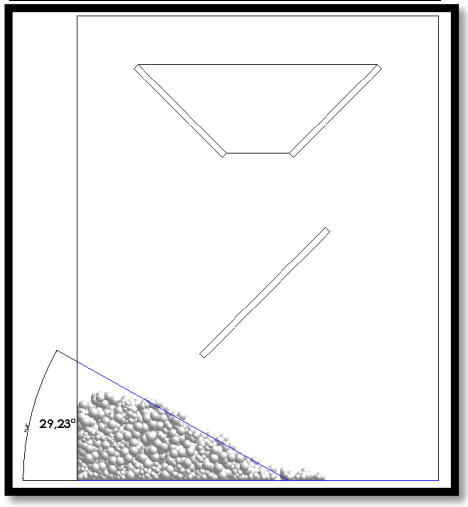

Static Friction Coefficient	0.6

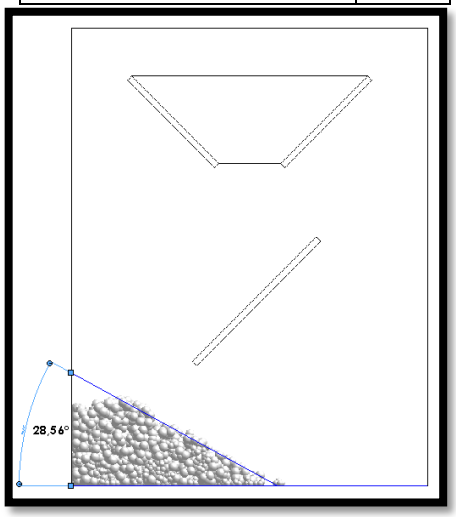

Static Friction Coefficient	0.7

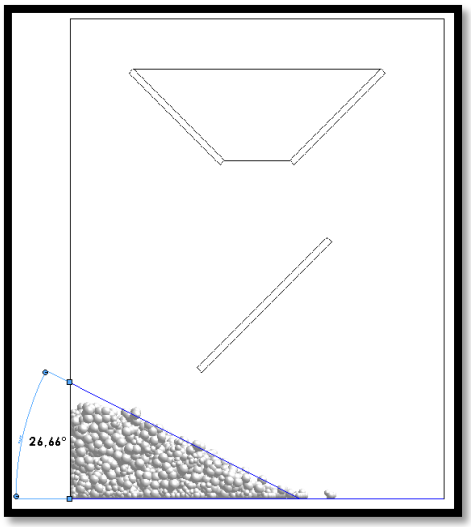

Static Friction Coefficient	0.8

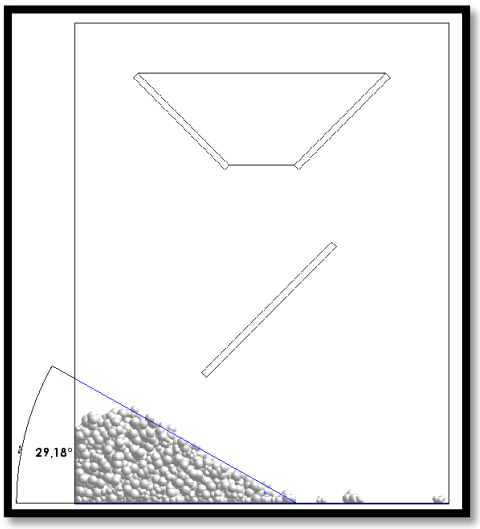

Static Friction Coefficient	0.9

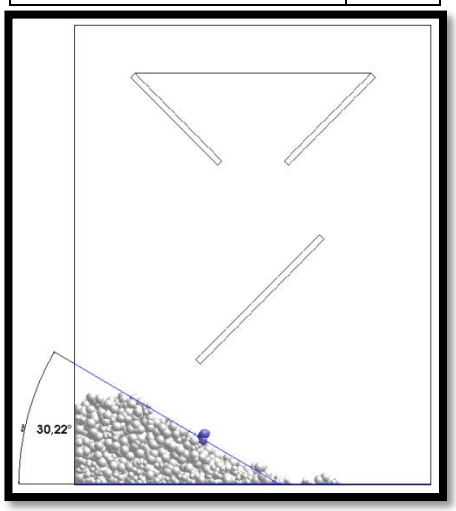

Static Friction Coefficient	1.0

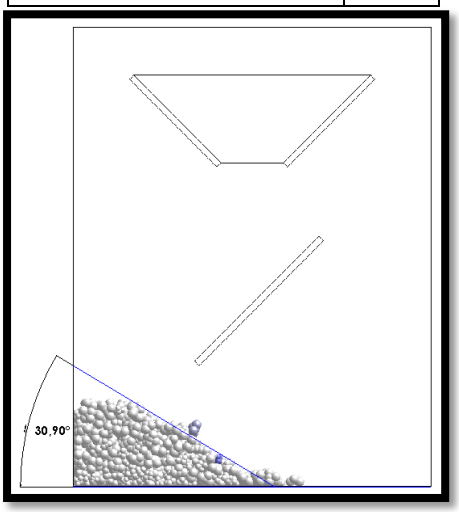

Static Friction Coefficient	1.2

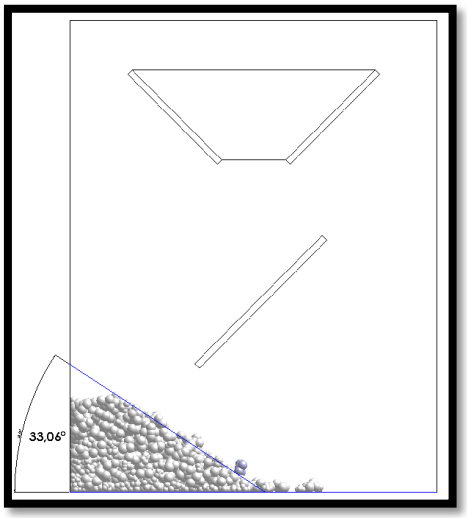

Static Friction Coefficient	1.4

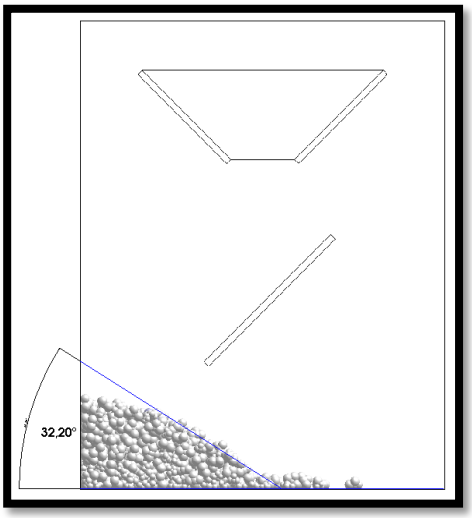

Static Friction Coefficient	1.6

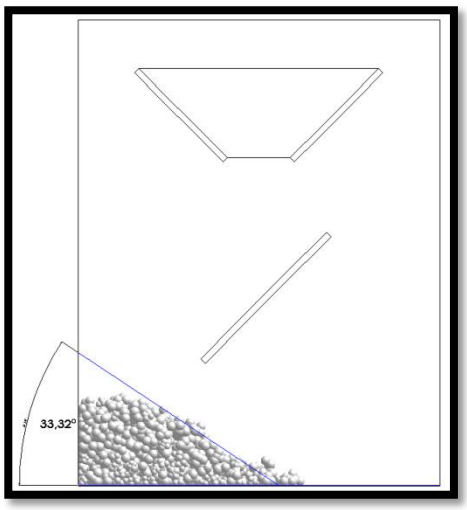

Static Friction Coefficient	1.8

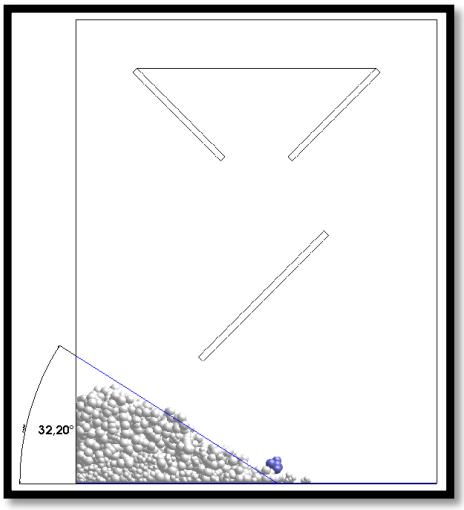

Static Friction Coefficient	2.0

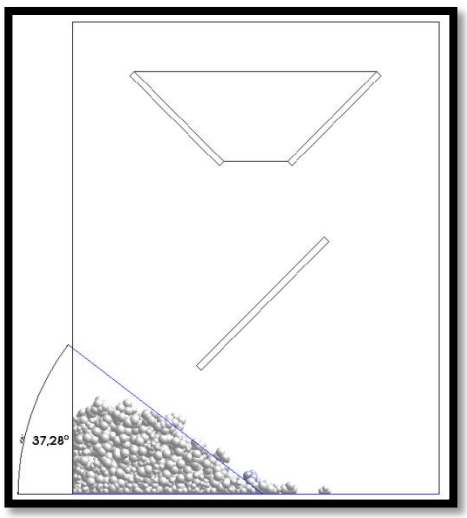

Static Friction Coefficient	2.2

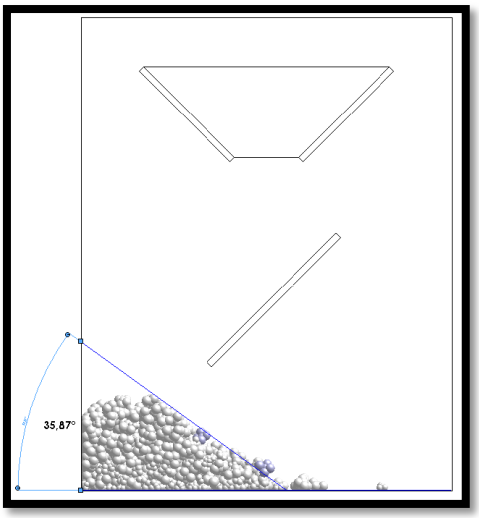

Static Friction Coefficient	2.4

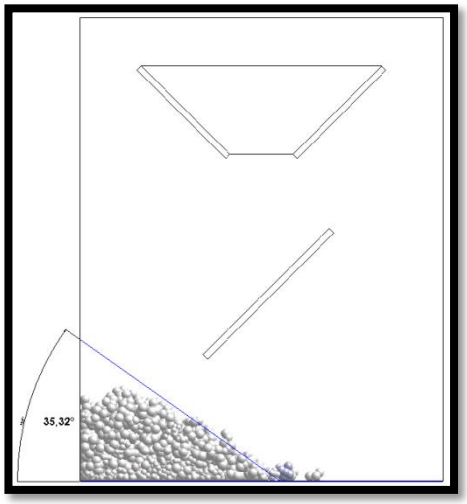

Static Friction Coefficient	3.5

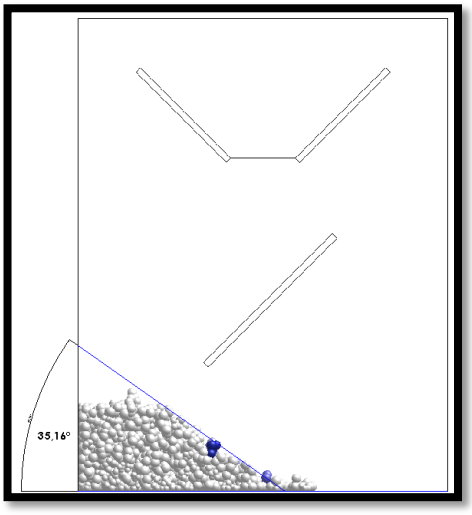

Static Friction Coefficient	4.5

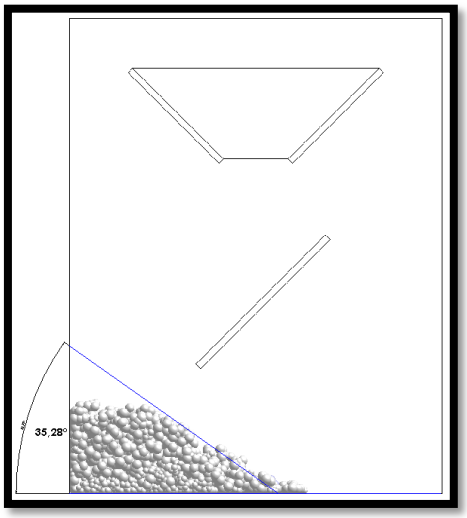

BIBLIOGRAPHY

1. Advanced Conveyor Technologies, 2018. *Newton.* [Online]
   Available at: http://www.demsoftware.net/software/
   [Accessed 13 August 2018].

2. Ai, J., Chen, J.-F., Rotter, M. J. & Ooi, J. Y., 2011. Assessment of rolling resistance models in discrete element simulations. *Powder Technology,* 206(3), pp. 269 - 282.

3. Asaf, Z., Rubinstein, D. & Shmulevich, I., 2007. Determination of discrete element model parameters required for soil tillage. *Soil and Tillage Research,* 92(1-2), pp. 227 - 242.

4. Canonical Ltd., 2018. *ESyS-Particle.* [Online]
   Available at: https://launchpad.net/esys-particle/
   [Accessed 13 August 2018].

5. Coetzee, C. J., 2016. Calibration of the discrete element method and the effect of particle shape. *Powder Technology,* pp. 50 - 70.

6. Coetzee, C. J., 2017. Review: Calibration of the discrete element method. *Powder Technology,* pp. 104-142.

7. Coetzee, C. J. & Els, D. N. J., 2009. Calibration of discrete element parameters and the modelling of silo discharge and bucket filling. *Computers and Electronics in Agriculture,* 65(2), pp. 198 - 212.

8. Cundall, P. A. & Strack, O. D. L., 1979. A discrete numerical model for granular assemblies. *Geotechnique,* Volume 29, pp. 47 - 65.

9. DCS Computing and CFDEMresearch, 2018. *CFDEM Project.* [Online]
   Available at: https://www.cfdem.com/liggghtsr-open-source-discrete-element-method-particle-simulation-code
   [Accessed 13 August 2018].

10. DEM Solutions Ltd, 2018. *EDEM Simulation.* [Online]
    Available at: https://www.edemsimulation.com/about/
    [Accessed 13 August 2018].

11. Engineering Simulation and Scientific Software, 2018. *Rocky.* [Online]
    Available at: https://rocky.esss.co
    [Accessed 13 August 2018].

12. Grima, A. P. & Wypych, P. W., 2011. Investigation into calibration of discrete element model parameters for scale-up and validation of particle–structure interactions under impact conditions. *Powder Technology,* pp. 198 - 209.

13. Haapakangas, J., 2016. *COKE PROPERTIES IN SIMULATED BLAST FURNACE CONDITIONS. INVESTIGATION ON HOT STRENGTH, CHEMICAL REACTIVITY AND REACTION MECHANISM,* s.l.: Acta Univ. Oul. C589.

14. Härtl, J. & Ooi, J. Y., 2011. Numerical investigation of particle shape and particle friction on limiting bulk friction in direct shear tests and comparison with experiments. *Powder Technology,* 212(1), pp. 231 - 239.

15. Höhner, D., Wirtz, S. & Scherer, V., 2015. A study on the influence of particle shape on the mechanical interactions of granular media in a hopper using the Discrete Element Method. *Powder Technology,* Volume 278, pp. 286-305.

16. Horn, E., 2012. *The Calibration of Material Properties for Use in Discrete Element Models,* Stellenbosch: Stellenbosch University.

17. ITASCA Consulting group, Inc., 2018. *PFC Version 6 General Purpose Distinct-Element Modeling Framework.* [Online]
Available at: https://www.itascacg.com
[Accessed 13 August 2018].

18. Just, S. et al., 2013. Experimental Analysis of Tablet Properties for Discrete Element Modeling of an Active Coating Process. *AAPS PharmSciTech,* 14(1), pp. 402-411.

19. Katterfeld, A., Groger, T. & Minkin, A., n.d. *Discrete Element Simulation of Transfer Stations and their Verification,* s.l.: s.n.

20. LI, Q., FENG, M. & ZOU, Z., 2013. Validation and Calibration Approach for Discrete Element Simulation of Burden Charging in Pre-reduction Shaft Furnace of COREX Process. *ISIJ International,* 53(8), pp. 1365-1371.

21. Lommen, S., Schot, D. & Lodewijks, G., 2014. DEM speedup: Stiffness effects on behavior of bulk material. *Particuology,* Volume 12, pp. 107-112.

22. Marigo, M. & Stitt, E. H., 2015. Discrete Element Method (DEM) for Industrial Applications: Comments on Calibration and Validation for the Modelling of Cylindrical Pellets. *KONA Powder and Particle Journal,* pp. 236 - 252.

23. Markauskas, D. & Kačianauskas, R., 2011. Investigation of rice grain flow by multi-sphere particle model with rolling resistance. *Granular Matter,* 13(2), pp. 143-148.

24. Minkin, A., Borsting, P. & Becker, N., 2016. A new Technology for Steep Incline High Capacity Open Pit Conveying. *Bulk Solids Handling.*

25. Nordell, L., 1997. *Particle Flow Modelling: Transfer chutes and other applications.* Johannesburg, s.n.

26. Pasha, M. et al., 2016. Effect of particle shape on flow in discrete element method simulation of a rotary batch seed coater. *Powder Technology,* Volume 296, pp. 29-36.

27. Paulick, M., Morgeneyer, M. & Kwade, A., 2015. Review on the influence of elastic particle properties on DEM simulation results. *Powder Technology,* Volume 283, pp. 66 - 76.

28. Quist, J. & Evertsson, M., 2015. *Framework for DEM Model Calibration and Validation.* Sweden, PROCEEDINGS OF THE 14TH EUROPEAN SYMPOSIUM ON COMMINUTION AND CLASSIFICATION.

29. Ricketts, J. A., 2012. *Blast Furnace Training.* Vanderbijlpark: s.n.

30. Roessler, T. & Katterfeld, A., 2016. Scalability of Angle of Repose Tests for the Calibration of DEM Parameters. *ICBMH2016 Conference,* pp. 201 - 211.

31. Shigeto, Y., Sakai, M. & Matsusaka, S., 2011. *Development of a large scale discrete element modeling for a fine particle conveying.* Sydney Australia, Engineers Australia.

32. Siemens PLM, 2018. *Fluid Dynamics Simulation.* [Online]
Available at: https://www.plm.automation.siemens.com/global/en/products/simulation-test/fluid-dynamics-simulation.html
[Accessed 13 August 2018].

33. Siemens Product Lifecycle Management Software Inc., 2018. *Simcenter STAR-CCM+.* [Online]
Available at:
https://documentation.thesteveportal.plm.automation.siemens.com/starccmplus_latest_en/index.html#page/STARCCMP%2FGUID-AD4497B4-33A5-4874-B0F7-E3EB762CDB5D%3Den%3D.html%23
[Accessed 4 October 2018].

34. Sinnot, M. D., Hilton, J. E., McBride, W. & Cleary, P. W., 2017. Coupled gas-particulate discharge from a bucket elevator. *Powder Technology,* Volume 314, pp. 203-217.

35. Thompson, M. E., 2008. *From the field to the computer - A case study on the developement of input parameters for DEM simulation purposes,* s.l.: IMHC.

36. Timoshenko, S., 1951. *Theory of Elasticity.* s.l.:McGraw-Hill Book Company.

37. Ucgul, M., Fielke, J. M. & Saunders, C., 2014. Three-dimensional discrete element modelling of tillage: Determination of a suitable contact model and parameters for a cohesionless soil. *Biosystems Engineering,* Volume 121, pp. 105 - 117.

38. University of Queensland, 2015. *MECHSYS MULTI-PHYSICS SIMULATION LIBRARY.* [Online]
Available at: http://mechsys.nongnu.org/index.html
[Accessed 13 August 2018].

39. Xie, L. et al., 2016. Wear process during granular flow transportation in conveyor transfer. *Powder Technology,* Volume 288, pp. 65-75.